[AMERICAN JOURNAL OF SCIENCE, VOL. 317, MARCH, 2017, P. 369-410, DOI 10.2475/03.2017.03]

CRUSTAL EVOLUTION IN THE GYEONGSANG ARC, SOUTHEASTERN KOREA: GEOCHRONOLOGICAL, GEOCHEMICAL AND Sr-Nd-Hf ISOTOPIC CONSTRAINTS FROM GRANITOID ROCKS

ALBERT CHANG-SIK CHEONG*,**,† and HUI JE JO**

ABSTRACT. A loosely assembled patchwork of Cretaceous to Paleogene granitoid plutons comprise the platform of the Gyeongsang Arc in southeastern Korea and represent a high-flux pulse of magmatism in Northeast Asia. The present study uses new and published zircon U-Pb ages, whole-rock geochemical and Sr-Nd isotopic data, and zircon Hf isotopic data of the plutons to decipher the crustal evolution in the Gyeongsang Arc and compare it with adjacent accretionary terranes. The ion microprobe zircon U-Pb ages range from 91 to 27 Ma, revealing the selective occurrence of Paleogene plutons in the eastern coastal area, to the east of the NNE-trending Yangsan fault system. Paleoproterozoic to Paleogene xenocrystic cores are occasionally observed in the zircon grains. The plutons are composed of dominantly magnesian, high- to medium-K calc-alkaline granites-granodiorites exhibiting typical geochemical characteristics of subduction zone magma, and less abundant ferroan alkaline granites. Their trace element patterns require residual amphibole and feldspar, but not garnet in the source. The whole-rock Sr-Nd and zircon Hf isotopic compositions of the granitoids (initial $^{87}Sr/^{86}Sr$ = 0.7043 to 0.7069; $\varepsilon_{Nd}(t)$ = –4.8 to +2.9; $\varepsilon_{Hf}(t)$ = –5.0 to +19.7) are distinctly more primitive than those of inland granitoids distributed outside of the Gyeongsang backarc basin. An important role of relatively young, most likely Paleozoic juvenile crust in the formation of the Late Cretaceous granitoids is suggested by the time-ε_{Hf} trend of high-ε_{Hf} zircons that converges toward data points of the Late Permian Yeongdeok adakite composing the arc basement. The asthenospheric mantle input is highlighted by significantly high (>+17) $\varepsilon_{Hf}(t)$ values of some zircons from the early Eocene alkaline plutons. Subsequent reworking of the rejuvenated crust yielded granitoid plutons possessing slightly but recognizably higher $\varepsilon_{Nd}(t)$ and $\varepsilon_{Hf}(t)$ values than the older plutons. These isotopic features demonstrate that the Cretaceous-Paleogene calc-alkaline granitoids in the Gyeongsang Arc are not "juvenile" (*sensu stricto*) despite their mostly positive epsilon Nd and Hf values, but are basically a product of crustal reworking. The Sr-Nd-Hf isotopic compositions of Late Cretaceous granitoids in the Gyeongsang Arc are comparatively more primitive than those in adjacent accretionary terranes such as Southwest Japan and Fujian province in southeastern China, reflecting differences in the formation age of the basement on which the arc system was built.

Key words: Gyeongsang Arc, southeastern Korea, granitoids, Sr-Nd isotopes, zircon age, zircon Hf isotope, crustal reworking, crustal rejuvenation

INTRODUCTION

Subduction systems have been active throughout much of Earth's history and provided an important driving force for the formation of the continents (Martin and others, 2005; Cawood and others, 2006, 2013; Hawkesworth and others, 2010). Arc magmatism is driven by dehydration reactions in the subducting oceanic lithosphere (Gill, 1981; Peacock and others, 1994; Tatsumi and Eggins, 1995; Tatsumi, 2005; Grove and others, 2012) and/or the supply of hydrous continental materials from the

* Division of Earth and Environmental Sciences, Korea Basic Science Institute, Chungbuk 28119, Republic of Korea

** Department of Isotope Geochemistry, Korea University of Science and Technology, Daejeon 34113, Republic of Korea

† Corresponding author: ccs@kbsi.re.kr; Tel: +82-43-240-5170; Fax: +82-43-240-5319; Mailing address: Korea Basic Science Institute, 162 Yeongudanji-ro, Cheongwon-gu, Cheongju, Chungbuk 28119, Republic of Korea

retroarc area to the arc root (Ducea, 2001; DeCelles and other, 2009). Whereas oceanic island arcs commonly produce basaltic to andesitic magmas, continental arc magmas are more silicic on average, thus requiring an additional differentiation step in the crust (Rudnick, 1995). Unlike oceanic arcs, many continental arcs exhibit a cyclicity of high-flux magmatic episodes (Armstrong, 1988; Barton, 1996; Ducea and others, 2015a, 2015b), attributable to cycles consisting of the influx of underthrusting continental lithosphere and gravitational removal of dense arc roots (Ducea, 2001; Ducea and Barton, 2007; DeCelles and other, 2009), or to repeated alternation from lithospheric extension to contraction typically caused by transient flat subduction (Collins, 2002; Li and Li, 2007; Li and others, 2012b; Zhu and others, 2014). The dominant portion of continental arc magma freezes at depth to form the batholithic root, rather than erupting at the surface (Paterson and others, 2011).

Prolonged subduction of the (paleo-)Pacific plate has left a huge, nearly continuous granitoid belt around the margins of the circum-Pacific. For example, the western North American Cordillera is composed mainly of Triassic to Eocene granitoid batholiths, such as the Peninsula Range batholith, the Sierra Nevada batholith, the Idaho batholith, and the Coast Mountains batholith, from south to north (Anderson, 1990). On the western Pacific side, the Phanerozoic granitoid belt extends from the Lachlan Fold Belt in eastern Australia through the Malay Peninsula, southeastern China, the Korean Peninsula, and the Japanese Islands to the Russian Far East. The eastern and western Pacific rims show fundamental differences in the gross long-term kinematic framework of the overriding plate (Cawood and others, 2009), as well as in the redox state of the granitoid and mineralization pattern (Ishihara, 1998).

The Cretaceous-Paleogene period marks a magmatic flare-up in Northeast Asia, as is the case for the eastern Pacific continental arcs (Ducea and others, 2015a, 2015b; Paterson and Ducea, 2015). The coastal areas of southeastern China are occupied predominantly by Cretaceous granitoids and volcanic rocks (Li, 2000; Li and others, 2014). Cretaceous to Paleogene granitoids and volcanic rocks are widespread in the Japanese Islands (Jahn, 2010, and references therein; Jahn and others, 2014), and the Gyeongsang Arc System [the term proposed by Chough and Sohn (2010) to collectively refer to the arc platform and adjacent to superjacent sedimentary basins] in the southeastern margin of the Korean Peninsula. Relatively little is known about the exact emplacement age and isotopic composition of granitoids in the Gyeongsang Arc, making it difficult to discuss the spatiotemporal trend and source characteristic of arc magmatism.

This study summarizes new and published geochronological, geochemical, and Sr-Nd-Hf isotopic data for Cretaceous-Paleogene granitoid plutons in the Gyeongsang Arc, and reveals that this ancient arc system has its own distinctive evolution style characterized by the reworking and rejuvenation of crustal protolith.

GEOLOGICAL BACKGROUND

Northeast Asia is a collage of several continental blocks successively isolated from the Gondwanan landmass (Li and Powell, 2001). The cratonal massifs in mainland Asia are bordered by Neoproterozoic-Early Mesozoic mobile belts (fig. 1; Ernst and others, 2007). On the other hand, Southwest Japan is composed of a series of accretionary complexes that have grown oceanward since the early Paleozoic (Isozaki and others, 2010). Widespread arc- or collision-related Phanerozoic granitoids occur approximately along the plate boundaries (fig. 1). After the Permian-Triassic amalgamation between the North and South China Blocks, the tectonic and magmatic evolution of Northeast Asia has primarily been governed by subduction of the (paleo)Pacific plate (Li and others, 2012a and references therein). As commonly observed in Phanerozoic supercontinents (Cawood and Buchan, 2007), the timing of subduction initiation in the Northeast Asian continental margin is nearly synchronous with internal collisional

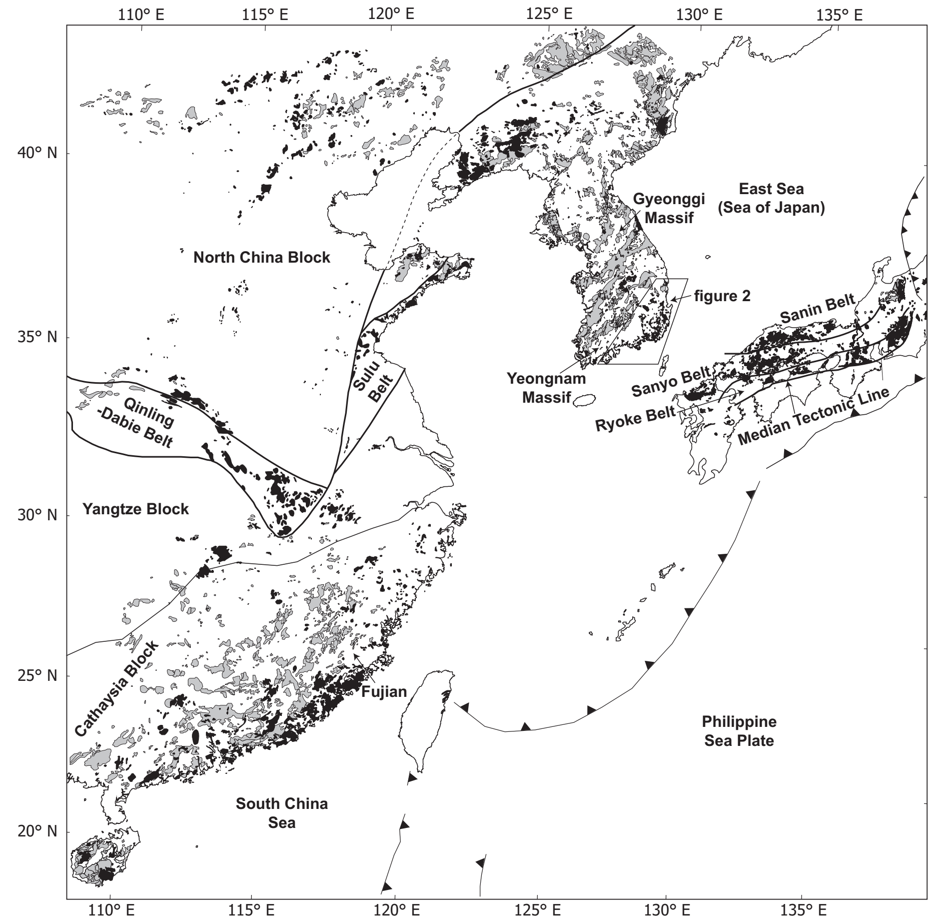

Fig. 1. Generalized tectonic map of Northeast Asia showing the distributions of Permian-Jurassic (in gray) and Cretaceous-Paleogene (in black) granitoids (compiled from KIGAM, 2001; Jahn, 2010; Cheong and Kim, 2012; Li and others, 2012b; Zhang and others, 2014).

orogenesis. The conversion to active continental margin is marked by the intrusion of Late Permian calc-alkaline granites on Hainan Island, southeastern China (Li and others, 2006) and Late Permian-Early Triassic adakite and sodic granitoids in southeastern Korea (Yi and others, 2012a; Cheong and others, 2014b). Thereafter, magmatic flare-ups occurred in the Jurassic and Cretaceous, with a lull especially prominent in South Korea (Sagong and others, 2005; Cheong and Kim, 2012). The present day Western Pacific-type plate margin was established in southeastern China in the late Early-early Late Cretaceous (Li and others, 2012b, 2014).

With the oblique subduction of the Izanagi Plate in the Early Cretaceous, the eastern margin of the Asian continent underwent left-lateral wrench tectonics (Klimetz, 1983; Engebretson and others, 1985). Several sedimentary basins, including the Gyeongsang Basin in southeastern Korea, formed in association with sinistral brittle shearing along strike-slip faults and continental arc magmatism. According to Chough and Sohn (2010), the Gyeongsang backarc basin was initiated in the Early Cretaceous as a narrow NS-trending trough that expanded progressively toward the east. The sedimentary strata crop out mainly in the northern and western parts of the basin

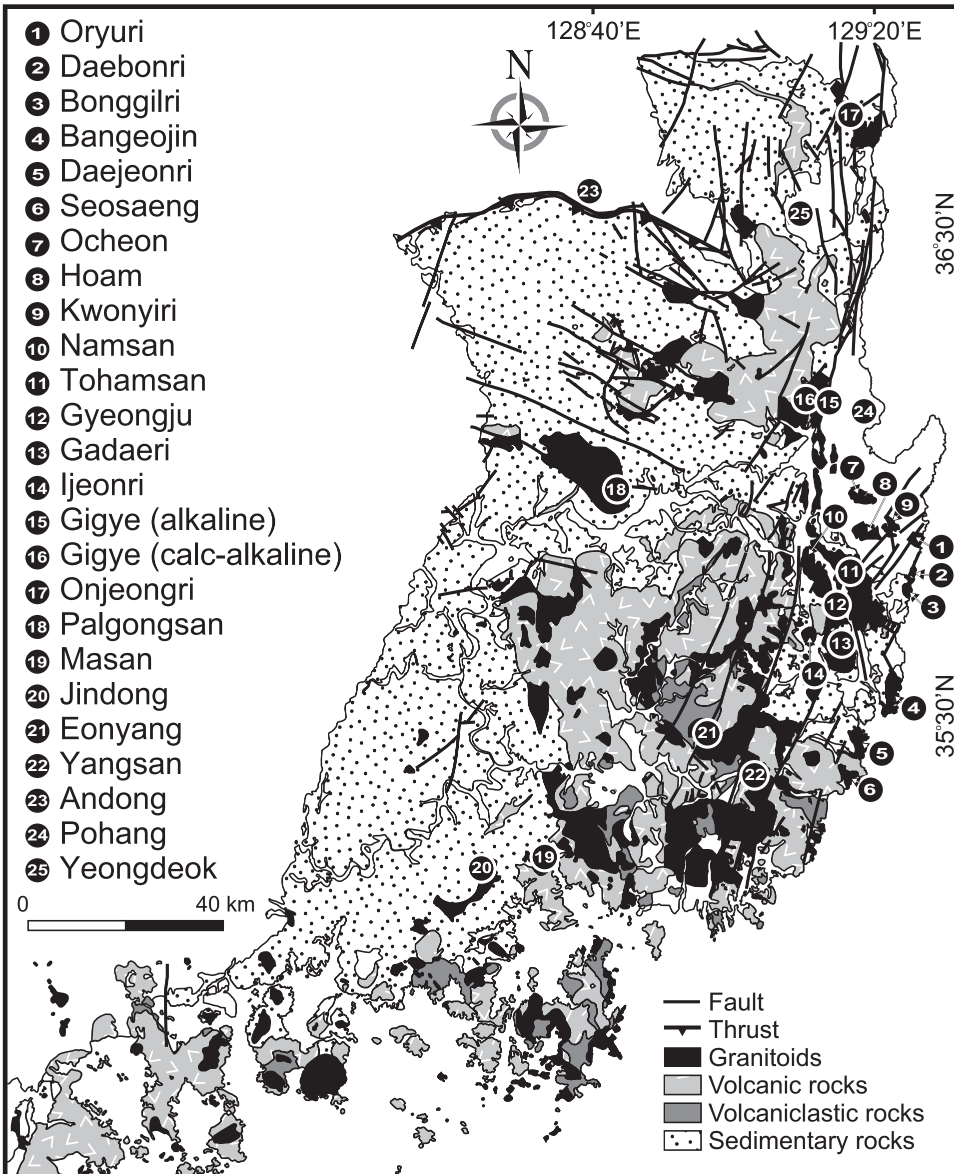

Fig. 2. Simplified geological map of the Gyeongsang Arc System in southeastern Korea (modified from Chough and Sohn, 2010), with sample locations of the present work and previous studies.

(fig. 2). They are composed of a thick succession of nonmarine sedimentary rocks such as conglomerate, sandstone, mudstone or shale, and some carbonate rocks, showing a temporal increase in the proportion of volcanogenic rocks. Extensive arc magmatism heralded by laterally continuous Cenomanian ignimbrites ("Gusandong Tuff"; Jwa and others, 2009; Sohn and others, 2009) has left a number of caldera complexes and a loosely assembled patchwork of granitoid plutons cropping out mainly in the southeastern part of the basin (fig. 2). This arc platform supplied a significant amount of volcanogenic material into the backarc basin via a fluvial network (Chough and Sohn, 2010). The plutons consist mainly of calc-alkaline I-type granites, granodiorites, and tonalites (Chough and others, 2000). Their shallow emplacement is indicated by occasionally observed miarolitic cavities, hornblende geobarometry (Cho and Kwon, 1994), and zircon oxygen and biotite magnesium isotope systematics (Jo and others, 2016). Paleogene alkaline granites containing riebeckite, arfvedsonite or annite occur along the NNE-trending Yangsan fault system bounding the Paleogene pull-apart basins in the eastern coastal area (Kim and Kim, 1997; Hwang and others, 2007, 2012). Hwang and others (2007) suggested that post-Eocene dextral strike slip movements along the Yangsan fault system separated the alkaline pluton, now in Gigye and Namsan (fig. 2), by approximately 20 km. The northern part of the Gyeongsang Basin is fault-bounded with schist and gneiss complexes in the Precambrian Yeongnam Massif and Jurassic granitoid batholiths (Choi and others, 2002).

The tectonic regime of the Gyeongsang Arc System is a controversial issue. Hwang and others (2008) explained the evolution of the Gyeongsang Basin in terms of the movement of conjugate fault sets and accompanying block rotation under a compressional stress regime. On the other hand, Chough and Sohn (2010) suggested an overall extensional or transtensional stress regime of the Gyeongsang Arc System and consequent weak coupling of the subducting slab with the overriding plate, on the basis of the development of volcanotectonic depressions or calderas and the virtual absence of syndepositional folds and thrusts. The latest prominent deformation in the southern Korean Peninsula is imprinted in the Early Cretaceous "Myogok" Formation overlain by sedimentary rocks of the northern Gyeongsang Basin (Lee and others, 2015).

MATERIALS AND METHODS

For this study, 25 rock samples were collected from 20 granitoid plutons within the Gyeongsang Arc System (fig. 2). Among them, two samples were taken from alkaline plutons in Namsan and Gigye, the mineralogy and geochemical signatures of which are typical of A-type granite (Koh and others, 1996; Kim and Kim, 1997; Hwang and others, 2012). The petrographic and mineralogical features of the investigated plutons are summarized in table 1.

Zircon grains were extracted from pulverized rock samples using conventional sieving, magnetic, and heavy liquid techniques. Cathodoluminescence (CL) images of zircon grains were obtained using a scanning electron microscope (JEOL JSM-6610LV) at the Korea Basic Science Institute (KBSI). Zircon U-Th-Pb isotopic analyses were performed using a KBSI Sensitive High-Resolution Ion Microprobe (SHRIMP IIe/MC). A 2 – 4 nA mass filtered O_2^- primary beam was focused to a spot *ca.* 25 μm diameter on the polished surface of zircon with an accelerating voltage of 10 kV. The collector slit was fixed at 100 μm in width, achieving a mass resolution of about 5,000 at 1 perecent peak height. FC1 (1099 Ma; Paces and Miller, 1993) and SL13 (U = 238 ppm) standard zircons were used for Pb/U calibration and to determine U abundance, respectively. Pb/U ratios were calibrated against FC1 according to the power law relationship between Pb^+/U^+ and UO^+/U^+, while Th/U ratios were estimated using a fractionation factor derived from the measured $^{232}Th^{16}O^+/^{238}U^{16}O^+$ versus $^{208}Pb/^{206}Pb$ of the SL13 standard. The common lead was removed by the ^{207}Pb (for spots <1,000 Ma) or ^{204}Pb (for spots >1,000 Ma) correction method (Williams, 1998) using the model of Stacy and Kramers (1975). Data processing was conducted using SQUID 2.50 and Isoplot 3.75 programs (Ludwig, 2008, 2009). Weighted mean ages were calculated after excluding the outliers with the t-test and reported at the 95 percent confidence level. Spots with high U concentrations (>2,000 ppm) were not considered in the age calculation (see White and Ireland, 2012). It should be noted that this study utilizes the geological time scale defined by Walker and others (2012).

TABLE 1

Petrographic and mineralogical summaries of granitoid samples collected from the Gyeongsang Arc, southeastern Korea

Pluton name	Lithology	Mineralogy	Texture
Oryuri	Coarse-grained granite with miarolitic cavities	Kfs + Pl + Qz + Bt ± Opq ± Zrn	Chlorite replacing biotite
Daebonri	Medium- to coarse-grained granite	Kfs + Pl + Qz + Hbl ± Bt ± Opq ± Mnz ± Ttn ± Zrn	Micrographic texture
Bonggilri	Medium- to coarse-grained granite to granodiorite with mafic microgranular enclaves	Pl + Qz + Kfs + (Hbl) + Bt ± Opq ± Ttn ± Mnz ± Zrn	Sericite replacing plagioclase and K-feldspar
Bangeojin	Fine- to medium-grained granite with mafic microgranular enclaves	Kfs + Qz + Pl + Bt ± Zrn ± Mag ± Mnz ± Ilm	Micrographic texture
Daejeonri	Fine- to medium-grained granite with mafic microgranular enclaves and sedimentary xenoliths	Qz + Pl + Kfs + Hbl + Bt ± Zrn ± Mag ± Ilm ± Mnz	Micrographic texture
Seosaeng	Fine- to medium-grained granite with mafic clots	Qz + Pl + Kfs + Hbl + Bt ± Zrn ± Mag ± Mnz ± Ilm ± Ttn	Compositional zoning pattern in plagioclase
Ocheon	Fine- to medium-grained porphyritic granite with miarolitic cavities	Kfs + Pl + Qz + Bt ± Zrn ±Opq ± Mnz ± Ttn	K-feldspar phenocryst, micrographic texture
Hoam	Medium- to coarse-grained granite	Kfs + Pl + Qz + Bt ± Mnz ± Mag ± Ilm ± Zrn	Chlorite replacing biotite
Kwonyiri	Medium- to coarse-grained porphyritic granodiorite with mafic clots	Kfs + Pl + Qz + Bt ± Zrn ± Mag ± Mnz ± Ilm	K-feldspar phenocryst, compositional zoning pattern in plagioclase
Namsan	Medium- to coarse-grained alkali granite	Kfs + Qz + Bt ± Zrn ± Ilm ± Mnz	Micrographic texture, interstitial biotite
Tohamsan	Fine- to medium-grained granodiorite	Pl + Qz + Bt + Hbl + Kfs ± Opq ± Zrn	Sericite replacing plagioclase and K-feldspar
Gyeongju	Fine- to medium-grained granite	Qz + Kfs + Pl + Bt ± Opq ± Zrn	Micrographic texture
Gadaeri	Fine-grained granite	Qz + Pl + Kfs + Bt ± Ms ± Zrn ± Mnz ± Ilm ± Ttn ± Mag	Micrographic texture
Ijeonri	Medium- to coarse-grained granite	Qz + Pl + Kfs + Bt + Hbl ± Ms ± Mnz ± Ttn ± Mag ± Ilm	Compositional zoning pattern in plagioclase
Gigye (alkaline)	Fine-grained alkali granite	Qz + Kfs + Bt ± Opq ± Zrn	Micrographic texture
Gigye (calc-alkaline)	Medium- to coarse-grained porphyritic granite	Kfs + Pl + Qz + Bt ± Mag ± Ilm ± Ttn ± Zrn ± Ap	K-feldspar phenocryst, compositional zoning pattern in plagioclase, micrographic texture
Onjeongri	Coarse-grained granodiorite	Kfs + Pl + Qz + Bt ± Opq ± Zrn	K-feldspar phenocryst, sericite replacing plagioclase
Palgongsan	Medium- to coarse-grained porphyritic granite with mafic microgranular enclaves	Pl + Kfs + Qz + Bt ± Mag ± Ilm ± Zrn ± Ap	K-feldspar phenocryst, compositional zoning pattern in plagioclase, ocellus quartz, acicular apatite
Masan	Medium- to coarse-grained granodiorite with mafic microgranular	Pl + Kfs + Qz + Bt + Hbl ± Opq ± Zrn	Sericite replacing plagioclase and K-feldspar
Jindong	Fine- to medium-grained granodiorite with mafic microgranular enclaves	Pl + Qz + Hbl + Bt + Kfs ± Opq ± Zrn	Sericite replacing plagioclase and K-feldspar

Mineral abbreviations: Ap, apatite; Bt, biotite; Hbl, hornblende; Ilm, ilmenite; Kfs, K-feldspar; Mag, magnetite; Mnz, monazite; Ms, muscovite; Opq, opaque mineral; Pl, plagioclase; Qz, quartz; Ttn, titanite; Zrn, zircon.

Whole-rock major element analyses were performed at Pukyong National University using an X-ray fluorescence spectrometer (XRF 1700, Shimadzu). Sample solutions for trace element analyses were prepared by low-dilution glass bead digestion (Park and others, 2013) and analyzed using a quadrupole inductively coupled plasma-mass spectrometer (ICP-MS) (X5, Thermo Elemental) at the KBSI. The geological reference material GSP-2 was used to monitor analyses. Discrepancies from recommended values were generally within 2 percent for major elements and 10 percent for trace elements.

Whole-rock Rb-Sr and Sm-Nd isotopic compositions were measured at the KBSI by isotope dilution-thermal ionization mass spectrometry (ID-TIMS). All analyses were carried out in a clean room equipped with laminar flow benches. Samples of approximately 50 mg of rock powder were mixed with highly enriched ^{87}Rb, ^{84}Sr, ^{149}Sm, and ^{150}Nd spikes and then dissolved with a mixed acid ($HF:HNO_3:HClO_4$ = 10:5:1) in PTFE digestion vessels. Rb, Sr, and rare earth element (REE) fractions were separated by the first step column filled with Dowex AG50W-X8 resin (H^+ form, 200 – 400 #). Sm and Nd fractions were separated from each other by second-step chromatography using Ln resin (2-ethylhexyl phosphoric acid). Isotopic ratios were measured using a multiple collector (MC) TIMS (IsoProbe-T; GV Instruments). Measured isotopic ratios were corrected mathematically for the added spikes (Cheong and others, 2014a). The effects of mass fractionation in Sr and Nd isotopic measurements were corrected by normalizing to ^{86}Sr/^{88}Sr = 0.1194 and ^{146}Nd/^{144}Nd = 0.7219, respectively. Replicate analyses of NBS 987 and JNdi-1 Nd yielded average ^{87}Sr/^{86}Sr of 0.710249 ± 0.000003 (n = 30, 2 standard error) and ^{143}Nd/^{144}Nd of 0.512101 ± 0.000002 (n = 30, 2 standard error), respectively. Total procedural blank levels were below 0.2 ng for Sr and 0.1 ng for Rb, Sm and Nd, and were therefore negligible. The epsilon Nd values were calculated using present day ^{143}Nd/^{144}Nd of 0.512638 and ^{147}Sm/^{144}Nd of 0.1967 assumed for a chondritic uniform reservoir (CHUR).

Zircon Lu-Yb-Hf isotopic compositions were analyzed using a 193 nm ArF excimer laser ablation system connected to a Neptune and Nu Plasma II MC-ICP-MS installed at the Tianjin Institute of Geology and Mineral Resources (TIGMR) and KBSI, respectively. Laser ablation was targeted for the analyzed SHRIMP points or new points within the same CL domains. The spot size was typically *ca.* 50 μm in diameter, but was reduced to *ca.* 30 μm for small CL domains. Instrumental operating parameters and data acquisition protocols were the same as reported in Cheong and others (2013) (for TIGMR Neptune) and Jo and others (2016) (for KBSI Nu Plasma II). The Yb and Lu isotopic compositions employed for the correction of mass bias and isobaric interference were adopted from Vervoort and others (2004) and Chu and others (2002), respectively. The isobaric interference-corrected ^{176}Hf/^{177}Hf ratios were exponentially normalized to ^{179}Hf/^{177}Hf = 0.7325. The ^{176}Lu/^{177}Hf and ^{176}Yb/^{177}Hf ratios were calculated after Iizuka and Hirata (2005). Initial epsilon Hf values were calculated using a ^{176}Lu decay constant of 1.865×10^{-11} year^{-1} (Scherer and others, 2001) and the chondritic values suggested by Blichert-Toft and Albarade (1997). During sample analysis at the TIGMR and KBSI, the GJ1, FC1, and 91500 zircons yielded ^{176}Hf/^{177}Hf ratios consistent with the values in the literature (Griffin and others, 2000; Woodhead and others, 2004; Gerdes and Zeh, 2006; Kemp and others, 2010). The internal precision of the ^{176}Hf/^{177}Hf ratio was proportional to the spot size. However, the accuracy was not seriously affected by the spot size (Jeong and others, 2015).

RESULTS

Zircon U-Pb Age

Representative CL images of newly dated zircon grains are shown in figure 3. The grains are generally prismatic and euhedral, and show clear oscillatory or banding zoning. Some grains contain rounded or resorbed cores texturally discordant to the magmatic rims. Zircon U-Th-Pb isotope data are listed in table 2. The ^{206}Pb/^{238}U and ^{207}Pb/^{206}Pb ratios in table 2 represent ^{208}Pb-corrected values. The magmatic origin of zircon grains is corroborated by their mostly high (>0.1) Th/U ratios (Rubatto, 2002). The uranium concentration is relatively high in zircon grains from the Gyeongju and Gigye (alkaline) plutons. Zircon grains from the Gigye sample are characterized by darker

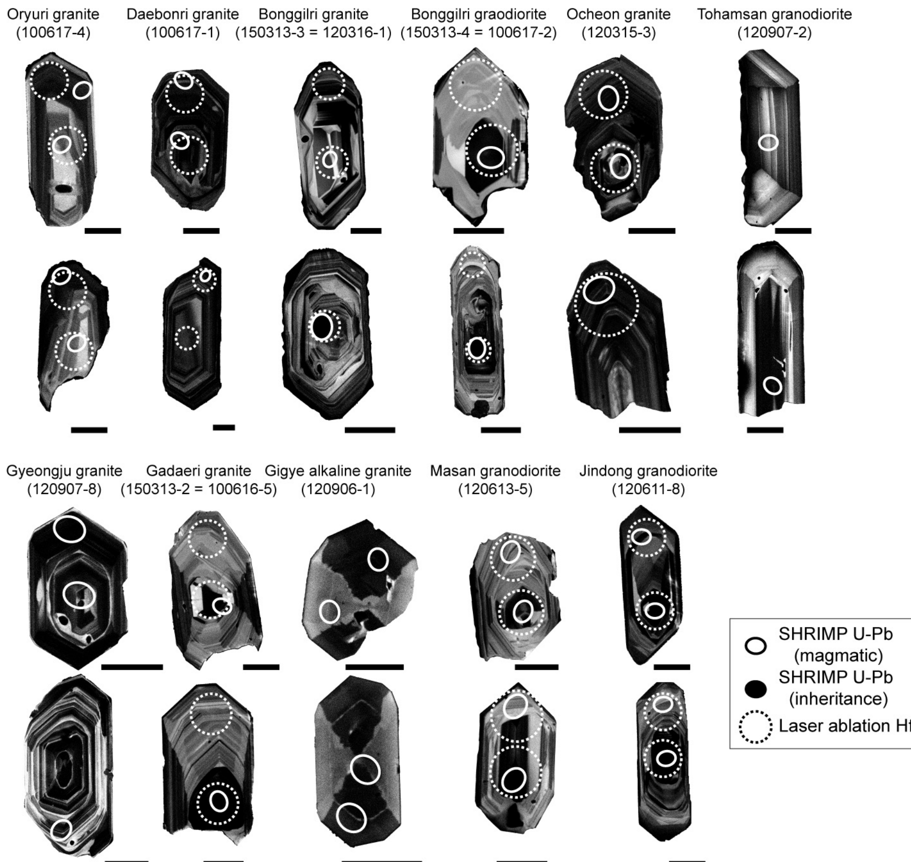

Fig. 3. Representative cathodoluminescence images of newly dated zircon grains recording locations for SHRIMP U-Pb dating and laser ablation-MC-ICP-MS Hf isotopic measurement. Scale bars are 50 μm.

and brighter CL patches (fig. 3). The common lead content ($^{206}Pb_{common}$) of zircon is generally lower than 2 percent.

Figure 4 illustrates zircon U-Pb isotopic compositions in the Tera-Wasserburg diagrams. It should be noted that most data plot on or near the concordia curve. The emplacement ages of the plutons would be best represented by the weighted means of $^{206}Pb/^{238}U$ dates, which correspond to the Late Cretaceous (Daebonri, Bonggilri, Gadaeri, Masan, and Jindong plutons), the Paleocene (Oryuri, Ocheon, and Tohamsan plutons), or the Eocene Epoch (Gyeongju and Gigye plutons). Zircon grains from the Bonggilri, Gadaeri, and Gyeongju plutons contain Paleoproterozoic, Triassic to Jurassic, and Paleogene xenocrystic cores. The Paleoproterozoic xenocrysts are not shown in figure 4 to save space.

Whole-Rock Geochemistry

The major and trace element compositions of 25 whole-rock samples are listed in table 3. Rb and Sr concentrations in table 3 represent the ID-TIMS results. Trace elements were not analyzed for three samples from Namsan and Gigye. Whole-rock geochemistry is described and discussed using these new data and published results for the Namsan, Tohamsan, Gyeongju, Gigye, Onjeongri, and Jindong plutons (Kim and Kim, 1997; Cheong and others, 1998; Hwang and others, 2012; Kim and others, 2016).

TABLE 2

SHRIMP U-Th-Pb results for zircon

Spot number*	Common ^{206}Pb (%)	U (ppm)	Th (ppm)	$\frac{Th}{U}$	$\frac{^{206}Pb}{^{238}U}$	±%**	$\frac{^{207}Pb}{^{206}Pb}$	±%**	date (Ma)***	
Oryuri granite (100617-4)										
1.1c	0.16	400	226	0.57	0.0109	0.9	0.0473	3.7	70.0	±0.6
1.2r	0.32	125	111	0.88	0.0103	1.6	0.0508	12.4	65.8	±0.8
2.1c	0.65	104	66	0.63	0.0099	1.5	0.0543	7.7	62.6	±0.8
2.2r		553	191	0.35	0.0101	0.9	0.0447	3.1	64.9	±0.5
3.1c	0.50	706	459	0.65	0.0100	1.1	0.0533	4.1	63.6	±0.6
3.2r	0.71	327	222	0.68	0.0101	1.1	0.0505	5.1	64.5	±0.6
5.1c		320	127	0.40	0.0101	1.6	0.0478	4.1	64.7	±1.0
5.2r	0.27	715	293	0.41	0.0102	1.5	0.0492	4.4	65.4	±0.9
6.1c	1.88	140	254	1.82	0.0099	3.8	0.0663	65.7	62.3	±1.5
7.2r	0.66	458	175	0.38	0.0099	1.3	0.0513	3.3	63.1	±0.7
8.2r	0.22	1114	323	0.29	0.0102	0.7	0.0501	2.0	65.5	±0.5
9.1r	0.64	152	183	1.21	0.0100	4.2	0.0436	29.8	64.5	±2.1
10.1r	0.59	211	249	1.18	0.0101	2.3	0.0549	17.9	64.3	±1.1
12.1r	0.48	146	179	1.23	0.0101	2.3	0.0505	27.6	64.4	±1.1
13.1r		209	324	1.55	0.0098	1.7	0.0406	57.7	63.4	±0.6
14.1r	0.19	239	314	1.31	0.0098	2.2	0.0467	27.8	62.7	±1.0
15.1r		547	181	0.33	0.0102	1.9	0.0459	3.3	65.5	±1.2
16.1r	0.87	167	140	0.84	0.0104	3.9	0.0359	17.3	67.5	±2.2
17.1r	0.08	799	360	0.45	0.0101	0.8	0.0487	2.5	64.9	±0.5
18.1r	0.08	817	336	0.41	0.0102	0.8	0.0461	2.6	65.3	±0.5
19.1r	0.32	148	255	1.72	0.0104	1.9	0.0645	52.9	65.5	±0.7
Daebonri granite (100617-1)										
1.1c	0.16	264	188	0.71	0.0094	1.2	0.0363	9.2	61.0	±0.6
1.2r		388	251	0.65	0.0102	2.8	0.0469	5.0	65.3	±1.6
2.1c	0.12	896	1098	1.22	0.0101	1.7	0.0496	10.8	64.4	±0.8
2.2r	0.49	259	155	0.60	0.0103	2.2	0.0489	5.3	66.0	±1.3
3.2r	0.48	282	176	0.62	0.0105	1.1	0.0517	4.7	66.7	±0.6
4.1c	0.22	223	185	0.83	0.0102	3.2	0.0531	7.8	65.0	±1.8
4.2r	0.03	150	80	0.54	0.0104	1.3	0.0564	5.2	66.2	±0.7
5.1c	0.66	142	95	0.67	0.0102	1.5	0.0463	9.1	65.6	±0.8
5.2r	0.19	1150	487	0.42	0.0100	0.8	0.0459	2.4	64.2	±0.5
6.1c	5.64	507	363	0.72	0.0104	1.2	0.0441	18.4	67.0	±0.9
6.2r	1.00	189	91	0.48	0.0104	2.0	0.0467	7.8	66.8	±1.2
7.1c	0.88	124	81	0.66	0.0104	1.7	0.0598	13.4	65.8	±1.1
7.2r	0.13	485	232	0.48	0.0100	2.7	0.0496	4.5	64.1	±1.6
8.1c	3.38	2536	579	0.23	0.0107	1.7	0.0535	3.3	67.9	±1.1
8.2r	0.55	515	309	0.60	0.0099	1.9	0.0463	6.3	63.4	±1.0
9.1c	1.09	82	38	0.46	0.0097	2.5	0.0410	11.3	62.8	±1.4
9.2r	0.18	696	334	0.48	0.0102	1.5	0.0468	3.1	65.4	±0.9
10.1c	0.03	1013	582	0.57	0.0106	1.1	0.0437	3.6	68.2	±0.6
10.2r	0.30	134	79	0.59	0.0105	1.5	0.0436	8.5	67.4	±0.8
11.1c	0.16	517	546	1.06	0.0106	1.5	0.0500	10.1	67.6	±0.8
11.2r	0.21	329	218	0.66	0.0107	1.4	0.0526	6.8	68.2	±0.6
12.1r	0.26	435	225	0.52	0.0107	1.0	0.0464	4.1	68.4	±0.6
13.1r	0.32	162	99	0.61	0.0103	1.3	0.0464	6.8	65.9	±0.7
14.1r	0.17	558	242	0.43	0.0106	0.9	0.0541	2.6	67.4	±0.5
15.2r	0.33	733	534	0.73	0.0104	1.0	0.0432	5.0	67.0	±0.5
16.1c	0.21	1551	1035	0.67	0.0105	1.3	0.0477	2.4	67.5	±0.8
16.2r		330	207	0.63	0.0105	1.1	0.0510	4.2	66.9	±0.6
17.1c	0.19	965	500	0.52	0.0108	0.8	0.0519	2.1	68.8	±0.5
17.2r	0.31	710	474	0.67	0.0104	1.3	0.0501	3.4	66.4	±0.8
18.1r	0.46	112	69	0.62	0.0100	1.5	0.0457	13.5	64.2	±0.9
19.1r		202	123	0.61	0.0103	2.3	0.0390	7.1	66.6	±1.3
20.1r		322	179	0.56	0.0100	2.4	0.0459	4.9	64.3	±1.4
Bonggilri granite (150313-3 = 120316-1)										
1.1c	0.41	109	103	0.94	0.0112	1.5	0.0576	13.1	71.2	±0.8
2.1c	0.01	712	745	1.05	0.0113	1.5	0.0483	8.7	72.3	±0.9

TABLE 2
(continued)

Spot number*	Common ^{206}Pb (%)	U (ppm)	Th (ppm)	$\frac{Th}{U}$	$\frac{^{206}Pb}{^{238}U}$	±%**	$\frac{^{207}Pb}{^{206}Pb}$	±%**	date (Ma)***	
Bonggilri granite (150313-3 = 120316-1)										
3.1r	0.21	173	84	0.48	0.0114	3.4	0.0462	6.3	73.3	±2.3
4.1c	0.43	138	126	0.91	0.0116	4.0	0.0566	10.9	73.7	±2.5
5.1c		208	104	0.50	0.0116	1.0	0.0394	5.9	75.3	±0.7
6.1c	0.86	167	131	0.79	0.0112	1.8	0.0490	9.2	71.4	±1.1
7.1c	0.37	166	108	0.65	0.0113	3.6	0.0463	7.8	72.8	±2.3
8.1c	0.44	201	96	0.48	0.0117	1.7	0.0556	4.5	74.5	±1.1
9.1c		224	143	0.64	0.0110	1.8	0.0439	8.2	70.8	±1.0
10.1c	0.02	121	101	0.84	0.0118	1.4	0.0445	12.8	75.7	±0.8
11.1c	0.15	401	309	0.77	0.0116	2.6	0.0446	6.1	74.6	±1.7
12.1c	0.36	126	97	0.77	0.0116	1.4	0.0518	9.1	74.1	±0.8
13.1ic		2430	2870	1.18	0.0325	0.7	0.0514	3.6	206.0	±1.2
14.1c	0.10	1065	722	0.68	0.0117	1.1	0.0502	2.6	74.9	±0.7
15.1c	0.23	233	175	0.75	0.0114	2.5	0.0419	8.1	73.8	±1.5
16.1c	0.64	219	142	0.65	0.0116	1.0	0.0548	5.0	73.4	±0.6
17.1c	0.33	268	123	0.46	0.0111	1.0	0.0465	4.6	71.3	±0.6
18.1c		122	112	0.92	0.0115	2.5	0.0441	15.5	73.9	±1.5
19.1c	0.45	928	159	0.17	0.0093	0.6	0.0469	2.8	59.7	±0.4
20.1c		397	407	1.03	0.0119	1.3	0.0446	10.8	76.5	±0.8
21.1c	0.28	309	204	0.66	0.0114	2.4	0.0370	8.0	74.2	±1.5
22.1c	0.04	174	115	0.66	0.0116	2.2	0.0464	7.2	74.4	±1.4
23.1ic	0.01	515	56	0.11	0.3580	2.6	0.1171	0.5	1915.1	±8.0
24.1c		393	365	0.93	0.0119	1.4	0.0399	10.4	76.7	±0.8
25.1c	0.84	95	42	0.44	0.0114	4.5	0.0430	10.7	73.6	±2.9
26.1ic	0.04	652	441	0.68	0.0338	0.8	0.0509	2.1	214.1	±1.4
27.1c		185	99	0.54	0.0111	1.2	0.0358	7.8	71.9	±0.7
28.1c	0.20	180	128	0.71	0.0120	1.2	0.0442	11.5	77.5	±0.8
29.1c	0.67	256	119	0.46	0.0119	2.4	0.0536	4.5	75.7	±1.6
30.1c	0.42	158	130	0.82	0.0117	3.1	0.0596	8.3	73.8	±2.0
31.1c	0.37	129	67	0.52	0.0111	1.3	0.0533	4.9	70.7	±0.8
32.1c		303	297	0.98	0.0117	1.1	0.0486	8.1	74.7	±0.7
33.1c	0.41	288	195	0.68	0.0112	1.5	0.0472	6.4	71.5	±0.9
34.1c	0.30	818	192	0.24	0.0119	1.7	0.0478	2.2	76.1	±1.3
35.1c	0.41	172	85	0.49	0.0115	2.0	0.0480	9.0	73.9	±1.4
36.1c	0.36	146	79	0.54	0.0119	1.3	0.0531	4.4	76.0	±0.8
37.1c	0.01	191	130	0.68	0.0115	1.8	0.0538	4.6	73.3	±1.2
38.1c		136	121	0.89	0.0116	1.5	0.0430	11.2	75.0	±0.9
39.1c		545	433	0.79	0.0123	1.0	0.0482	5.0	78.5	±0.7
40.1c	0.33	146	135	0.92	0.0127	1.3	0.0548	9.2	80.4	±0.8
41.1c	0.51	182	142	0.78	0.0117	3.4	0.0496	7.3	75.0	±2.2
42.1ic		390	219	0.56	0.0336	0.8	0.0512	2.7	213.0	±1.6
44.1ic	0.05	184	140	0.76	0.0328	1.9	0.0476	6.8	208.8	±3.5
45.1ic	0.77	95	37	0.39	0.0234	1.3	0.0457	5.3	149.7	±1.8
46.1c	0.61	163	103	0.63	0.0117	2.6	0.0507	5.6	74.8	±1.7
47.1c		248	224	0.91	0.0120	1.1	0.0497	7.7	76.8	±0.7
48.1c	0.17	157	128	0.81	0.0122	1.8	0.0555	6.7	77.7	±1.2
50.1c		272	210	0.77	0.0118	1.6	0.0460	8.5	75.7	±1.0
51.1c		305	318	1.04	0.0116	1.2	0.0506	9.8	74.3	±0.7
52.1c	0.00	629	603	0.96	0.0119	0.9	0.0496	5.3	76.2	±0.6
53.1ic		84	47	0.56	0.0393	1.4	0.0503	3.8	248.7	±3.0
54.1c	0.20	478	343	0.72	0.0120	1.2	0.0480	3.5	77.2	±0.8
55.1c	1.13	207	125	0.60	0.0116	2.2	0.0511	5.7	74.0	±1.4
56.1c	0.86	137	80	0.59	0.0116	2.5	0.0566	4.8	73.8	±1.6
57.1c		222	116	0.52	0.0119	2.1	0.0425	4.5	76.8	±1.4
58.1c	0.16	283	175	0.62	0.0115	0.9	0.0451	4.1	74.0	±0.6
59.1c	0.13	205	77	0.37	0.0121	1.5	0.0446	5.3	78.1	±1.1
60.1c	0.03	98	46	0.47	0.0118	2.8	0.0460	6.2	76.0	±2.0
61.1c	0.21	467	546	1.17	0.0116	2.6	0.0475	10.7	74.5	±1.5

TABLE 2

(continued)

Spot number*	Common ^{206}Pb (%)	U (ppm)	Th (ppm)	$\frac{Th}{U}$	$\frac{^{206}Pb}{^{238}U}$	±%**	$\frac{^{207}Pb}{^{206}Pb}$	±%**	date (Ma)***	
Bonggilri granite (150313-3 = 120316-1)										
62.1ic	0.00	425	253	0.59	0.0325	1.3	0.0510	1.9	205.8	±2.3
63.1c	16.94	147	77	0.53	0.0123	3.8	0.0367	15.5	80.1	±2.2
64.1c		161	104	0.64	0.0118	1.1	0.0405	9.3	76.5	±0.8
65.1c	0.02	411	380	0.93	0.0119	1.2	0.0428	7.1	76.8	±0.8
Bonggilri granodiorite (150313-4 = 100617-2)										
1.1c	1.55	108	101	0.93	0.0120	1.5	0.0683	10.8	75.0	±0.8
2.1c	0.45	1007	1722	1.71	0.0116	1.5	0.0508	25.7	74.0	±0.7
3.1c	0.16	1016	1168	1.15	0.0114	0.8	0.0473	9.1	72.8	±0.5
4.1c		293	101	0.34	0.0117	1.6	0.0445	4.6	75.3	±1.1
5.1c	0.16	522	701	1.34	0.0120	1.6	0.0546	16.3	76.5	±0.9
6.1ic	0.13	588	464	0.79	0.0297	0.8	0.0514	2.8	188.0	±1.3
7.1c		534	228	0.43	0.0136	0.8	0.0436	3.3	87.4	±0.6
8.1c		1092	567	0.52	0.0114	0.7	0.0466	2.3	73.1	±0.5
9.1c		184	139	0.75	0.0111	3.1	0.0468	7.2	71.4	±1.9
10.1c	64.42	178	123	0.69	0.0141	63.4	0.0433	297.0	90.7	±20.1
11.1c		155	148	0.95	0.0116	2.2	0.0506	11.2	74.3	±1.3
12.1ic		462	259	0.56	0.0327	0.8	0.0516	1.7	207.3	±1.5
13.1c	1.41	444	612	1.38	0.0120	1.1	0.0529	16.2	76.4	±0.6
14.1c	0.12	158	127	0.80	0.0111	2.3	0.0513	7.8	71.1	±1.4
15.1c	0.01	309	353	1.14	0.0116	1.1	0.0484	12.9	74.4	±0.6
16.1c	0.80	56	36	0.63	0.0114	4.9	0.0530	9.8	72.3	±3.2
17.1c	0.22	144	122	0.85	0.0114	1.4	0.0427	11.2	73.6	±0.8
18.1c	2.65	116	108	0.93	0.0117	1.8	0.0266	37.8	77.2	±0.9
19.1c	2.30	99	66	0.67	0.0117	2.1	0.0588	13.6	74.1	±1.5
20.1c	4.24	109	90	0.83	0.0115	2.6	0.0554	27.1	72.8	±1.1
22.1c	1.48	176	154	0.88	0.0117	2.2	0.0453	18.0	75.2	±1.5
23.1ic	0.04	711	632	0.89	0.0332	0.8	0.0531	2.9	209.6	±1.3
24.1c	1.29	194	127	0.65	0.0114	2.2	0.0512	6.6	72.6	±1.4
27.1c	1.12	92	50	0.54	0.0120	2.5	0.0585	6.2	76.1	±1.7
29.1c	0.08	74	46	0.63	0.0118	3.8	0.0410	11.8	76.5	±2.5
30.1c		1639	97	0.06	0.0119	1.2	0.0473	1.7	76.4	±0.9
31.1c	0.56	150	111	0.74	0.0114	1.2	0.0457	9.1	73.0	±0.7
33.1c		152	132	0.87	0.0119	4.5	0.0535	9.8	75.5	±2.9
34.1c		103	65	0.63	0.0124	1.4	0.0501	7.7	78.9	±0.9
35.1c	1.22	117	78	0.66	0.0118	3.3	0.0586	7.5	74.8	±2.2
36.1c	0.46	167	145	0.87	0.0118	1.3	0.0464	11.5	75.7	±0.7
37.1c	0.08	106	82	0.78	0.0120	8.3	0.0424	18.2	77.4	±5.5
38.1c		201	192	0.95	0.0118	1.3	0.0411	15.4	76.5	±0.7
39.1c	0.05	98	70	0.72	0.0121	1.6	0.0441	11.5	77.9	±1.0
40.1c	0.10	2491	130	0.05	0.0119	1.3	0.0470	1.5	76.4	±1.0
42.1c		235	211	0.90	0.0111	1.8	0.0421	9.8	71.9	±1.0
43.1c	0.52	148	71	0.48	0.0118	1.6	0.0581	4.1	74.5	±1.1
Ocheon granite (120315-3)										
1.2r	0.58	97	63	0.64	0.0101	1.2	0.0525	4.0	64.7	±0.7
2.2r		99	69	0.70	0.0103	1.0	0.0469	8.0	66.0	±0.6
5.2r	0.49	207	239	1.15	0.0100	1.3	0.0421	15.4	64.6	±0.6
6.2r	0.16	272	183	0.67	0.0104	0.8	0.0489	4.5	66.9	±0.5
7.1c	0.58	75	70	0.92	0.0101	2.2	0.0465	10.8	65.2	±1.1
7.2r	0.47	84	42	0.50	0.0102	1.0	0.0490	3.9	65.5	±0.5
8.1c	0.24	403	582	1.44	0.0102	0.9	0.0512	13.4	65.4	±0.4
8.2r	1.47	87	54	0.62	0.0103	2.1	0.0420	6.0	66.4	±1.2
9.1c	0.95	86	46	0.54	0.0105	1.1	0.0488	4.9	67.4	±0.6
9.2r	2.49	38	20	0.52	0.0103	1.3	0.0611	5.1	64.8	±0.7
10.2r	0.88	137	172	1.25	0.0101	1.1	0.0516	15.8	64.4	±0.5
11.1c	1.12	360	231	0.64	0.0102	0.7	0.0441	3.3	65.9	±0.4
12.2r	0.90	92	58	0.63	0.0103	1.0	0.0477	4.7	65.9	±0.5
13.1c	2.89	75	70	0.93	0.0104	1.3	0.0579	10.0	65.7	±0.6

Table 2

(continued)

Spot number*	Common ^{206}Pb (%)	U (ppm)	Th (ppm)	$\frac{Th}{U}$	$\frac{^{206}Pb}{^{238}U}$	±%**	$\frac{^{207}Pb}{^{206}Pb}$	±%**	date (Ma)***	
Ocheon granite (120315-3)										
13.2r	0.20	213	134	0.63	0.0104	0.8	0.0475	2.9	66.5	±0.4
17.1r	0.98	111	77	0.70	0.0099	1.1	0.0462	6.9	63.7	±0.5
19.1r	0.38	146	134	0.92	0.0104	1.0	0.0430	8.6	66.8	±0.5
20.1r	0.68	78	46	0.59	0.0101	1.0	0.0491	4.3	64.4	±0.5
21.1r	0.25	202	278	1.38	0.0103	1.0	0.0504	16.9	65.7	±0.4
Tohamsan granodiorite (120907-2)										
1.1c	4.96	409	424	1.03	0.0086	2.1	0.0485	17.8	55.1	±0.8
1.2r	4.15	381	462	1.21	0.0085	2.1	0.0498	23.9	54.4	±0.8
2.1c	0.20	600	63	0.11	0.0088	1.4	0.0428	4.3	57.1	±0.8
3.1c	0.45	1257	106	0.08	0.0090	1.3	0.0485	2.7	57.5	±0.7
3.2r	0.94	329	398	1.21	0.0091	2.0	0.0555	20.2	57.6	±0.8
4.1c	0.63	722	1442	2.00	0.0095	2.2	0.0701	43.1	59.1	±0.8
5.1c	0.65	551	826	1.50	0.0086	2.1	0.0380	45.9	55.9	±0.8
6.1c	0.40	1081	73	0.07	0.0093	1.3	0.0487	2.9	59.6	±0.8
6.2r	5.16	129	126	0.97	0.0086	4.9	0.0458	28.2	55.1	±2.1
7.1c	1.11	1200	51	0.04	0.0088	2.2	0.0477	5.6	56.6	±1.2
7.2r	5.26	793	257	0.32	0.0085	2.1	0.0519	5.8	54.1	±1.0
8.1c	8.93	101	86	0.85	0.0091	2.9	0.0359	35.9	59.0	±1.2
12.1c	1.78	602	1016	1.69	0.0090	2.1	0.0584	36.6	56.8	±0.8
13.1c	0.79	547	917	1.68	0.0090	2.1	0.0553	38.9	57.1	±0.8
14.1c	1.58	383	453	1.18	0.0085	2.8	0.0508	20.9	54.3	±1.1
15.1r	2.56	290	201	0.69	0.0086	3.1	0.0352	23.6	56.3	±1.3
Gyeongju granite (120907-8)										
1.2r	0.19	2035	2247	1.10	0.0080	2.8	0.0407	16.3	51.7	±1.1
2.1c	4.89	649	464	0.71	0.0082	1.3	0.0563	6.1	51.9	±0.5
3.2r	1.13	2456	1808	0.74	0.0085	1.1	0.0521	3.1	54.4	±0.5
4.1c	0.79	839	570	0.68	0.0084	1.2	0.0489	4.8	53.9	±0.5
4.2r	0.25	1687	1792	1.06	0.0082	1.2	0.0486	7.9	52.5	±0.5
5.2r	32.89	522	438	0.84	0.0078	2.4	0.0449	25.3	50.0	±0.7
6.2r	0.49	1823	1820	1.00	0.0084	1.3	0.0527	6.3	53.4	±0.6
7.1c	2.54	714	762	1.07	0.0088	1.4	0.0632	10.4	55.5	±0.6
7.2r	0.80	2802	3145	1.12	0.0088	1.2	0.0518	7.4	56.2	±0.5
8.1c	0.57	1267	1613	1.27	0.0086	1.3	0.0597	11.8	54.6	±0.5
9.1c	0.39	1050	762	0.73	0.0084	1.3	0.0497	4.4	53.7	±0.6
10.1ic	0.64	732	557	0.76	0.0097	1.2	0.0498	9.7	62.3	±0.7
11.1c	0.77	438	276	0.63	0.0083	2.4	0.0465	11.1	53.0	±1.2
11.2r	0.14	1975	2294	1.16	0.0084	1.0	0.0524	6.9	53.5	±0.4
12.1c	0.05	586	438	0.75	0.0085	2.1	0.0469	5.5	54.5	±1.0
12.2r	0.54	475	324	0.68	0.0084	1.6	0.0451	5.6	53.8	±0.7
13.1c		1719	1615	0.94	0.0087	1.0	0.0451	5.0	56.3	±0.5
13.2r	0.32	1423	1307	0.92	0.0085	1.4	0.0515	4.7	54.5	±0.6
15.1c	0.19	1383	1061	0.77	0.0085	1.0	0.0461	3.9	54.5	±0.5
15.2r	0.17	1870	1740	0.93	0.0086	1.0	0.0529	4.3	54.6	±0.5
16.1c	0.12	1301	840	0.65	0.0084	1.0	0.0494	3.1	53.9	±0.5
17.1r	0.16	894	795	0.89	0.0084	1.1	0.0538	5.4	53.2	±0.5
Gadaeri granite (150313-2 = 100616-5)										
2.1c	0.19	76	43	0.57	0.0107	3.8	0.0427	11.1	69.0	±2.3
3.1c	47.79	676	1199	1.77	0.0095	4.0	0.0335	144.8	62.3	±1.3
4.1c	0.16	1060	2243	2.12	0.0111	1.8	0.0535	46.6	70.4	±0.8
5.1c	0.10	1010	2766	2.74	0.0108	2.8	0.0467	224.2	69.3	±0.9
6.1c	0.28	510	798	1.56	0.0109	1.2	0.0428	35.2	70.3	±0.5
7.1c	0.03	628	1207	1.92	0.0109	1.2	0.0569	41.4	69.3	±0.5
8.1c	0.06	175	198	1.13	0.0109	2.1	0.0473	20.9	69.9	±1.1
9.1c	0.59	121	84	0.70	0.0103	1.5	0.0437	10.4	66.6	±0.8
10.1c		545	753	1.38	0.0105	1.9	0.0404	26.5	67.8	±0.9
11.1c	0.07	429	723	1.68	0.0109	1.7	0.0602	56.9	68.7	±0.5
12.1ic		471	77	0.16	0.3055	1.0	0.1149	0.5	1878.3	±8.6

Table 2

(continued)

Spot number*	Common ^{206}Pb (%)	U (ppm)	Th (ppm)	$\frac{Th}{U}$	$\frac{^{206}Pb}{^{238}U}$	±%**	$\frac{^{207}Pb}{^{206}Pb}$	±%**	date (Ma)***	
Gadaeri granite (150313-2 = 100616-5)										
13.1c	0.25	1077	2632	2.44	0.0109	2.8	0.0541	73.1	69.4	±1.1
14.1c	1.47	112	85	0.77	0.0099	1.5	0.0455	13.2	63.5	±0.7
15.1c		140	125	0.89	0.0105	1.8	0.0455	13.0	67.3	±0.9
16.1c	0.48	282	374	1.33	0.0110	1.7	0.0474	26.7	70.4	±0.8
17.1c	0.12	143	147	1.03	0.0106	3.7	0.0406	21.5	68.7	±2.0
18.1c		494	832	1.69	0.0108	3.0	0.0464	39.2	69.6	±1.5
20.1c	0.61	865	1648	1.90	0.0107	1.1	0.0465	43.9	68.8	±0.4
21.1c	0.58	74	47	0.64	0.0118	3.2	0.0537	9.1	74.8	±2.1
23.1c	0.13	761	1632	2.14	0.0105	2.3	0.0570	53.4	66.5	±0.9
24.1c		288	498	1.73	0.0110	1.4	0.0542	44.7	69.9	±0.5
25.1c	1.46	541	1128	2.08	0.0106	3.1	0.0466	73.8	68.2	±1.3
26.1c		491	701	1.43	0.0108	2.3	0.0483	23.4	69.1	±1.1
27.1c	0.14	390	742	1.90	0.0113	1.9	0.0646	43.9	70.7	±0.8
28.1c	0.14	394	582	1.48	0.0109	3.0	0.0520	28.6	69.3	±1.5
30.1c	0.85	221	213	0.96	0.0105	2.9	0.0468	13.3	67.7	±1.6
31.1c	4.63	99	95	0.96	0.0106	1.8	0.0301	37.6	69.5	±1.0
32.1c	0.22	165	208	1.26	0.0100	1.5	0.0498	23.5	63.7	±0.6
33.1c	0.11	92	53	0.57	0.0110	1.6	0.0394	8.6	71.0	±1.0
34.1c		93	62	0.66	0.0107	3.0	0.0500	7.7	68.2	±1.8
35.1c		150	129	0.86	0.0107	2.1	0.0452	10.6	68.9	±1.2
36.1c		316	424	1.34	0.0110	1.8	0.0520	18.7	70.3	±0.9
37.1c		78	73	0.93	0.0107	2.8	0.0391	19.2	69.5	±1.6
38.1c		64	43	0.67	0.0109	3.6	0.0467	10.5	70.1	±2.2
39.1c	0.17	88	56	0.63	0.0111	3.4	0.0528	7.7	70.4	±2.1
40.1c	0.06	154	134	0.87	0.0113	1.4	0.0446	10.8	72.9	±0.8
41.1c		46	23	0.51	0.0108	2.0	0.0320	14.9	70.7	±1.2
42.1c	0.11	93	75	0.81	0.0110	4.9	0.0441	12.8	71.1	±3.0
43.1c		104	98	0.94	0.0109	4.6	0.0504	13.6	69.9	±2.7
44.1c		71	42	0.60	0.0105	2.6	0.0464	8.6	67.3	±1.5
45.1c	0.10	81	51	0.62	0.0110	3.1	0.0480	8.3	70.3	±1.9
Gigye alkali granite (120906-1)										
1-1.1c	3.39	1689	2669	1.58	0.0086	1.3	0.0520	19.3	54.6	±0.5
1-1.2r	7.16	1060	1011	0.95	0.0085	1.2	0.0737	5.8	53.0	±0.5
1-2.1c	0.36	2331	3699	1.59	0.0090	1.2	0.0529	15.3	57.2	±0.5
1-2.2r	3.25	1397	1378	0.99	0.0085	1.2	0.0497	7.8	54.5	±0.5
1-3.2r	1.38	1012	557	0.55	0.0082	1.0	0.0469	3.6	52.5	±0.5
1-4.1c	4.55	844	545	0.65	0.0084	1.7	0.0451	16.5	54.0	±0.9
1-4.2r	5.34	1143	923	0.81	0.0083	1.2	0.0486	6.2	53.2	±0.5
1-5.1c	2.11	1839	1740	0.95	0.0088	1.3	0.0524	12.9	56.2	±0.6
1-5.2r	22.88	1381	1446	1.05	0.0085	2.8	0.0702	33.7	53.2	±0.9
1-6.1c	0.38	1393	1139	0.82	0.0087	1.3	0.0554	8.8	55.3	±0.5
1-6.2r	0.68	1409	1360	0.96	0.0083	1.1	0.0480	6.8	53.5	±0.5
1-7.1c	0.75	525	328	0.62	0.0085	1.2	0.0466	10.5	54.5	±0.6
1-7.2r	0.46	1813	1207	0.67	0.0087	1.5	0.0494	3.1	55.8	±0.8
1-8.1r	1.36	1548	1496	0.97	0.0085	1.1	0.0480	6.2	54.7	±0.5
1-9.1r	1.28	1507	1512	1.00	0.0084	1.1	0.0509	6.5	53.9	±0.5
1-10.1r	5.37	612	421	0.69	0.0084	2.3	0.0591	13.7	52.8	±0.9
1-11.1r	0.76	1257	981	0.78	0.0085	1.1	0.0583	3.7	53.9	±0.5
1-12.1c	33.71	491	134	0.27	0.0081	2.0	0.0536	14.0	51.7	±0.7
1-12.2r	6.69	783	466	0.60	0.0086	1.2	0.0446	6.4	55.1	±0.5
1-13.1r	7.95	691	478	0.69	0.0084	1.3	0.0484	16.3	53.9	±0.7
1-14.1r	5.43	811	607	0.75	0.0079	1.5	0.0539	16.6	50.3	±0.7
2-1.1c	0.37	805	536	0.67	0.0084	1.0	0.0523	3.1	53.4	±0.5
2-1.2r		1596	1675	1.05	0.0085	1.1	0.0486	5.5	54.5	±0.5
2-2.1c	90.88	281	84	0.30	0.0083	84.9	0.0915	78.1	50.4	±6.0
2-2.2r	91.46	330	90	0.27	0.0084	91.8	0.1894	74.6	44.3	±3.8

Table 2
(continued)

Spot number*	Common ^{206}Pb (%)	U (ppm)	Th (ppm)	$\frac{Th}{U}$	$\frac{^{206}Pb}{^{238}U}$	±%**	$\frac{^{207}Pb}{^{206}Pb}$	±%**	date (Ma)***	
Gigye alkali granite (120906-1)										
2-3.1c	2.56	1431	1259	0.88	0.0081	1.0	0.0479	8.8	51.9	±0.4
2-3.2r	0.71	1692	1315	0.78	0.0083	1.4	0.0470	4.2	53.6	±0.6
2-4.1c	6.21	1797	1895	1.05	0.0085	3.2	0.0451	50.9	55.0	±1.4
2-4.2r	0.78	1282	1188	0.93	0.0082	1.1	0.0510	3.8	52.5	±0.5
2-5.1c	18.99	934	796	0.85	0.0079	9.3	0.0475	97.7	50.7	±3.7
2-5.2r	0.18	1310	1261	0.96	0.0081	1.2	0.0512	4.4	51.7	±0.5
2-6.1c	0.19	1007	699	0.69	0.0084	0.8	0.0491	3.2	53.5	±0.4
2-6.2r	4.18	577	367	0.64	0.0085	5.2	0.0540	30.4	54.4	±2.5
2-7.1c	0.90	1195	1022	0.86	0.0083	0.7	0.0496	4.1	53.1	±0.3
2-7.2r	0.12	2064	2241	1.09	0.0086	1.1	0.0515	5.1	55.1	±0.5
2-7.1c		683	459	0.67	0.0084	1.5	0.0468	3.7	54.2	±0.7
2-8.2r	3.29	750	491	0.65	0.0079	0.8	0.0491	6.6	50.6	±0.4
2-9.1c	0.17	1443	1233	0.85	0.0085	0.9	0.0431	8.0	54.7	±0.4
2-9.2r	0.33	1492	1535	1.03	0.0083	0.7	0.0466	5.1	53.4	±0.3
2-10.1c	0.20	3539	6869	1.94	0.0089	1.9	0.0588	43.9	56.6	±0.7
2-10.2r	0.02	1543	1588	1.03	0.0083	1.0	0.0491	4.7	53.3	±0.4
2-11.1c	0.52	1042	709	0.68	0.0081	2.0	0.0494	6.5	52.1	±0.9
2-11.2r	1.23	1256	1184	0.94	0.0084	0.9	0.0509	4.7	53.5	±0.4
2-12.1c	1.61	1291	1138	0.88	0.0082	1.4	0.0486	6.7	52.7	±0.6
2-12.1r	0.06	2033	2213	1.09	0.0086	1.0	0.0477	4.5	55.0	±0.4
2-13.1c	2.17	691	329	0.48	0.0083	0.7	0.0455	8.5	53.7	±0.4
2-13.2r	0.01	1247	1128	0.90	0.0084	1.1	0.0492	5.4	53.5	±0.4
2-14.1r	0.03	1167	739	0.63	0.0082	1.0	0.0474	3.3	52.9	±0.5
2-14.2r	0.14	1647	1762	1.07	0.0084	0.8	0.0480	4.9	53.7	±0.4
2-15.1r	0.12	1312	799	0.61	0.0085	0.9	0.0476	2.1	54.6	±0.4
2-15.2r	0.14	1649	1784	1.08	0.0085	0.8	0.0503	9.6	54.6	±0.3
Masan granodiorite (120613-5)										
1.1c	0.32	795	979	1.23	0.0146	2.5	0.0532	8.5	92.8	±1.8
1.2r	1.13	326	149	0.46	0.0139	4.7	0.0516	9.0	88.7	±3.9
2.1c	1.69	231	171	0.74	0.0145	2.5	0.0573	8.3	91.6	±2.0
2.2r	1.14	468	333	0.71	0.0142	2.3	0.0519	4.8	90.4	±1.8
3.1c	2.19	659	336	0.51	0.0141	2.2	0.0527	3.4	89.7	±1.8
3.2r	0.31	1304	727	0.56	0.0146	2.2	0.0440	3.8	93.6	±1.8
4.2r	1.63	159	86	0.54	0.0150	4.4	0.0522	9.7	95.2	±3.8
5.1c	2.74	175	68	0.39	0.0142	2.5	0.0468	6.7	90.9	±2.1
5.2r	2.13	191	119	0.63	0.0146	3.4	0.0563	13.5	92.6	±2.9
6.1c	1.33	329	260	0.79	0.0138	2.6	0.0475	8.0	88.2	±1.9
6.2r	1.20	209	105	0.50	0.0148	2.4	0.0468	5.9	94.9	±2.1
7.1c	1.12	285	164	0.58	0.0147	2.4	0.0512	9.1	93.4	±2.0
7.2r	1.64	207	104	0.50	0.0144	2.6	0.0492	13.8	92.2	±2.2
8.1c	0.36	615	327	0.53	0.0143	2.2	0.0469	3.4	91.7	±1.8
9.1c	0.16	1667	2999	1.80	0.0149	2.7	0.0735	13.8	92.5	±1.8
9.2r	0.93	272	162	0.60	0.0141	2.4	0.0517	5.5	89.9	±1.9
10.1c	1.04	379	277	0.73	0.0138	3.3	0.0520	7.4	88.2	±2.5
10.2r	0.73	664	613	0.92	0.0133	2.4	0.0565	5.8	84.5	±1.7
11.1c	2.16	141	76	0.54	0.0137	3.0	0.0510	14.8	87.5	±2.3
Jindong granodiorite (120611-8)										
1.2r	8.51	49	29	0.60	0.0139	2.6	0.0423	40.4	89.5	±2.5
2.1r	7.83	34	18	0.52	0.0134	8.6	0.0737	26.1	83.0	±6.5
2.2c	5.85	57	58	1.01	0.0145	2.6	0.0797	25.2	89.1	±2.6
3.1c	5.29	61	39	0.64	0.0132	2.0	0.0615	15.5	83.3	±1.6
3.2r	6.47	40	23	0.58	0.0149	7.1	0.0584	12.4	94.1	±5.7
4.1c	1.47	88	80	0.91	0.0141	1.8	0.0711	8.3	87.8	±1.3
4.2r	5.08	43	32	0.74	0.0138	2.8	0.0511	27.2	87.8	±2.3
5.1c	2.96	83	85	1.03	0.0138	2.7	0.0627	34.6	86.7	±2.0
5.2r	9.63	34	17	0.52	0.0129	5.8	0.0475	44.0	82.5	±4.1

TABLE 2

(continued)

Spot number*	Common ^{206}Pb (%)	U (ppm)	Th (ppm)	$\frac{Th}{U}$	$\frac{^{206}Pb}{^{238}U}$	±%**	$\frac{^{207}Pb}{^{206}Pb}$	±%**	date (Ma)***	
Jindong granodiorite (120611-8)										
6.2r	5.37	41	22	0.52	0.0137	4.6	0.0575	12.7	86.6	±3.0
7.1c	5.19	50	38	0.76	0.0135	2.3	0.0479	23.1	86.2	±1.8
7.2r	4.30	81	38	0.47	0.0141	5.8	0.0225	58.7	93.2	±4.7
8.1c	4.17	99	75	0.76	0.0133	2.3	0.0503	16.7	84.6	±1.3
8.2r	4.39	57	30	0.53	0.0128	7.9	0.0355	37.1	83.2	±5.7
9.1c	4.66	52	43	0.84	0.0132	3.2	0.0345	55.4	85.9	±2.1
9.2r	7.31	39	23	0.61	0.0137	5.9	0.0563	29.4	86.5	±4.6
10.1c	0.84	360	399	1.11	0.0146	1.3	0.0663	7.7	91.1	±0.9
10.2r	2.09	59	34	0.59	0.0136	1.9	0.0477	9.5	87.3	±1.4
11.2r	6.58	44	24	0.54	0.0142	2.4	0.0571	12.5	89.6	±1.8
11.1c	2.60	101	64	0.63	0.0133	3.2	0.0620	6.7	83.6	±2.4

* c, core; ic, inherited xenocrystic core; r, rim.
** Relative errors at 1σ.
*** ^{207}Pb-corrected ^{206}Pb/^{238}U (<1000 Ma) and ^{204}Pb-corrected ^{207}Pb/^{206}Pb dates (>1000 Ma). Errors are absolute, and at 1σ.

The whole-rock samples vary in SiO_2 content from 61.9 to 79.0 weight percent. They are normatively classified as "granite" or "granodiorite." Some major element classification diagrams are presented in figure 5. In the classification scheme of Frost and others (2001), the alkaline granites from Namsan and Gigye are invariably "ferroan," whereas most of the other samples are "magnesian" (fig. 5A). In figure 5B, the samples are scattered between "alkali-calcic" and "calc-alkalic" fields. They also straddle the boundary between metaluminous and peraluminous fields in figure 5C but their A/CNK ratios are all below 1.1, the conventionally accepted boundary value between I- and S-type granites (Chappell and White, 1992). The samples are plotted dominantly in the high-K series field (Rickwood, 1989) (fig. 5D).

Figure 6 illustrates normalized geochemical patterns of the granitoids. In the normal-mid oceanic ridge basalt (N-MORB)-normalized spider diagram arranging the elements according to their compatibilities with the basaltic liquid (fig. 6A), the granitoid samples exhibit a typical arc affinity characterized by enrichment in large-ion-lithophile elements and relative depletion in high-field-strength elements. Negative troughs for Ba, Nb, Sr, P, and Ti are prominent in most samples, particularly in the alkaline granites. Th, Zr, Y, and REE contents are relatively high in the alkaline granites. Chondrite-normalized REE patterns are presented in figure 6B. The granitoids consistently show enrichment of light REEs (LREEs) (up to 100× chondrite), flat to slightly concave patterns in the middle and heavy REE (MREE and HREE, respectively) region, and conspicuous Eu negative anomalies. The alkaline granites have higher HREE contents and stronger negative Eu anomalies ($Eu/Eu^* < 0.1$) than the other samples. Their ferroan composition and high Zr and HREE concentrations are typical of A-type granitoids, which are commonly, although not always, related to an extensional environment (Whalen and others, 1987; Eby, 1990; Frost and others, 2001). It is noted that adakitic geochemical features (that is, high La/Yb and Sr/Y) of the Jindong pluton suggested by Wee and others (2007) are not verified by analytical results of Kim and others (2016) and this study.

Whole-Rock Sr-Nd Isotopes

Whole-rock Rb-Sr and Sm-Nd isotopic data are listed in table 4. The initial $^{87}Sr/^{86}Sr$ ratios calculated based on the SHRIMP zircon ages range from 0.7043 to

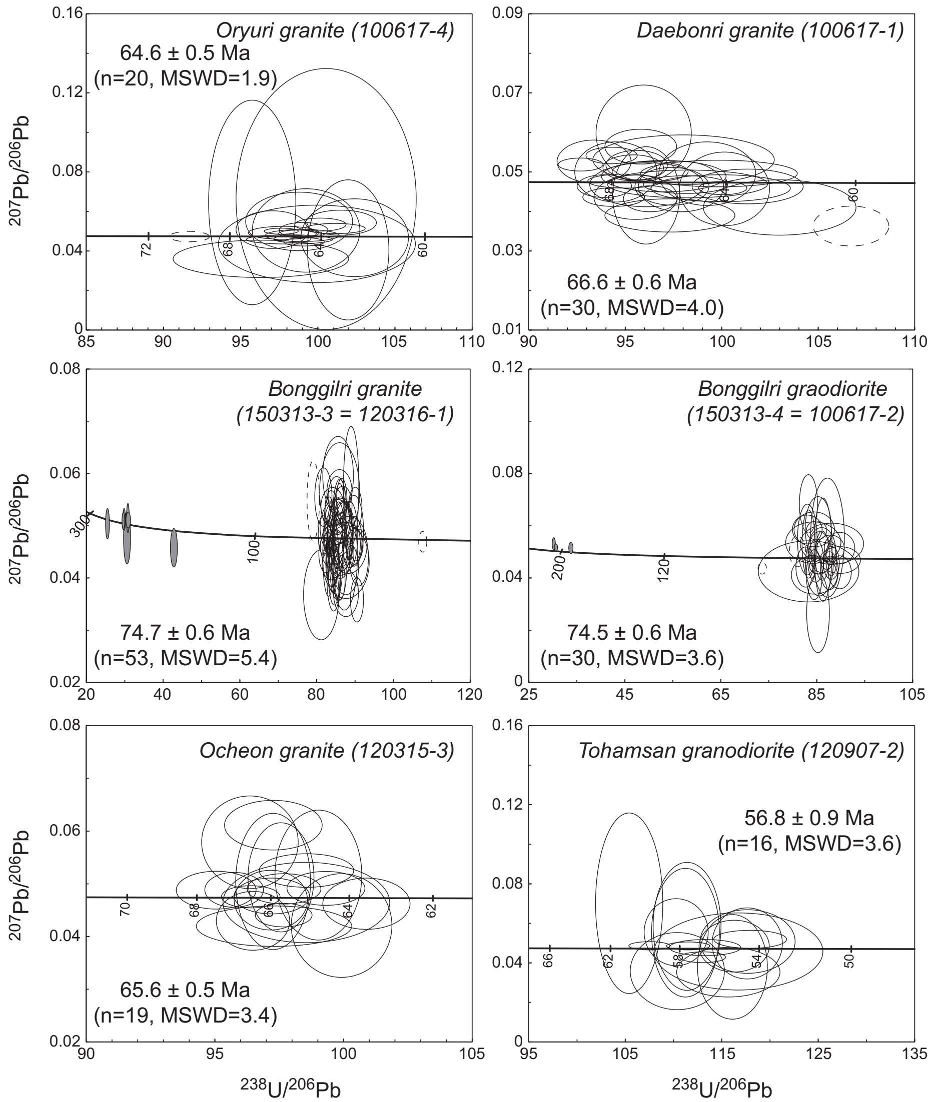

Fig. 4. Tera-Wasserburg concordia diagrams of SHRIMP zircon U-Pb data, with weighted mean $^{206}Pb/^{238}U$ ages, uncertainties at the 95% confidence level, and statistical parameters. Error ellipses are at the 1-sigma level. Gray and dashed ellipses represent the xenocrystic cores and outliers determined by t-tests in calculation of the weighted mean ages, respectively. Data points represent ^{208}Pb-corrected ratios. For clarity, data for the Paleoproterozoic xenocrysts in the Bonggilri (sample 150313-3) and Gadaeri (sample 150313-2) granites are not shown.

0.7069. The initial $^{87}Sr/^{86}Sr$ ratios of three samples from the Oryuri, Namsan, and Gigye (alkaline) plutons were not considered in this study, because their high $^{87}Rb/^{86}Sr$ ratios (>10) make the calculation of initial Sr isotopic composition inappropriate. Two samples from the Palgongsan pluton have the highest initial $^{87}Sr/^{86}Sr$ ratios and exceptionally low (≤ -4) $\varepsilon_{Nd}(t)$ values. The other samples have CHUR-like (near "0") or positive $\varepsilon_{Nd}(t)$ values. The alkaline granites have the highest (>+2.8) $\varepsilon_{Nd}(t)$ values. Single-stage Sm-Nd model ages (T_{DM}) calculated by assuming present

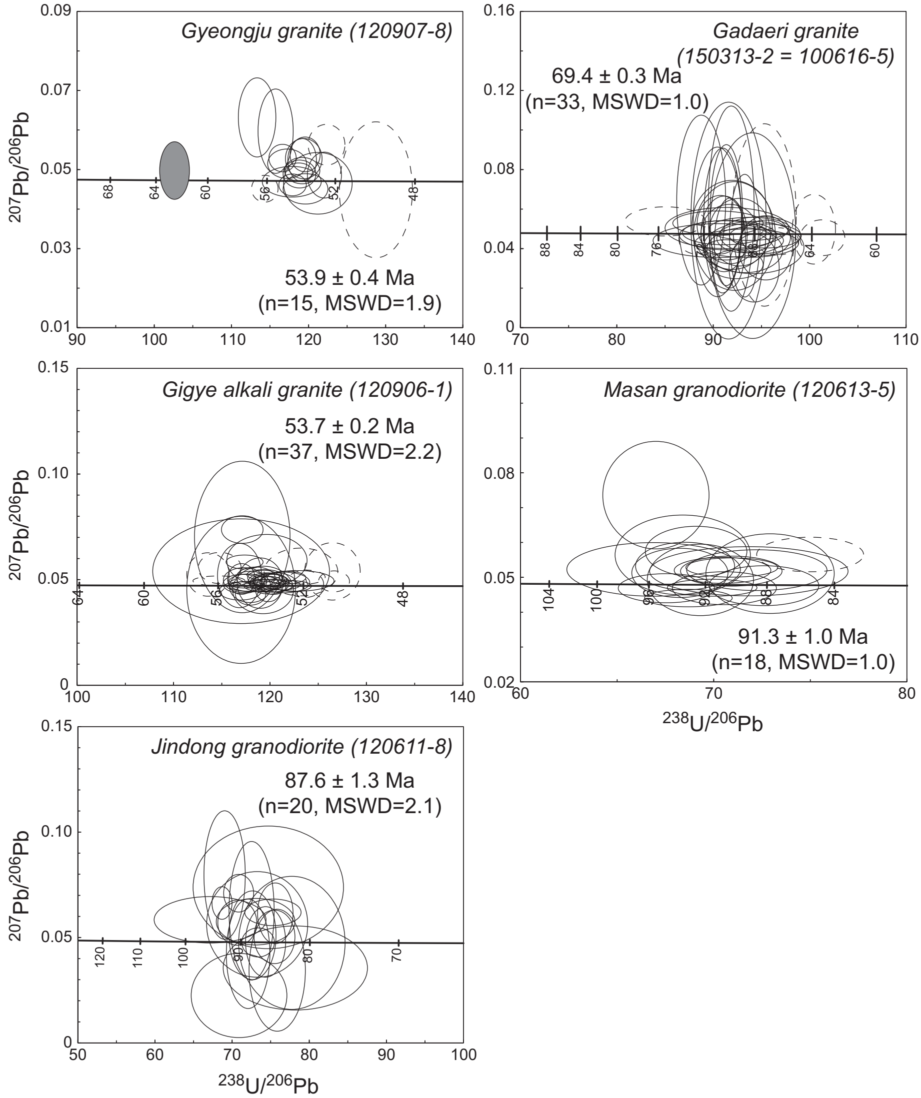

Fig. 4 (continued).

day $^{143}Nd/^{144}Nd$ of 0.51315 and $^{147}Sm/^{144}Nd$ of 0.2137 for the depleted mantle range from *ca.* 1500 to 600 Ma. The range of two-stage model ages (T_{2DM}; Keto and Jacobsen, 1987), when adopting $^{147}Sm/^{144}Nd$ of 0.118 for the average continental crust, are scattered slightly less between *ca.* 1300 and 600 Ma.

Zircon Hf Isotopes

The zircon Lu-Yb-Hf isotopic compositions of the granitoids are given in table 5. Notably, zircon grains from all individual rock samples have variable $\varepsilon_{Hf}(t)$ values, certainly beyond analytical uncertainties. As can be inferred from whole-rock Sr and

Table 3

Whole-rock major and trace element compositions

Sample No.	100617-3	100617-4	100617-1	100617-2	120316-1	100616-2	100616-3	120316-3	120317-1
Locality	Oryuri	Oryuri	Daebonri	Bonggilri	Bonggilri	Bangeojin	Bangeojin	Daejeonri	Seosaeng
Rock type	granite	granite	granite	granodiorite	granite	granite	granite	granite	granite
Major elements (in weight %)									
SiO_2	77.64	77.57	69.22	66.93	69.87	76.78	76.79	68.51	68.59
Al_2O_3	12.58	12.70	14.96	14.85	14.63	12.88	12.82	15.16	14.33
TiO_2	0.12	0.10	0.47	0.56	0.36	0.12	0.15	0.48	0.40
$Fe_2O_3^{total}$	0.45	0.26	3.51	4.47	3.10	0.51	0.43	3.20	3.44
MnO	0.02	0.02	0.12	0.13	0.09	0.04	0.03	0.10	0.07
MgO	0.13	0.06	1.06	1.49	1.17	0.12	0.27	0.82	1.71
CaO	0.30	0.29	2.65	3.36	2.62	0.43	0.63	1.82	3.09
Na_2O	4.18	4.16	4.15	4.13	4.38	3.34	2.93	5.65	3.55
K_2O	4.02	4.38	3.05	3.24	2.93	5.43	5.50	3.24	3.59
P_2O_5	0.02	0.01	0.11	0.12	0.10	0.02	0.03	0.13	0.08
LOI	0.42	0.28	0.52	0.53	0.66	0.21	0.32	0.76	1.04
total	99.88	99.81	99.83	99.81	99.91	99.87	99.90	99.87	99.89
A/CNK	1.07	1.05	1.00	0.90	0.97	1.06	1.08	0.94	0.93
A/NK	1.12	1.10	1.48	1.44	1.41	1.13	1.19	1.18	1.47
Trace elements (in ppm)									
Ba	388	418	485	453	464	115	405	565	542
Sr	18	19	231	258	239	33	162	238	188
Rb	150	150	106	97	103	89	199	61	132
V	3.5	4.2	64	94	43	3.6	9.3	26	67
Cr	1.6	0.5	2.0	5.2	1.1	0.5	3.9	n.d.	12
Ni	6.1	3.7	5.7	5.0	2.7	2.3	2.9	0.8	5.0
Y	31	29	28	29	19	33	21	27	22
Zr	51	58	143	197	211	36	361	426	200
Nb	14	13	13	10	10	21	5.4	35	9.6
Cs	3.6	2.1	3.0	4.5	6.2	2.0	4.1	2.1	5.9
Hf	2.5	2.7	4.5	5.9	6.0	1.9	5.8	10	6.0
Pb	17	15	13	18	8.5	20	13	24	12
Th	11	12	12	7.7	14	13	16	9.1	13
U	2.4	2.2	3.7	2.2	3.6	3.6	3.6	1.9	3.0
La	11	15	26	25	25	10	15	26	15
Ce	25	34	52	51	53	21	31	56	32
Pr	2.87	3.89	5.64	5.82	5.79	2.28	3.24	6.46	3.84
Nd	10.7	14.4	21.7	23.2	21.5	7.9	11.2	24.8	15.4
Sm	2.86	3.44	4.40	4.79	4.01	2.05	2.06	4.82	3.48
Eu	0.32	0.41	0.89	1.00	0.71	0.18	0.36	1.10	0.61
Gd	3.14	3.41	3.97	4.64	3.39	2.38	1.80	4.33	3.18
Tb	0.59	0.62	0.64	0.72	0.53	0.56	0.31	0.70	0.56
Dy	4.39	4.09	4.17	4.46	3.39	4.23	2.07	4.18	3.51
Ho	0.93	0.87	0.85	0.91	0.71	0.95	0.44	0.89	0.75
Er	3.02	2.74	2.62	2.72	2.10	3.05	1.38	2.86	2.31
Tm	0.46	0.42	0.39	0.40	0.33	0.45	0.21	0.43	0.35
Yb	3.27	3.13	2.82	2.73	2.53	3.21	1.58	2.97	2.39
Lu	0.51	0.45	0.44	0.43	0.39	0.43	0.24	0.49	0.37
Σ REE	69	87	126	128	123	59	70	136	84
Eu/Eu*	0.33	0.36	0.65	0.65	0.59	0.25	0.57	0.74	0.56
$(La/Yb)_N$	2.28	3.35	6.23	6.23	6.77	2.18	6.46	6.02	4.16

TABLE 3

(continued)

Sample No.	120315-3	110418-1	120315-4	120907-11	120907-2	120907-8	100616-5	100616-6
Locality	Ocheon	Hoam	Kwonyiri	Namsan	Tohamsan	Gyeongju	Gadaeri	Gadaeri
Rock type	granite	granite	granodiorite	alkali granite	granodiorite	granite	granite	granite
Major elements (in weight %)								
SiO_2	69.23	74.68	67.10	77.33	63.62	76.54	73.20	68.93
Al_2O_3	14.50	13.12	15.75	11.94	17.14	12.74	13.76	15.20
TiO_2	0.38	0.13	0.40	0.05	0.65	0.13	0.31	0.34
$Fe_2O_3^{total}$	2.75	1.25	3.56	1.32	4.80	0.99	2.10	3.40
MnO	0.09	0.06	0.10	0.02	0.09	0.03	0.07	0.08
MgO	1.07	0.41	1.61	0.01	2.01	0.08	0.40	0.48
CaO	2.23	0.76	3.02	0.38	4.48	0.55	0.57	1.61
Na_2O	4.29	4.49	4.68	4.05	4.00	3.40	4.63	5.43
K_2O	3.50	4.28	2.47	4.08	2.06	4.69	4.07	3.45
P_2O_5	0.09	0.02	0.13	0.01	0.18	0.03	0.07	0.08
LOI	1.71	0.63	1.01	0.63	0.76	0.59	0.61	0.79
total	99.84	99.82	99.82	99.82	99.78	99.77	99.78	99.79
A/CNK	0.97	0.98	0.99	1.01	1.01	1.09	1.05	0.97
A/NK	1.34	1.09	1.52	1.08	1.95	1.20	1.14	1.20
Trace elements (in ppm)								
Ba	489	276	589	n.d.	454	349	668	609
Sr	174	62	321	n.d.	428	66	85	195
Rb	97	123	57	n.d.	50	210	112	87
V	41	6.8	55	n.d.	73	3.5	11	7.3
Cr	3.2	1.5	0.6	n.d.	15	0.8	1.4	1.3
Ni	2.1	3.2	1.4	n.d.	22	1.5	19	5.5
Y	19	35	19	n.d.	17	23	41	38
Zr	150	213	180	n.d.	152	139	279	370
Nb	10	23	9.9	n.d.	5.2	6.7	24	23
Cs	3.3	3.0	2.0	n.d.	2.7	3.7	2.3	3.1
Hf	4.4	7.9	5.2	n.d.	4.0	4.5	8.2	9.3
Pb	26	23	8.9	n.d.	13	36	23	17
Th	11	17	8.8	n.d.	5.4	19	12	11
U	3.3	3.5	1.6	n.d.	1.6	4.2	3.1	2.8
La	20	38	22	n.d.	21	42	43	42
Ce	41	80	44	n.d.	45	80	90	85
Pr	4.53	8.75	4.91	n.d.	5.43	8.70	10.28	9.69
Nd	17.3	31.3	18.3	n.d.	21.8	28.7	39.0	37.0
Sm	3.56	6.18	3.43	n.d.	4.33	4.87	7.30	6.89
Eu	0.65	0.30	0.91	n.d.	1.19	0.34	1.05	1.50
Gd	3.04	5.10	3.00	n.d.	3.32	3.23	6.00	5.69
Tb	0.51	0.87	0.49	n.d.	0.48	0.50	0.98	0.91
Dy	3.24	5.43	2.88	n.d.	3.18	3.86	6.33	5.70
Ho	0.67	1.17	0.61	n.d.	0.63	0.80	1.29	1.21
Er	2.12	3.52	1.88	n.d.	1.90	2.48	3.96	3.82
Tm	0.35	0.55	0.28	n.d.	0.26	0.39	0.63	0.57
Yb	2.43	3.74	1.96	n.d.	1.84	2.83	4.34	4.05
Lu	0.37	0.60	0.34	n.d.	0.28	0.42	0.66	0.61
Σ REE	100	185	105		111	178	215	205
Eu/Eu*	0.60	0.16	0.86		0.96	0.26	0.48	0.73
$(La/Yb)_N$	5.70	6.88	7.57		7.89	9.98	6.80	7.10

TABLE 3
(continued)

Sample No.	100616-7	100616-8	120906-1	120906-4	120614-1	120614-4	120613-5	120611-8
Locality	Ijeonri	Ijeonri	Gigye	Gigye	Palgongsan	Palgongsan	Masan	Jindong
Rock type	granite	granodiorite	alkali granite	granite	granite	granodiorite	granodiorite	granodiorite
Major elements (in weight %)								
SiO_2	68.55	66.73	75.96	69.60	71.12	63.40	66.21	64.31
Al_2O_3	14.99	14.88	11.87	15.27	14.58	15.22	15.56	15.39
TiO_2	0.40	0.46	0.09	0.45	0.31	0.57	0.49	0.55
$Fe_2O_3^{total}$	3.38	4.22	2.35	2.71	2.38	3.97	4.83	6.05
MnO	0.06	0.08	0.09	0.09	0.09	0.05	0.09	0.14
MgO	1.27	1.49	0.08	0.63	0.65	2.73	1.77	1.81
CaO	2.80	3.09	0.17	1.80	1.83	3.29	4.07	3.72
Na_2O	3.13	3.09	3.65	4.41	4.08	3.16	3.31	2.97
K_2O	4.18	3.80	4.43	3.67	4.09	5.26	2.78	2.95
P_2O_5	0.09	0.10	0.01	0.14	0.09	0.22	0.10	0.13
LOI	0.99	1.95	1.10	1.03	0.56	1.65	0.67	1.75
total	99.85	99.91	99.81	99.80	99.79	99.54	99.87	99.76
A/CNK	1.02	1.00	1.07	1.05	1.01	0.90	0.98	1.04
A/NK	1.55	1.62	1.10	1.36	1.31	1.40	1.84	1.91
Trace elements (in ppm)								
Ba	679	687	n.d.	n.d.	912	831	565	802
Sr	282	300	n.d.	n.d.	213	349	298	411
Rb	185	162	n.d.	n.d.	118	152	99	78
V	71	87	n.d.	n.d.	20	44	67	74
Cr	11	15	n.d.	n.d.	0.1	5.3	5.0	7.0
Ni	6.6	8.0	n.d.	n.d.	1.2	3.2	3.8	4.2
Y	29	33	n.d.	n.d.	19	18	17	31
Zr	438	438	n.d.	n.d.	252	237	167	221
Nb	4.1	6.8	n.d.	n.d.	7.9	6.8	2.2	4.4
Cs	4.9	6.4	n.d.	n.d.	8.0	6.7	5.2	1.1
Hf	8.4	9.1	n.d.	n.d.	6.1	6.0	4.5	5.9
Pb	11	35	n.d.	n.d.	25	14	5.5	9.4
Th	21	21	n.d.	n.d.	14	13	9.9	11
U	4.3	6.8	n.d.	n.d.	3.3	3.1	2.4	3.0
La	31	43	n.d.	n.d.	42	18	20	31
Ce	69	93	n.d.	n.d.	80	39	43	67
Pr	7.26	9.77	n.d.	n.d.	8.29	4.05	4.74	8.44
Nd	27.1	35.8	n.d.	n.d.	27.8	16.8	18.2	32.8
Sm	5.43	6.82	n.d.	n.d.	4.56	3.72	3.51	6.84
Eu	0.93	1.13	n.d.	n.d.	0.81	0.97	0.84	1.17
Gd	4.83	5.62	n.d.	n.d.	2.92	2.85	2.55	4.92
Tb	0.80	0.92	n.d.	n.d.	0.44	0.43	0.38	0.78
Dy	5.09	5.81	n.d.	n.d.	3.21	3.03	2.78	5.24
Ho	1.07	1.21	n.d.	n.d.	0.69	0.65	0.59	1.11
Er	3.18	3.71	n.d.	n.d.	2.27	2.13	1.79	3.43
Tm	0.48	0.58	n.d.	n.d.	0.35	0.30	0.26	0.50
Yb	3.17	3.78	n.d.	n.d.	2.39	2.13	1.73	3.39
Lu	0.50	0.59	n.d.	n.d.	0.34	0.34	0.28	0.49
Σ REE	160	212			177	95	100	168
Eu/Eu*	0.55	0.55			0.67	0.91	0.86	0.62
$(La/Yb)_N$	6.69	7.77			12.09	5.65	7.67	6.30

LOI; Loss on ignition, A/CNK; molar $Al_2O_3/(CaO+Na_2O+K_2O)$, A/NK; molar $Al_2O_3/(Na_2O+K_2O)$.

ΣREE; Total rare earth element content, Eu* = $(Sm \times Gd)^{0.5}_{chondrite\text{-}normalized}$, $(La/Yb)_N$; chondrite-normalized ratio.

n.d.; not determined.

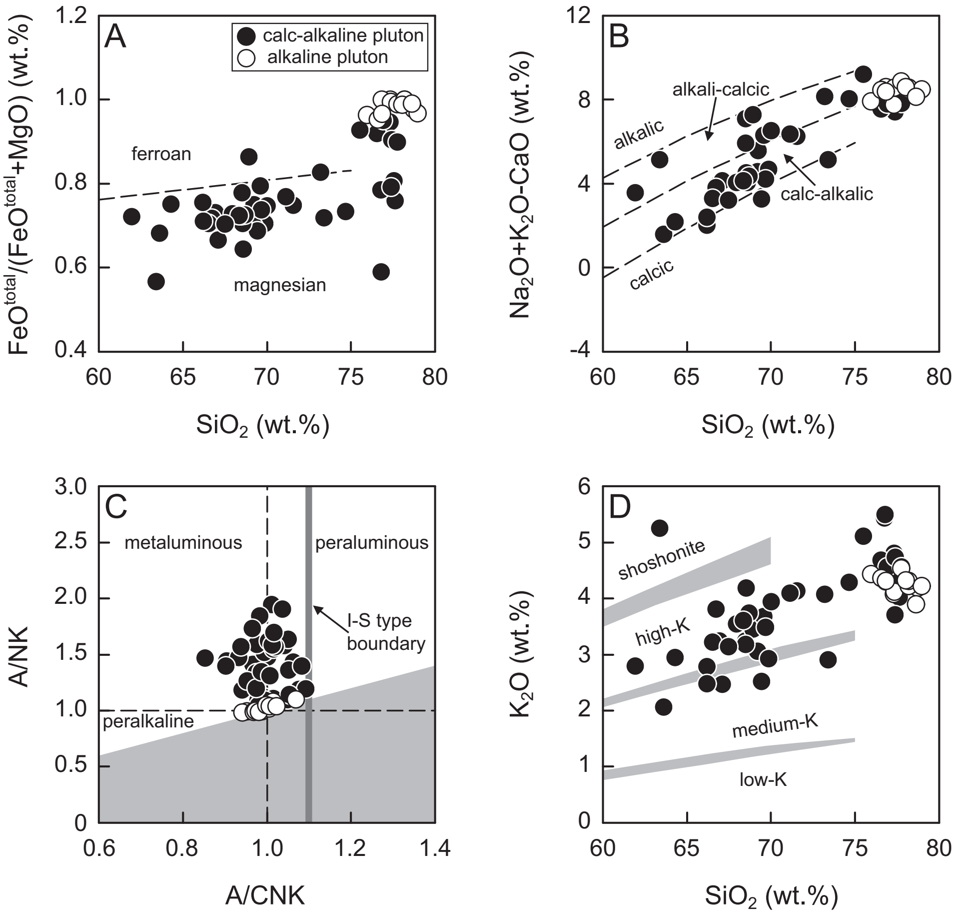

Fig. 5. Major element classification diagrams for the Cretaceous to Paleogene granitoids from the Gyeongsang Arc analyzed in this study and previous works (Kim and Kim, 1997; Cheong and others, 1998; Hwang and others, 2012; Kim and others, 2016). (A) $FeO^{total}/(FeO^{total} + MgO)$ versus SiO_2 plot showing the ranges of ferroan and magnesian fields (Frost and others, 2001). (B) (Na_2O + K_2O − CaO) versus SiO_2 plot showing the ranges of alkalic, alkali-calcic, calc-alkalic and calcic rock fields (Frost and others, 2001). (C) A/NK (molar $Al_2O_3/(Na_2O + K_2O)$) versus A/CNK (molar $Al_2O_3/(CaO + Na_2O + K_2O)$) plot, with the suggested boundary between I- and S-type granites (A/CNK = 1.1; Chappell and White, 1992). (D) K_2O versus SiO_2 plot showing the shoshonite, high-K, medium-K, and low-K series fields (Rickwood, 1989).

Nd data, all zircon grains show positive $\varepsilon_{Hf}(t)$ values, with the exception of some grains from the Palgongsan pluton, which have negative values as low as –5. Some zircon spots from the Gigye alkaline pluton have significantly high $\varepsilon_{Hf}(t)$ (>+17) exceeding the MORB value. The $\varepsilon_{Hf}(t)$ values of Triassic to Jurassic xenocrysts from the Bonggilri and Gadaeri plutons vary between +4.4 and +13.4. The Paleoproterozoic zircon cores from the two plutons have negative $\varepsilon_{Hf}(t)$ values (–1.6 and –4.2). Two-stage Hf model ages of magmatic (that is, not inherited) zircon domains (563 ± 136 Ma; mean ± standard deviation), calculated using the Lu/Hf ratio of average continental crust suggested by Rudnick and Gao (2003), are systematically younger than Nd model ages of their respective host rocks.

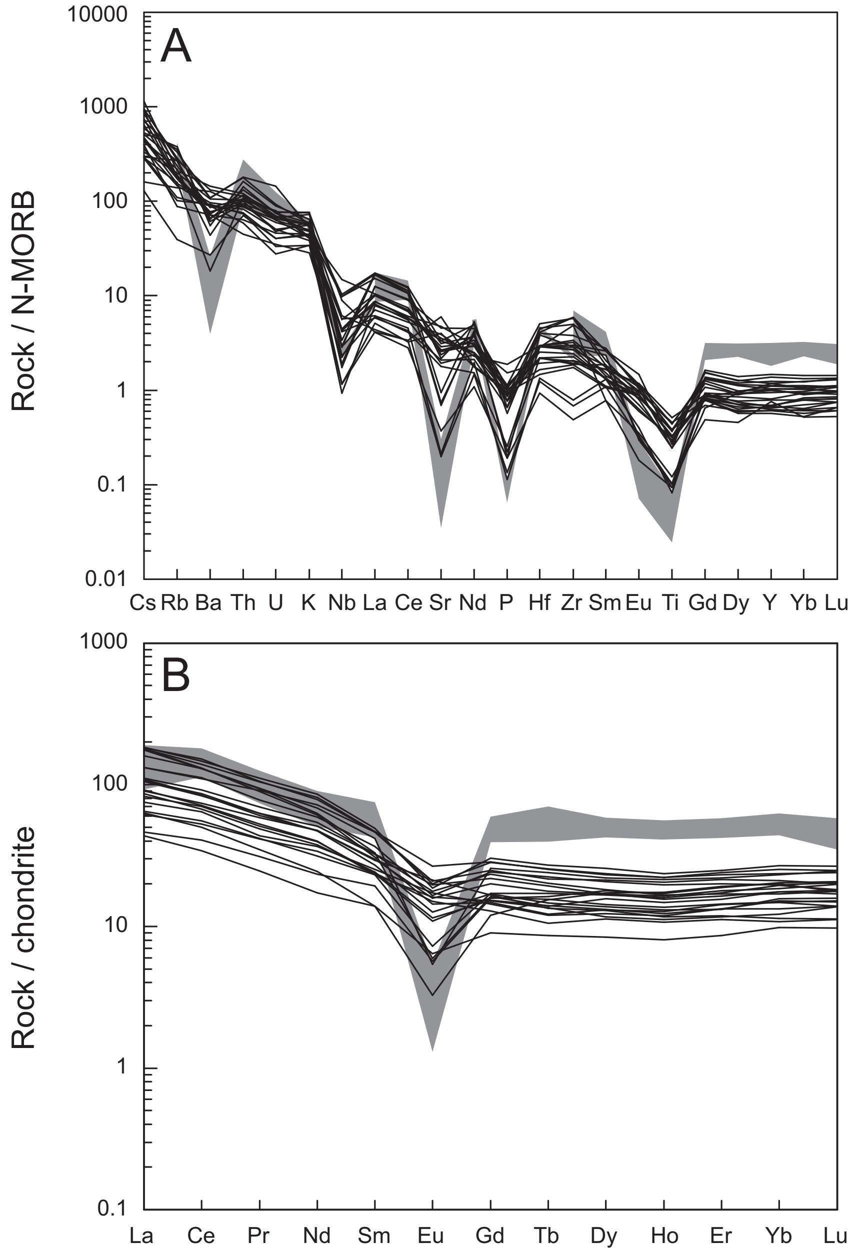

Fig. 6. (A) Normal-mid oceanic ridge basalt (N-MORB)-normalized patterns of the Cretaceous to Paleogene granitoids from the Gyeongsang Arc (Kim and Kim, 1997; Cheong and others, 1998; Hwang and others, 2012; Kim and others, 2016; this study). The N-MORB values are from Sun and McDonough (1989). (B) Chondrite-normalized REE patterns of the granitoids. The chondrite values are from McDonough and Sun (1995). In (A) and (B), the shaded area represents the range of alkaline granites from Namsan and Gigye.

TABLE 4

Whole-rock Rb-Sr and Sm-Nd isotopic compositions

Sample No.	Locality	$\frac{^{87}Rb}{^{86}Sr}$	$\frac{^{87}Sr}{^{86}Sr}$		$\frac{^{87}Sr}{^{86}Sr_{initial}}$	$\frac{^{147}Sm}{^{144}Nd}$	$\frac{^{143}Nd}{^{144}Nd}$		$\varepsilon_{Nd}(t)$	T_{DM} (Ma)	T_{2DM} (Ma)
100617-4	Oryuri	23.0	0.724650	(5)	0.7036*	0.1564	0.512652	(11)	0.61	1322	818
100617-1	Daebonri	1.32	0.706129	(5)	0.7049	0.1246	0.512632	(3)	0.50	886	830
100617-2	Bonggilri	1.08	0.705868	(6)	0.7047	0.1295	0.512692	(2)	1.69	830	739
120316-1	Bonggilri	1.25	0.706068	(5)	0.7047	0.1067	0.512665	(2)	1.38	691	765
100616-3	Bangeojin	3.56	0.707670	(5)	0.7047	0.1133	0.512598	(21)	-0.15	838	877
120316-3	Daejeonri	0.746	0.705008	(5)	0.7045	0.1219	0.512750	(2)	2.64	665	640
120317-1	Seosaeng	2.03	0.707057	(4)	0.7051	0.1398	0.512612	(5)	-0.01	1109	873
120315-3	Ocheon	1.61	0.706364	(4)	0.7049	0.1221	0.512613	(7)	0.14	894	858
110418-1	Hoam	5.71	0.708914	(5)	0.7048	0.1214	0.512683	(5)	1.36	773	747
120315-4	Kwonyiri	0.511	0.704610	(5)	0.7044	0.1146	0.512721	(5)	1.90	660	683
120907-11	Namsan	113	0.783539	(9)	0.6966*	0.1530	0.512774	(2)	2.95	945	619
120907-2	Tohamsan	0.334	0.705249	(7)	0.7050	0.1307	0.512613	(3)	0.00	985	862
120907-8	Gyeongju	9.21	0.711400	(7)	0.7043	0.1048	0.512725	(4)	2.34	595	670
100616-5	Gadaeri	3.80	0.708977	(6)	0.7052	0.1185	0.512589	(3)	-0.26	898	894
100616-7	Ijeonri	1.90	0.706881	(5)	0.7046	0.1282	0.512679	(3)	1.56	840	759
120906-1	Gigye	58.8	0.749312	(6)	0.7041*	0.1567	0.512768	(3)	2.82	1020	630
120906-4	Gigye	1.12	0.706179	(5)	0.7051	0.1136	0.512585	(3)	-0.34	861	898
120614-1	Palgongsan	1.60	0.708175	(7)	0.7065	0.1053	0.512391	(6)	-3.97	1067	1199
120614-4	Palgongsan	1.26	0.708157	(6)	0.7069	0.1359	0.512362	(5)	-4.82	1547	1266
120613-5	Masan	0.958	0.705968	(5)	0.7047	0.1260	0.512641	(4)	0.88	885	818
120611-8	Jindong	0.546	0.705960	(6)	0.7053	0.1295	0.512644	(3)	0.87	916	816

Numbers in parentheses refer to least significant digit and $\pm 2\sigma$ SE.
T_{DM}; single-stage model age, T_{2DM}; two-stage model age. See text for the model parameters.
*These values are not considered in this study because of high (>10) $^{87}Rb/^{86}Sr$.

DISCUSSION

Spatiotemporal Pattern of Zircon Age

In the southern Korean Peninsula, Cretaceous to Paleogene arc magmatism occurred predominantly in its southeastern part after a magmatic lull of approximately 50 Myr between the Late Jurassic to the Early Cretaceous (Sagong and others, 2005; Cheong and Kim, 2012). The initiation of extensive magmatism in the Gyeongsang Arc was heralded by the earliest Late Cretaceous basin-wide eruption of rhyolitic to rhyodacitic ignimbrite that produced the so called Gusandong Tuff (Sohn and others, 2009), although the earlier clues of volcanism, such as volcanogenic plagioclase grains (Noh and Park, 1990) and glass shards and their alteration products (Cheong and Kim, 1996), are observed in the Early Cretaceous sedimentary rocks.

Table 6 lists the available ion microprobe zircon U-Pb ages of Cretaceous to Paleogene granitoids in the Gyeongsang Arc from new analyses presented here and in the literature (Hwang, 2012; Hwang and others, 2012; Zhang and others, 2012; Yi and others, 2012b; Cheong and others, 2013; Jo and others, 2016; Kim and others, 2016). In table 6, the crystallization age of the Ijeonri pluton (86.1 $\pm$ 0.4 Ma) represents a newly calculated weighted mean of two $^{206}Pb/^{238}U$ data sets from Cheong and others (2013) and Jo and others (2016). The intraplutonic consistency of age data is verified by different rock samples of the Bonggilri, Tohamsan, Gadaeri, Gigye, and Jindong plutons. We note that sample number "0316-3" (from Daejeonri pluton) in Cheong and others (2013) should be corrected to "0419-2" (from Tohamsan pluton).

The SHRIMP zircon ages of the Gyeongju, Oryuri, and Namsan plutons are consistently *ca.* 5 Ma older than their respective whole-rock Rb-Sr ages presented in the literature (Kim and others, 1995; Kim and Kim, 1997). This difference seems reasonable,

TABLE 5

Zircon Lu-Yb-Hf isotopic compositions

Spot number*	Date (Ma)*	$^{176}Hf/^{177}Hf$	2σ (ppm)	$^{176}Lu/^{177}Hf$	2σ (%)	$^{176}Yb/^{177}Hf$	2σ (%)	$\varepsilon_{Hf}(t)$	T_{DM} (Ma)	T_{2DM} (Ma)
Oryuri granite (100617-4)										
1.1c	70	0.282901	92	0.0012	3.2	0.0365	3.3	5.9	501	670
1.2r	66	0.282900	99	0.0008	1.6	0.0263	2.2	5.9	497	671
2.1c	63	0.282923	117	0.0024	0.4	0.0732	0.2	6.7	485	630
2.2r	65	0.282942	156	0.0025	1.1	0.0783	1.1	7.3	459	592
5.1c	65	0.282947	99	0.0019	1.8	0.0592	2.0	7.5	444	581
5.2r	65	0.282964	127	0.0035	1.2	0.0980	0.6	8.1	437	551
7.1c		0.282952	117	0.0018	1.0	0.0535	1.3	7.7	435	571
7.2r	63	0.282912	106	0.0023	2.2	0.0687	1.6	6.3	500	651
8.1c		0.282947	110	0.0020	2.6	0.0578	1.9	7.5	444	581
8.2r	65	0.282997	106	0.0023	2.5	0.0700	3.1	9.3	375	482
9.1r	64	0.282968	99	0.0013	0.5	0.0416	1.3	8.3	407	538
10.1r	64	0.282918	127	0.0022	1.1	0.0642	0.5	6.5	489	639
17.2c		0.282948	127	0.0017	1.5	0.0563	1.6	7.6	440	578
17.1r	65	0.283015	131	0.0030	0.5	0.0882	1.1	9.9	354	448
20.1r		0.282968	113	0.0014	1.5	0.0382	0.8	8.3	407	538
Daebonri granite (100617-1)										
2.1c	64	0.282945	117	0.0011	4.5	0.0309	5.2	7.5	437	582
2.2r	66	0.282924	95	0.0015	1.7	0.0431	1.5	6.8	471	625
3.1c		0.282951	110	0.0018	1.9	0.0482	3.1	7.7	436	572
5.1c	66	0.282925	173	0.0046	1.2	0.1390	1.3	6.7	512	630
5.2r	64	0.282939	99	0.0021	2.4	0.0634	2.8	7.3	457	596
8.1c	68	0.282921	110	0.0026	0.9	0.0774	0.9	6.6	491	633
8.2r	63	0.282922	67	0.0008	0.7	0.0207	0.7	6.7	466	627
10.1c	68	0.282950	127	0.0019	1.0	0.0544	1.1	7.7	439	574
10.2r	67	0.282954	92	0.0013	0.3	0.0393	0.6	7.8	426	565
15.1c		0.282785	103	0.0012	2.7	0.0390	2.6	1.9	667	899
15.2r	67	0.282846	106	0.0017	2.0	0.0496	1.2	4.0	587	780
17.1c	69	0.282852	124	0.0025	5.6	0.0765	5.6	4.2	591	770
17.2r	66	0.282939	88	0.0017	0.4	0.0493	0.3	7.3	452	595
19.1r	67	0.282925	110	0.0016	1.3	0.0459	2.0	6.8	471	623
20.2c		0.282841	163	0.0043	3.0	0.1283	2.8	3.7	639	796
20.1r	64	0.282924	124	0.0014	1.0	0.0417	1.1	6.8	471	624
Bonggilri granite (150313-3 = 120316-1)										
12.1c	74	0.282905	163	0.0009	2.0	0.0259	2.3	6.3	491	658
12.2r		0.282934	99	0.0008	4.6	0.0192	3.8	7.3	449	600
13.1ic	206	0.283036	314	0.0033	7.3	0.0919	8.6	13.4	326	363
13.2r		0.283011	173	0.0013	1.6	0.0320	2.3	10.0	344	448
18.1c	74	0.282953	113	0.0009	5.5	0.0227	6.2	8.0	422	562
18.2r		0.282963	88	0.0007	2.1	0.0187	2.8	8.4	407	542
23.1ic	1915	0.281555	146	0.0010	4.9	0.0268	4.9	-1.6	2375	2558
23.2r		0.282947	194	0.0009	2.4	0.0227	2.1	7.8	432	574
26.1ic	214	0.282946	262	0.0021	1.1	0.0685	0.7	10.6	447	530
28.1c	77	0.282958	124	0.0017	3.7	0.0448	4.0	8.1	425	555
28.2r		0.282958	88	0.0007	0.6	0.0185	0.8	8.2	414	552
42.1ic	213	0.282990	127	0.0022	4.6	0.0650	5.7	12.1	383	443
44.1ic	209	0.282955	258	0.0028	4.0	0.0731	4.7	10.7	442	519
44.2r		0.282999	163	0.0009	1.6	0.0214	1.2	9.6	358	471
45.1ic	150	0.282810	813	0.0027	13.6	0.0687	13.5	4.4	656	825
47.1c	77	0.282969	131	0.0010	2.9	0.0257	3.1	8.6	401	531
47.2r		0.282923	95	0.0006	0.5	0.0170	0.4	6.9	462	621
48.1c	78	0.282958	113	0.0016	3.1	0.0449	2.9	8.1	424	554
48.2r		0.282958	102	0.0012	2.2	0.0326	2.8	8.2	419	553
53.1ic	249	0.282929	148	0.0005	2.8	0.0110	3.0	10.9	452	536
62.1ic	206	0.282954	254	0.0021	7.9	0.0547	8.2	10.7	436	517
64.1c	76	0.282953	88	0.0010	3.4	0.0278	2.7	8.0	424	563
64.2r		0.282947	99	0.0011	3.6	0.0265	2.9	7.8	433	575
66.1c		0.282924	92	0.0009	1.8	0.0255	2.1	7.0	465	620

TABLE 5

(continued)

Spot number*	Date (Ma)*	$^{176}Hf/^{177}Hf$	2σ (ppm)	$^{176}Lu/^{177}Hf$	2σ (%)	$^{176}Yb/^{177}Hf$	2σ (%)	$\varepsilon_{Hf}(t)$	T_{DM} (Ma)	T_{2DM} (Ma)
Bonggilri granite (150313-3 = 120316-1)										
66.2r		0.282944	88	0.0007	0.5	0.0183	0.8	7.7	434	580
67.1c		0.282969	187	0.0025	1.6	0.0676	1.2	8.5	419	535
68.2r		0.282950	99	0.0008	0.5	0.0209	1.0	7.9	426	568
69.1c		0.282951	110	0.0013	3.4	0.0337	4.2	7.9	430	567
69.2r		0.282954	95	0.0008	0.6	0.0196	0.9	8.0	420	560
70.1c		0.282977	173	0.0010	3.7	0.0261	3.8	8.8	390	515
70.2r		0.282957	131	0.0012	1.9	0.0287	1.2	8.1	420	555
71.1c		0.282946	117	0.0011	3.1	0.0303	3.6	7.7	435	577
71.2r		0.282980	163	0.0010	3.1	0.0287	3.2	8.9	386	509
72.1c		0.282979	110	0.0009	1.0	0.0269	0.7	8.9	387	511
72.2r		0.282993	124	0.0007	0.3	0.0195	1.5	9.4	365	482
73.1c		0.282943	92	0.0010	1.6	0.0274	1.8	7.6	439	583
73.1r		0.282957	95	0.0010	1.4	0.0256	1.0	8.1	419	555
Bonggilri granodiorite (150313-4 = 100617-2)										
1.1c	75	0.282962	138	0.0016	2.2	0.0430	2.8	8.3	418	547
1.2r		0.282970	102	0.0007	2.0	0.0179	1.3	8.6	397	529
6.1ic	188	0.282929	240	0.0016	5.8	0.0422	5.9	9.5	466	570
6.2r		0.282975	127	0.0009	0.5	0.0222	1.0	8.8	392	519
7.1c	87	0.282956	117	0.0011	2.9	0.0292	2.8	8.1	422	558
7.2r		0.282972	145	0.0007	2.1	0.0174	1.8	8.7	394	524
12.1ic	207	0.282910	389	0.0023	7.4	0.0655	8.5	9.1	502	605
23.1ic	210	0.282977	205	0.0027	7.7	0.0811	8.4	11.5	408	475
23.2ir		0.282969	152	0.0010	7.7	0.0295	8.8	11.4	401	477
23.3r		0.282945	117	0.0007	0.3	0.0186	0.6	7.7	432	578
33.1c	76	0.282917	117	0.0007	5.9	0.0193	6.2	6.7	472	634
33.2r		0.282951	95	0.0008	3.2	0.0211	2.4	7.9	425	567
61.1c		0.282988	138	0.0015	5.4	0.0429	6.1	9.2	380	495
61.2r		0.282990	113	0.0011	3.6	0.0283	4.6	9.3	372	490
62.1c		0.282979	113	0.0011	0.7	0.0304	1.2	8.9	388	512
62.2r		0.282978	102	0.0008	1.5	0.0201	0.5	8.9	387	513
63.1c		0.282961	127	0.0019	5.9	0.0533	6.6	8.2	423	550
63.2r		0.282948	92	0.0008	0.8	0.0198	0.8	7.8	429	572
64.1c		0.282983	102	0.0010	2.3	0.0274	3.0	9.0	382	504
64.2r		0.282973	92	0.0011	0.3	0.0277	0.9	8.7	397	524
65.1c		0.282968	173	0.0019	0.7	0.0527	0.9	8.5	413	536
65.2r		0.282948	113	0.0005	1.7	0.0127	0.9	7.8	426	572
66.1c		0.282970	106	0.0011	3.9	0.0291	4.1	8.6	401	530
66.2r		0.282952	95	0.0010	1.6	0.0271	1.8	7.9	426	565
67.1c		0.282996	110	0.0008	1.2	0.0224	1.7	9.5	362	477
67.2r		0.282964	102	0.0007	1.0	0.0175	0.6	8.4	405	540
68.1c		0.282978	102	0.0008	6.6	0.0215	7.4	8.9	387	513
68.2r		0.282958	85	0.0006	0.2	0.0156	0.4	8.2	413	552
69.1c		0.282991	138	0.0016	1.8	0.0453	2.4	9.3	376	489
69.2r		0.282969	127	0.0018	2.1	0.0507	2.4	8.5	410	533
70.1c		0.283011	110	0.0009	7.2	0.0251	8.4	10.0	341	448
70.2r		0.282974	120	0.0007	2.0	0.0184	1.3	8.7	391	521
Ocheon granite (120315-3)										
1.1c		0.283062	187	0.0015	3.1	0.0396	7.3	11.6	273	351
3.1c		0.283031	138	0.0015	9.6	0.0390	12.6	10.5	317	412
7.2r	66	0.282901	216	0.0016	0.5	0.0454	3.3	5.9	506	671
11.1c	66	0.282936	177	0.0017	2.7	0.0465	3.0	7.2	456	602
11.2r		0.282937	329	0.0018	2.7	0.0515	1.2	7.2	457	600
13.1c	66	0.283062	251	0.0022	8.5	0.0653	11.5	11.6	278	352
13.2r	67	0.282937	99	0.0014	0.9	0.0382	1.4	7.2	451	599
14.1c		0.282992	187	0.0021	10.7	0.0603	13.1	9.1	379	491
17.1r	64	0.283018	173	0.0021	3.6	0.0623	6.4	10.0	342	440
20.1r	64	0.283053	170	0.0019	1.3	0.0506	3.0	11.3	288	369

TABLE 5
(continued)

Spot number*	Date (Ma)*	$^{176}Hf/^{177}Hf$	2σ (ppm)	$^{176}Lu/^{177}Hf$	2σ (%)	$^{176}Yb/^{177}Hf$	2σ (%)	$\varepsilon_{Hf}(t)$	T_{DM} (Ma)	T_{2DM} (Ma)
Ocheon granite (120315-3)										
61.1c		0.282982	102	0.0011	4.8	0.0307	7.5	8.8	384	509
61.2r		0.282914	286	0.0024	8.5	0.0556	4.0	6.4	497	647
62.1		0.282926	173	0.0013	1.9	0.0360	1.0	6.8	467	621
62.2		0.282913	110	0.0016	1.6	0.0423	2.8	6.4	489	647
63.1c		0.282918	134	0.0015	2.9	0.0432	1.2	6.5	480	637
63.2r		0.282938	201	0.0019	6.9	0.0560	7.9	7.2	456	598
64.1c		0.283012	131	0.0018	20.3	0.0540	24.1	9.8	347	451
Tohamsan granodiorite (120907-2)										
1.1c	55	0.282958	152	0.0025	5.1	0.0859	6.1	7.7	435	563
3.1c	57	0.282903	127	0.0021	1.6	0.0649	1.2	5.8	510	671
5.1c	56	0.282929	173	0.0036	3.0	0.1214	3.0	6.7	492	623
5.2r		0.282926	113	0.0014	2.0	0.0455	2.6	6.6	467	624
19.1c		0.282883	156	0.0023	3.2	0.0748	2.9	5.1	543	711
20.1c		0.282905	265	0.0033	3.6	0.1159	1.6	5.8	525	670
20.2r		0.283015	212	0.0021	2.7	0.0655	1.5	9.8	346	449
21.1c		0.282884	177	0.0048	1.2	0.1571	1.2	5.0	581	714
22.1r		0.282919	113	0.0020	3.4	0.0574	2.4	6.4	486	639
28.1c		0.282945	156	0.0038	2.9	0.1193	3.5	7.2	470	591
28.2r		0.282906	110	0.0019	3.2	0.0625	4.0	5.9	504	665
29.1r		0.282955	138	0.0013	1.1	0.0381	1.8	7.7	425	566
30.1c		0.282862	163	0.0042	1.9	0.1339	2.2	4.3	605	757
30.2r		0.282955	120	0.0021	0.5	0.0627	1.6	7.6	434	568
Gyeongju granite (120907-8)										
2.1c	52	0.283114	76	0.0020	0.2	0.0915	0.5	13.2	199	251
2.2r		0.282996	101	0.0026	0.7	0.1239	0.4	9.0	379	488
4.1c	54	0.282937	131	0.0026	0.3	0.1214	0.2	6.9	467	605
4.2r	52	0.283086	79	0.0026	0.7	0.1130	0.4	12.2	246	310
5.1c		0.283054	97	0.0025	0.3	0.1191	0.5	11.1	292	373
5.2r	50	0.282979	81	0.0020	0.2	0.0935	0.4	8.4	397	520
7.1c	55	0.282991	86	0.0033	0.2	0.1387	0.4	8.8	394	500
8.1c	55	0.283128	82	0.0030	0.1	0.1225	0.3	13.6	185	227
8.2r		0.283003	103	0.0041	0.4	0.1358	0.8	9.2	384	478
10.1ic	62	0.282986	84	0.0021	0.2	0.0851	0.3	8.8	389	505
10.2r		0.282922	126	0.0024	0.4	0.0936	0.4	6.4	485	635
11.1c	53	0.283039	63	0.0025	0.1	0.1033	0.2	10.5	315	404
12.1c	54	0.283045	77	0.0022	1.0	0.0931	1.2	10.7	303	391
12.2r	54	0.283042	87	0.0023	0.8	0.0962	0.9	10.6	308	396
Gadaeri granite (150313-2 = 100616-5)										
10.1c	68	0.282877	223	0.0066	2.3	0.2028	2.6	4.9	625	729
10.2r		0.282867	99	0.0008	0.3	0.0226	0.6	4.8	544	735
12.1ic	1878	0.281475	78	0.0002	7.2	0.0050	5.0	-4.2	2432	2669
12.2r		0.282874	99	0.0010	0.3	0.0254	0.8	5.1	536	721
14.1c	63	0.282861	120	0.0015	1.0	0.0403	0.9	4.6	563	748
14.2r		0.282901	88	0.0009	0.2	0.0230	0.4	6.0	496	667
18.1c	70	0.282886	177	0.0009	2.6	0.0240	2.8	5.5	517	697
18.2r		0.282882	148	0.0012	0.5	0.0317	1.1	5.4	528	706
25.1c	68	0.282852	166	0.0012	1.4	0.0347	1.3	4.3	571	765
25.2r		0.282947	163	0.0012	2.3	0.0332	1.2	7.7	435	577
38.1c	70	0.282870	103	0.0012	2.2	0.0316	2.3	4.9	545	729
38.2r		0.282897	117	0.0009	0.4	0.0229	0.7	5.9	501	675
43.1c	70	0.282892	138	0.0019	0.9	0.0537	1.4	5.7	523	688
43.2r		0.282862	145	0.0013	3.7	0.0334	2.6	4.6	557	746
44.1c	67	0.282843	113	0.0012	3.3	0.0332	3.0	4.0	584	783
44.2r		0.282913	124	0.0010	0.9	0.0269	0.6	6.5	481	644
45.1c	70	0.282847	117	0.0014	2.1	0.0384	1.8	4.1	580	776
45.2r		0.282872	106	0.0011	2.1	0.0301	1.8	5.0	540	725
61.1c		0.282844	95	0.0009	3.8	0.0249	3.7	4.0	577	780

Table 5
(continued)

Spot number*	Date (Ma)*	$^{176}Hf/^{177}Hf$	2σ (ppm)	$^{176}Lu/^{177}Hf$	2σ (%)	$^{176}Yb/^{177}Hf$	2σ (%)	$\varepsilon_{Hf}(t)$	T_{DM} (Ma)	T_{2DM} (Ma)
Gadaeri granite (150313-2 = 100616-5)										
61.2r		0.282885	92	0.0011	1.6	0.0285	1.1	5.5	522	699
62.1c		0.282862	113	0.0018	4.0	0.0525	4.6	4.6	566	747
62.2r		0.282891	103	0.0011	1.4	0.0291	0.7	5.7	513	687
63.1c		0.282867	113	0.0014	1.5	0.0374	1.3	4.8	551	736
63.2r		0.282852	110	0.0012	0.7	0.0313	0.4	4.3	570	765
64.1c		0.282787	180	0.0013	5.5	0.0373	5.1	2.0	665	894
64.2r		0.282888	251	0.0016	1.7	0.0447	2.1	5.6	524	695
65.1c		0.282853	145	0.0020	4.6	0.0539	5.4	4.3	581	765
65.2r		0.282859	106	0.0010	1.1	0.0266	0.7	4.6	557	751
66.1c		0.282881	177	0.0016	6.4	0.0455	7.0	5.3	534	708
66.1r		0.282897	226	0.0014	3.1	0.0373	2.5	5.9	508	676
67.1c		0.282867	163	0.0020	4.6	0.0555	4.0	4.8	561	737
67.2r		0.282853	113	0.0015	1.6	0.0418	1.3	4.3	574	764
Gigye alkaline granite (120906-1)										
1.1c	55	0.283235	104	0.0042	0.2	0.2091	0.3	17.4	24	16
2.1c	57	0.283228	138	0.0068	0.8	0.3319	0.9	17.1	37	34
2.2r	55	0.283094	141	0.0067	0.4	0.2912	0.7	12.3	264	303
3.2r	52	0.283013	77	0.0047	1.1	0.1991	1.1	9.5	376	459
4.1c	54	0.283041	75	0.0040	0.8	0.2126	0.8	10.5	326	402
4.2r	53	0.283052	97	0.0066	0.8	0.2632	1.1	10.9	333	384
5.1c	56	0.283053	77	0.0053	0.3	0.2259	0.4	10.9	317	380
6.1c	55	0.283058	77	0.0031	0.7	0.1513	0.5	11.2	291	367
6.2r	53	0.283030	89	0.0051	1.0	0.2156	1.2	10.1	353	426
7.1c	54	0.283024	78	0.0046	0.4	0.2271	0.5	9.9	358	437
7.2r	56	0.283176	90	0.0047	0.7	0.1921	0.5	15.3	117	133
8.1r	55	0.283030	88	0.0069	0.2	0.2840	0.7	10.1	373	430
9.1r	54	0.283096	103	0.0056	0.3	0.2791	0.2	12.5	251	295
10.1r	53	0.282755	118	0.0070	0.0	0.3485	0.2	0.3	839	974
11.1r	54	0.282927	117	0.0070	0.1	0.3467	0.2	6.4	548	633
12.1	52	0.283055	49	0.0004	0.7	0.0246	1.4	11.2	275	367
13.1r	54	0.283242	137	0.0069	0.1	0.3342	0.3	17.6	13	6
14.1r	50	0.283157	139	0.0079	0.2	0.3892	0.2	14.5	163	178
15.1r		0.283069	63	0.0014	2.0	0.0843	0.7	11.6	262	341
Masan granodiorite (120613-5)										
1.1c	93	0.282951	47	0.0014	0.4	0.0503	0.5	8.3	431	561
1.2r	89	0.282971	56	0.0010	0.3	0.0285	0.4	9.0	399	520
2.1c	92	0.282858	59	0.0016	0.3	0.0607	0.3	4.9	568	747
2.2r	90	0.282906	43	0.0009	0.8	0.0281	0.6	6.7	490	649
3.1c	90	0.282963	53	0.0016	0.4	0.0553	0.6	8.6	417	539
3.2r	94	0.283041	70	0.0026	0.3	0.0730	0.7	11.4	311	386
4.1c		0.282949	54	0.0013	0.7	0.0535	0.8	8.2	434	566
4.2r	95	0.282909	53	0.0009	0.9	0.0353	0.9	6.8	485	642
5.1c	91	0.282943	61	0.0014	1.7	0.0523	1.9	8.0	443	577
5.2r	93	0.282961	50	0.0008	0.1	0.0264	0.3	8.6	410	539
6.1c	88	0.282953	59	0.0010	0.6	0.0373	0.7	8.3	424	556
7.1c	93	0.282923	57	0.0013	0.2	0.0474	0.2	7.3	470	617
7.2r	92	0.282944	51	0.0007	0.2	0.0239	0.1	8.0	434	573
8.1c	92	0.282946	56	0.0010	1.2	0.0354	1.1	8.1	434	570
8.2r		0.282921	62	0.0009	0.4	0.0307	0.4	7.2	469	620
9.1c	92	0.282996	80	0.0013	2.1	0.0437	2.8	9.8	366	472
9.2r	90	0.282966	69	0.0010	1.5	0.0323	1.7	8.8	406	531
10.1c	88	0.282993	84	0.0012	3.9	0.0413	4.9	9.7	370	478
11.1c	87	0.282935	67	0.0009	0.9	0.0327	0.7	7.7	448	591
11.1r		0.282967	67	0.0009	0.3	0.0303	0.5	8.9	402	527
12.1c		0.282954	70	0.0013	1.4	0.0491	1.1	8.3	427	556
12.2r		0.282945	51	0.0005	0.2	0.0160	0.4	8.1	429	569
13.1		0.282922	61	0.0011	0.2	0.0429	0.5	7.2	470	618

Table 5

(continued)

Spot number*	Date (Ma)*	$^{176}Hf/^{177}Hf$	2σ (ppm)	$^{176}Lu/^{177}Hf$	2σ (%)	$^{176}Yb/^{177}Hf$	2σ (%)	$\varepsilon_{Hf}(t)$	T_{DM} (Ma)	T_{2DM} (Ma)
Masan granodiorite (120613-5)										
13.2		0.282913	50	0.0006	0.2	0.0207	0.4	6.9	476	635
14.1c		0.282997	87	0.0017	0.3	0.0672	0.6	9.9	368	471
14.2r		0.282950	50	0.0009	0.4	0.0310	0.7	8.2	428	563
15.1c		0.282984	53	0.0010	0.4	0.0332	0.6	9.4	380	495
15.2r		0.282946	53	0.0006	0.1	0.0201	0.1	8.1	430	569
Jindong granodiorite (120611-8)										
1.2r	90	0.282967	136	0.0012	3.5	0.0559	2.1	8.7	407	531
2.1r	83	0.282962	101	0.0005	0.6	0.0257	0.9	8.6	406	539
2.2c	89	0.282897	106	0.0009	0.3	0.0479	0.5	6.3	502	668
3.1c	83	0.282926	92	0.0011	0.4	0.0506	0.4	7.3	464	612
3.2r	94	0.282956	109	0.0011	0.2	0.0489	0.4	8.4	422	552
4.1c	88	0.282962	137	0.0014	0.3	0.0719	0.4	8.6	415	540
4.2r	88	0.282941	108	0.0007	0.8	0.0373	0.9	7.9	438	581
5.1c	87	0.283049	136	0.0030	2.6	0.1617	3.1	11.5	304	374
5.2r	82	0.283042	96	0.0006	0.8	0.0272	0.3	11.4	294	379
6.2r	87	0.282926	105	0.0005	0.4	0.0263	0.6	7.3	456	609
6.3r		0.282997	120	0.0007	0.2	0.0339	0.2	9.8	358	469
7.1c	86	0.282949	97	0.0014	0.4	0.0616	0.4	8.1	433	566
7.2r	93	0.282870	77	0.0006	0.3	0.0278	0.2	5.3	537	721
8.1c	85	0.282867	92	0.0013	0.4	0.0596	0.6	5.2	552	730
8.2r	83	0.282960	80	0.0008	0.3	0.0329	0.4	8.5	412	543
9.1c	86	0.282917	73	0.0010	0.7	0.0422	1.0	7.0	474	628
9.2r	87	0.282966	79	0.0006	0.1	0.0259	0.1	8.7	401	530
10.1c	91	0.283060	101	0.0027	2.7	0.1272	3.1	11.9	285	351
10.2r	87	0.282917	65	0.0007	0.3	0.0259	0.5	7.0	471	627
11.2r	90	0.282906	66	0.0007	0.3	0.0274	0.3	6.6	488	650
11.1c	84	0.282830	76	0.0008	2.3	0.0340	2.4	3.9	596	800

* Spot numbers and dates are taken from table 2.

because the zircon U-Pb system typically has a higher closure temperature than that of the whole-rock Rb-Sr system by about 300 °C (Chiaradia and others, 2013). On the other hand, previous Rb-Sr ages of the Daebonri, Hoam, Masan, and Jindong plutons (Kim and others, 1995; Lee and others, 1995; Wee and others, 2006) randomly deviate from their respective SHRIMP zircon ages by up to 20 Myr. We found that their $^{87}Rb/^{86}Sr$ spreads (0.7–2.3) were much smaller than those in the Gyeongju, Oryuri, and Namsan plutons (> 20). In this case, initial Sr isotopic heterogeneity and/or wall-rock assimilation may have affected sensitively to the apparent Rb-Sr isochron age.

The zircon ages compiled in table 6 range from 91 to 27 Ma, confirming that the magmatic platform of the Gyeongsang Arc has been constructed extensively after deposition of the Gusandong Tuff. In the Gyeongsang Arc, the early Late Cretaceous (Turonian to Coniacian; 93.9–86.3 Ma) zircon ages are yielded only by two plutons in the western part (Masan and Jindong; fig. 2). The subsequent Santonian to Maastrichtian (86.3–66.0 Ma) plutons (Daebonri, Bonggilri, Seosaeng, Gadaeri, Eonyang-Yangsan, Ijeonri, Onjeongri, and Palgongsan) show no particular spatiotemporal trend. The Paleogene plutons (Oryuri, Bangeojin, Daejeonri, Ocheon, Hoam, Kwonyiri, Namsan, Tohamsan, Gyeongju, and Gigye) are distributed selectively in the eastern coastal area, to the east or in the central part of the NNE-trending Yangsan fault system (fig. 2). To our knowledge, the Chattian age of the Kwonyiri pluton (27.1 ± 0.5 Ma) represents the youngest record among mappable granitoid plutons in South Korea. It should be noted that post-Eocene strike-slip movements along the Yangsan fault system

TABLE 6

Summary of ion microprobe zircon U-Pb ages for Cretaceous to Paleogene granitoid plutons in the Gyeongsang Arc, southeastern Korea

Pluton name	Sample number	Zircon crystallization age (Ma)	n	MSWD	Zircon inheritance (Ma)	Source
Oryuri	100617-4	64.6 ± 0.5	20	1.9		this study
Daebonri	100617-1	66.6 ± 0.6	30	4.0		this study
Bonggilri	150313-3 (=120316-1)	74.7 ± 0.6	53	5.4	206–249, 1915	this study
	150313-4 (=100617-2)	74.5 ± 0.6	30	3.6	188–210	this study
Bangeojin	616-3	58.4 ± 0.7	26	3.6	66	Jo and others (2016)
Daejeonri	316-3*	48.0 ± 0.5	26	1.3	75	Jo and others (2016)
Seosaeng	317-1	68.7 ± 0.5	33	2.5		Jo and others (2016)
Ocheon	120315-3	65.6 ± 0.5	19	3.4		this study
Hoam	0418-5	50.8 ± 0.4	15	2.7		Cheong and others (2013)
Kwonyiri	315-4	27.1 ± 0.5	12	1.7	66	Jo and others (2016)
Namsan	907-11	54.4 ± 0.4	17	1.5		Jo and others (2016)
Tohamsan	120907-2	56.8 ± 0.9	16	3.6		this study
	0419-2*	57.5 ± 0.5	16	2.6		Cheong and others (2013)
Gyeongju	120907-8	53.9 ± 0.4	15	1.9	62	this study
Gadaeri	150313-2 (=100616-5)	69.4 ± 0.3	33	1.0	1878	this study
	0616-5	69.3 ± 0.8	24	1.9		Cheong and others (2013)
Eonyang	B-228	73.3 ± 2.0	8	3.7		Hwang (2012)
Eonyang-Yangsan	090616-5	72.4 ± 0.7	14	0.8		Zhang and others (2012)
Ijeonri	616-7	86.1 ± 0.4	20	0.96	262	Jo and others (2016) Cheong and others (2013)
Gigye(alkaline)	120906-1	53.7 ± 0.2	37	2.2		this study
	B-262	53.9 ± 0.3	8	1.5		Hwang and others (2012)
Gigye(calc-alkaline)	906-4	65.8 ± 1.6	14	8.5	202, 1981	Jo and others (2016)
	B-263	65.7 ± 0.7	9	1.46		Hwang and others (2012)
Onjeongri	0423-3	83.4 ± 1.3	14	1.6	1834	Yi and others(2012b)
Palgongsan	614-1	72.2 ± 1.0	15	4.3	169	Jo and others (2016)
Masan	120613-5	91.3 ± 1.0	18	1.0		this study
Jindong	120611-8	87.6 ± 1.3	20	2.1		this study
	MS-1	90.3 ± 1.3	14	1.2		Kim and others (2016)

* Sample number "0316-3" in Cheong and others (2013) should be corrected to "0419-2".

have displaced the original emplacement positions of some plutons by more than 20 km (Hwang and others, 2007). Therefore, although it is evident that the Cretaceous granitoids in the Gyeongsang Arc are consistently younger than those in the northern and central parts of the Korean Peninsula, which are mostly Albian to Cenomanian (113–93.9 Ma) in zircon U-Pb age (Wu and others, 2007; Kim and others, 2012; Yi and others, 2014), the along-arc age pattern of Turonian-Maastrichtian plutons remains unclear.

The SHRIMP dates of xenocrystic zircon cores from the Gyeongsang granitoids represent either the earlier episodes of Cretaceous-Paleogene arc magmatism or the older Paleoproterozoic and Permian to Jurassic events probably related to the buildup and remobilization of the crustal basement (that is, Cheong and others, 2013).

Crustal Reworking and Rejuvenation in the Gyeongsang Arc System

The presence of xenocrystic zircon cores (fig. 3, table 6), as well as dominantly high-K calc-alkaline composition (fig. 5D), Ti and Nb negative troughs in the spider diagram (fig. 6A), and prominent Eu negative anomalies (fig. 6B) of whole-rock samples, suggests the involvement of crustal materials in the formation of granitoid rocks composing the Gyeongsang Arc. The LREE enrichment and flat or concave patterns in the MREE-HREE region of the normalized diagram (fig. 6B) indicate that the source residue was rich in amphibole, which preferentially incorporates MREEs and HREEs rather than LREEs in andesitic and rhyolitic melts (Rollinson, 1993). In addition, the presence of feldspar in the source residue is evidenced by negative troughs in Ba and Sr and conspicuous Eu negative anomalies displayed by almost all samples (figs. 6A and 6B). On the other hand, these REE trends clearly negate the presence of garnet in the residue, and are thus indicative of relatively shallow melting (depth $<$ *ca.* 30km; see Qian and Hermann, 2013 and references therein). Recently, Jo and others (2016) provided compelling evidence for the involvement of upper crustal rocks into the shallow magma system within the Gyeongsang Arc. The authors found that single magmatic zircon crystals became progressively enriched in the light oxygen isotope toward their rims, in granite samples from the Daejeonri, Namsan, Ijeonri, and Gigye (calc-alkaline) plutons that contain biotite enriched in the heavy magnesium isotope. Such concomitant isotopic variation can be explained by the involvement of weathered surface rocks that experienced hydrothermal alteration after crystallization of the zircon core. This situation would have been best achieved through assimilation of roof rocks around the volcanic center, which is conventionally referred to as "crustal cannibalization" (Valley, 2003; Bindeman, 2008).

Figure 7 illustrates the available whole-rock Sr and Nd isotopic data of the granitoid plutons located within the Gyeongsang Arc System from the present analyses and the literature (Kim and others, 1995; Lee and others, 1995, 2014; Kim and Kim, 1997; Cheong and others, 1998, 2002; Wee and others, 2006; Yi and others, 2012a). In figure 7A, the initial ε_{Nd} values show the expected negative correlation with initial Sr ratios. The initial Sr ratios of the Eocene alkaline granites cannot be calculated precisely due to their extremely high $^{87}Rb/^{86}Sr$ ratios (58 – 221), and are therefore not shown in this figure. The ε_{Nd} values are plotted against zircon crystallization ages in figure 7B. Most samples have positive $\varepsilon_{Nd}(t)$ values regardless of their age. This is in sharp contrast to the significantly negative $\varepsilon_{Nd}(t)$ values (*ca.* –20 to –10) of Mesozoic granitoids in the central Korean Peninsula, outside of the Gyeongsang backarc basin (Cheong and Chang, 1997; Chough and others, 2000; Lee and others, 2010; Kim and others, 2011). As shown in figure 7B, the Permian to Jurassic granitoids from Yeongdeok and Pohang within the Gyeongsang Arc area (see fig. 2 for location) have $\varepsilon_{Nd}(t)$ values that plot marginally above the average crustal line projected from the mean two-stage Nd model age of the Cretaceous-Paleogene granitoids (=833 Ma). This approximate correspondence implies a common origin of Phanerozoic granitoids in the Gyeongsang Arc. We also note the adakitic geochemical signatures of the latest Permian (*ca.* 253 Ma) Yeongdeok pluton, such as the significantly high La/Yb (38 – 115) and Sr/Y ratios (138 – 214), intermediate to felsic composition (SiO_2 = 63 – 72 wt.%), and weak or no Eu anomalies (Eu/Eu^* = 0.92 – 1.31) (Cheong and others, 2002; Yi and others, 2012a). The intrusion of Yeongdeok adakite represents the addition of new mantle material via slab melting and consequent crustal growth. Approximately coeval (262 – 252 Ma) SHRIMP zircon ages were yielded by granites and gabbros recovered from a drill core (*ca.* 2700 – 3400 m in depth) in Pohang (Lee and others, 2014), suggesting that Late Permian granitoids comprise the upper part of arc basement. Based on the Nd isotopic range, these Permian granitoids could be considered as candidate source materials of the Late Cretaceous granitoids. Bulk isotopic data, however, provide limited information about the source and process because whole-rock samples are the end product of magmatic evolution and therefore only represent the average composition of the involved source materials. On the other

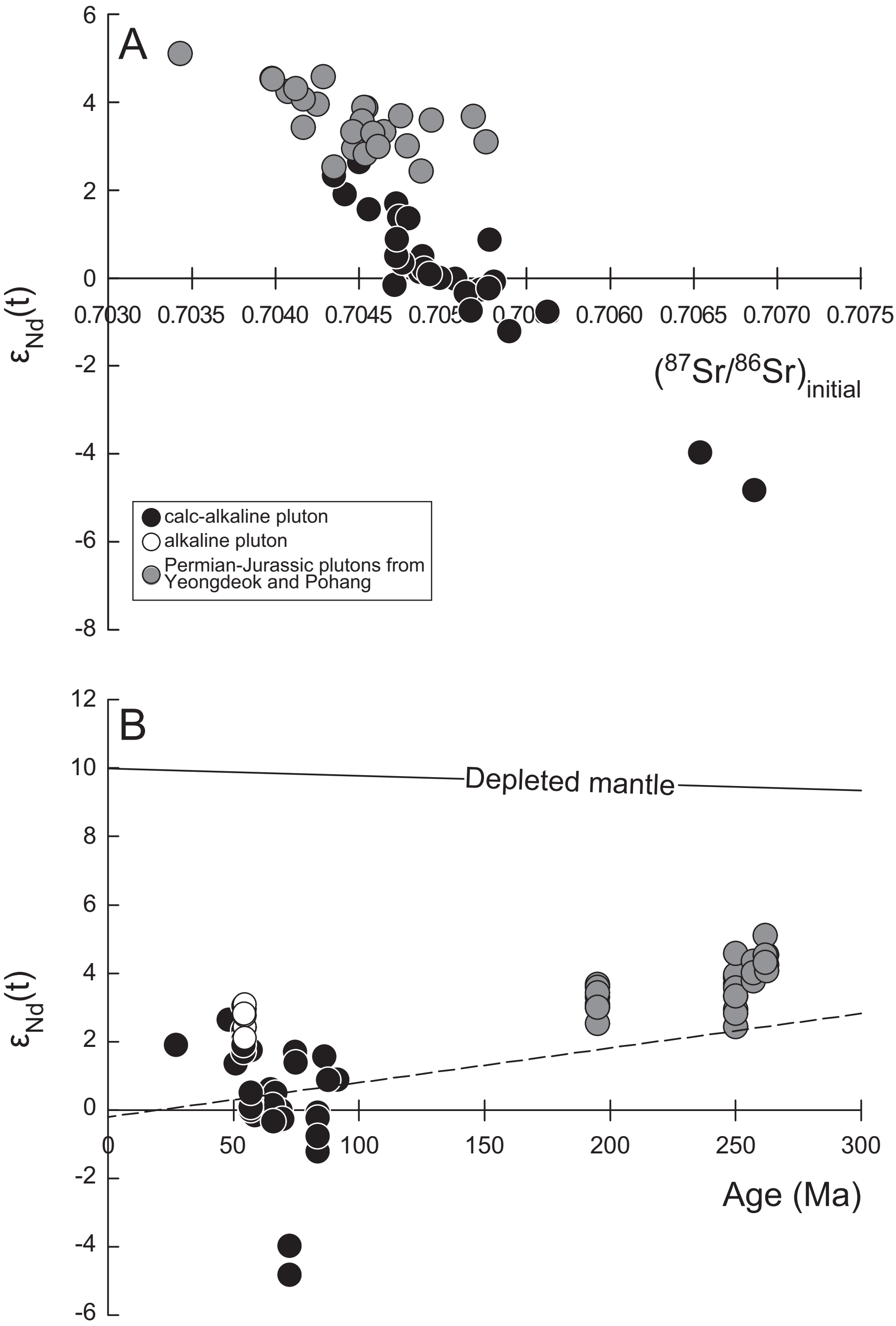

Fig. 7. (A) Initial $^{87}Sr/^{86}Sr$ versus initial ε_{Nd} for the Phanerozoic plutons in the Gyeongsang Arc area. (B) Plot of ε_{Nd} versus zircon crystallization ages. The evolutionary path of the depleted mantle is based on present day $^{143}Nd/^{144}Nd$ of 0.51315 and $^{147}Sm/^{144}Nd$ of 0.2137. The dashed line represents the evolutionary path of average continental crust ($^{147}Sm/^{144}Nd$ = 0.118) projected from the mean two-stage Nd model age of Cretaceous-Paleogene granitoids (=833 Ma). Data sources: Kim and others, 1995; Lee and others, 1995, 2014; Kim and Kim, 1997; Cheong and others, 1998, 2002; Wee and others, 2006; Yi and others, 2012a; this study.

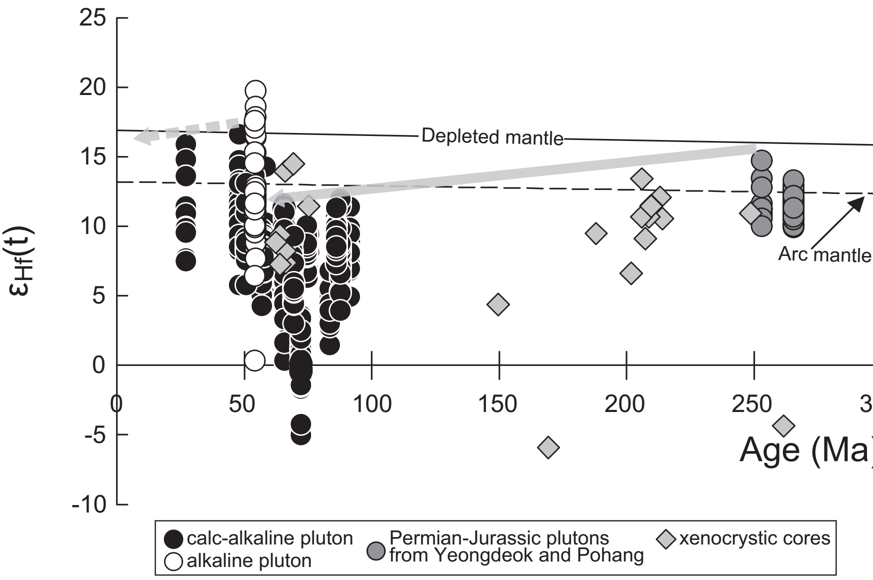

Fig. 8. Plot of zircon ε_{Hf} versus crystallization ages. The evolutionary path of the depleted mantle is based on $^{176}Hf/^{177}Hf$ and $^{176}Lu/^{177}Hf$ ratios from Griffin and others (2000). The evolution line of "arc mantle" (Dhuime and others, 2011) is also shown for reference. The arrowed solid line represents the evolutionary path of the Paleozoic basement beneath the Gyeongsang Arc. After the early Eocene rejuvenation, the basement path followed the arrowed dashed line (see text). It should be noted that there are significantly negative zircon ε_{Hf} values of Precambrian basement rocks in the adjacent Yeongnam Massif (Kim and others, 2014) and Jurassic granitoids in central Korea (Cheong and others, 2013) that plot beyond the range of the y axis in this diagram. Data sources: Cheong and others, 2013; Jo and others, 2016; this study.

hand, the laser ablation system affords sufficient spatial resolution to trace subgrain Hf isotopic variation across different zircon domains that grew independently from one another. Furthermore, zircon Hf isotopes provide a more complete record of the nature of the source by virtue of sluggish diffusion in the crystal lattice (Cherniak and others, 1997) and negligible *in situ* radiogenic growth.

Zircon Hf isotopic data from the present work and our previous studies (Cheong and others, 2013; Jo and others, 2016) are plotted in figure 8 as a function of crystallization age. Paleoproterozoic xenocryst data from the Bonggilri, Gadaeri, and Gigye (calc-alkaline) plutons are not shown in this figure for clarity. The general trend of Hf data is the same as that shown by Nd data but zircon spots from magmatic domains that represent the crystallization age of each pluton show significant spreads in initial ε_{Hf}, clearly outside analytical uncertainties (= *ca.* ± 1 unit at 2 sigma standard error). This internal variation attests to the interaction between primitive melts and pre-existing crustal materials during the crystallization of zircon. Figure 9 displays the core-to-rim variations of ε_{Hf} values for the magmatic grains. Isotopically opposite trends commonly observed in the zircon grains preclude a simple progressive magmatic evolution. It is evident that most grains have been grown by repeated interactions of magma with more primitive melts and pre-existing crustal materials. In this case, whole-rock Nd isotopes merely provide the average crustal residence time of involved source materials (Arndt and Goldstein, 1987). This can be resolved by examining subgrain Hf isotope data.

It is noteworthy that the line connecting the upper parts of $\varepsilon_{Hf}(t)$ values for magmatic zircon domains and xenocrystic cores from the Late Cretaceous plutons in figure 8 (arrowed solid line) converges toward zircon $\varepsilon_{Hf}(t)$ of the Yeongdeok pluton,

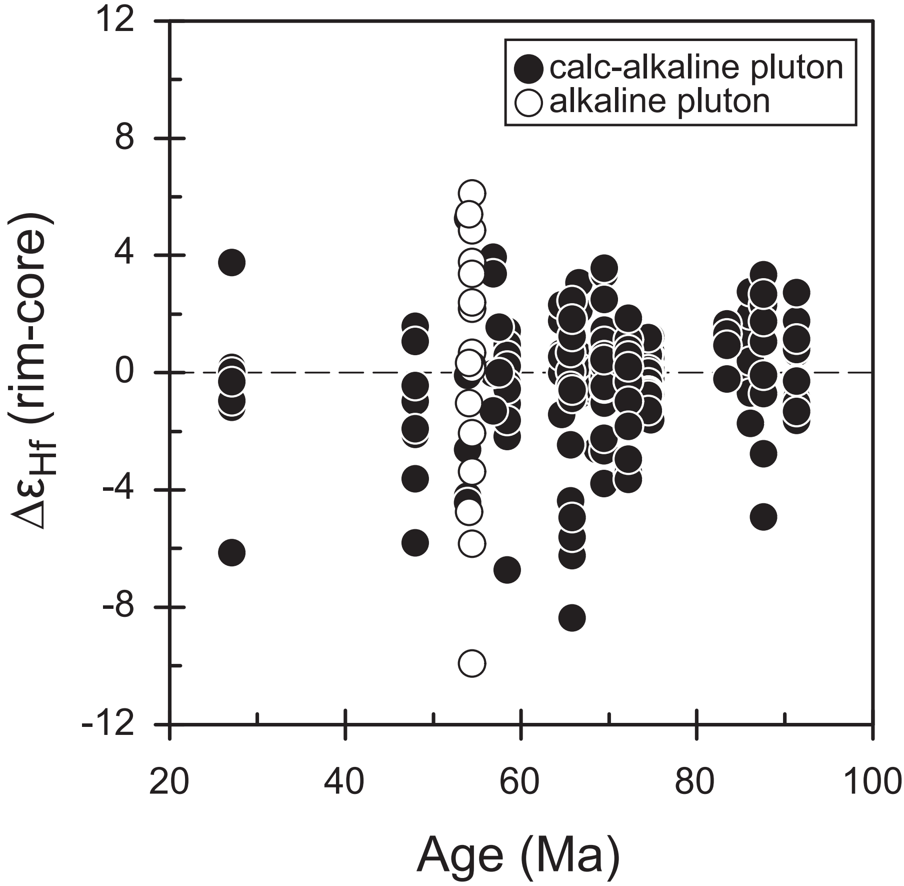

Fig. 9. Core-to-rim variations of magmatic zircon grains from the granitoids. The $\Delta\varepsilon_{Hf}$ (rim-core) values are plotted against the crystallization age. Data sources: Cheong and others, 2013; Jo and others, 2016; this study.

with a slope consistent with the Lu/Hf ratio of typical continental crust (= *ca.* 0.08; Rudnick and Gao, 2003). We interpret this line as representing the evolutionary path of juvenile Paleozoic basement involved in the Gyeongsang granitoids. The crustal residence time of such a young basement is estimated to be *ca.* 360 Myr, assuming its separation from the depleted mantle represented by the MORB data. Recently, Dhuime and others (2011) suggested that the model ages of continental crust formation should be calculated relative to the isotopic composition of new crust represented by island arc rocks. The authors introduced the evolution line of the new continental crust (or "arc mantle"; Arndt, 2013) projecting from the present-day Hf isotopic composition of island arc rocks (weighted average ε_{Hf} = 13.2 ± 1.1). Interestingly, this model line intersects with the evolutionary path of the young basement approximately at the intrusion age of the Yeongdeok adakite (fig. 8). This correspondence implies that the melting of subducting oceanic lithosphere could be considered as one important mechanism to produce new juvenile crust. The Silurian-Devonian magmatism recorded in detrital zircons from Andong, located close to the Gyeongsang Arc area (fig. 2), may also represent the production of Paleozoic arc basement (Cheong and others, 2015). The wide Hf isotopic variation of the detrital zircon (*ca.* +6 to –18; Cheong and others, 2015) suggests an extensive interaction between primitive magma and pre-existing crustal materials during arc magmatism.

The involvement of isotopically enriched source materials in the Gyeongsang granitoids is indicated by the presence of Paleoproterozoic and Jurassic xenocrysts (table 6) and a significant drop of ε_{Hf} in plutons proximal to the basin boundaries (Onjeongri and Palgongsan plutons; see fig. 2). Such enriched reservoirs could be easily identified as Precambrian basement rocks and Jurassic granitoids that are widespread in adjacent areas to the north and west of the Gyeongsang backarc basin. Highly negative ε_{Hf} values were reported from zircon grains in Paleoproterozoic (meta)granitoids and metasedimentary rocks in the Yeongnam Massif (average ± standard deviation = –52 ± 8, T_{2DM} = 2889 ± 303 Ma; Kim and others, 2014) and Middle Jurassic granitoids in the central Korean Peninsula (average ± standard deviation = –22 ± 3, T_{2DM} = 2079 ± 167 Ma; Cheong and others, 2013). We conclude that the Late Cretaceous granitoids in the Gyeongsang Arc are a mixing product between the juvenile Paleozoic basement and isotopically enriched Precambrian rocks (or their Mesozoic derivatives). They are not "juvenile" (*sensu stricto*) despite their mostly positive epsilon Nd and Hf values but are basically a reworking product of pre-existing crustal materials.

Some zircon grains from the Namsan and Gigye plutons show ε_{Hf} values sufficiently higher than the depleted mantle value. This asthenospheric signal is not identified in the other plutons in the Gyeongsang Arc. The extension-related geochemistry and highly primitive Nd-Hf isotopic signatures of the two alkaline plutons suggest that the upwelling asthenosphere in the backarc side finally participated significantly in the generation of A-type magma in the early Eocene. Subsequent reworking of such a "rejuvenated" crustal basement yielded granitoid plutons (that is, Daejeonri, Hoam, and Kwonyiri plutons) that have slightly, but recognizably higher ε_{Hf} (and ε_{Nd}) values than the older plutons (see the arrowed dashed line in fig. 8). In summary, the young basement beneath the Gyeongsang Arc was formed most likely in the Paleozoic through subduction zone processes including the melting of descending oceanic lithosphere, and rejuvenated in the early Eocene by the asthenospheric invasion in the backarc side. Repeated reworking of such a young basement and the Precambrian crust (and its derivatives) produced the Cretaceous-Paleogene granitoids in the Gyeongsang Arc System.

Comparison with Southwest Japan and Southeastern China

The continental side of the Median Tectonic Line (= Inner Zone) in Southwest Japan is further divided into three zones (Sanin, Sanyo, and Ryoke Belts; fig. 1) based on granite petrography and emplacement age (Murakami, 1974). Recently, the younging trend of granite ages from the Pacific side (Ryoke Belt) to the continental side (Sanin Belt) was verified by comprehensive zircon U-Pb dating that yielded Late Cretaceous to Eocene ages (93–33 Ma; Iida and others, 2015). Such continentward migration could be caused by flat slab subduction or tectonic erosion possibly associated with ridge subduction (Maruyama and others, 1996). The latter possibility is supported by contrasting age patterns of detrital zircons from Cretaceous accretionary complexes and their high pressure equivalents in Southwest Japan (Isozaki and others, 2010; Aoki and others, 2012). Regardless, this Andean-type advancing accretionary system induces coupling between the overriding and subducting plates and consequent development of foreland fold and thrust belts (Cawood and others, 2009).

It is worthwhile to note that Early Cretaceous (>100 Ma) zircon ages are reported for granitoids from central Korea and southeastern China but not within the Gyeongsang Arc and Southwest Japan. Zircon ages compiled by Li and others (2014) reveal that extension-related A-type magmatism initiated in Fujian province, southeastern China at *ca.* 125 to 119 Ma. Although no particular spatiotemporal trends were recognized in the zircon ages of the Cretaceous granitoids, A-type magmatism and subsequent bimodal igneous activities indicate that the southeastern margin of South China was chiefly governed by the retreating-type accretionary system during the Early Cretaceous. Such an extensional setting may have been induced by break-off and rollback of the subducting paleo-Pacific plate associated with the delamination of flat slabs (Li and Li, 2007; Li and others, 2012b, 2014; Zhu and others, 2014). The selective occurrence of the Early Cretaceous granitoids in central Korea, and the inland-directed increasing trend of U-Pb ages found in Cretaceous detrital zircons from modern river sediments in South Korea (Choi and others, 2012) suggest that the Korean Peninsula was also under an overall extensional or transtensional stress regime during the late Early Cretaceous.

The continentward younging trend of Late Cretaceous granitoids from Southwest Japan (Iida and others, 2015), as well as the age patterns of detrital zircons (Isozaki and others, 2010; Aoki and others, 2012), suggests a compressional arc setting and crustal thickening that may have focused in the more softened backarc area, represented by the Gyeongsang Basin. This apparently contradicts the absence of prominent syndepositional folds and thrusts in the Gyeongsang backarc basin (Chough and Sohn, 2010) but is consistent with the geometric model of conjugate faulting that indicates a compressional stress regime (Hwang and others, 2008). It should be noted again that the original age pattern of Late Cretaceous granitoids within the Gyeongsang Arc was disturbed by strike-slip movements along the Yangsan fault system (Hwang and others, 2007, 2008).

Figure 10 shows a comparison of whole-rock Sr-Nd and zircon Hf isotopic compositions of the Gyeongsang granitoids with literature data from Southwest Japan (Jahn, 2010 and references therein; Imaoka and others, 2011) and Fujian province (Chen and others, 2014; Li and others, 2014 and references therein; Li and others, 2015). As can be seen in this figure, the Cretaceous granitoids from the Gyeongsang Arc have slightly, but recognizably more primitive Sr-Nd-Hf isotopic compositions than those from the two adjacent terranes. Granitoids from Southwest Japan and Fujian province are similar in their Sr-Nd isotopic ranges, as reported by Jahn (2010). He advocated the longstanding idea that proto-Japan was initially developed along the southeastern margin of the South China Block (Maruyama and others, 1997; Isozaki and others, 2010), based on the unexpectedly crust-like Sr-Nd isotopic signatures of granitoids from Southwest Japan. Jahn's research group also suggested a tectonic correlation between Southwest Japan and Sikhote-Alin in the Russian Far East (Jahn and others, 2015) because granitoids from the two regions show Sr-Nd isotopic similarities. The relatively more primitive Sr-Nd-Hf isotopic compositions of Late Cretaceous granitoids from the Gyeongsang Arc cannot be ascribed to the selective involvement of the mantle component, because their zircon Hf isotopic compositions principally represent the evolution of the Paleozoic basement beneath the arc system (see fig. 8). Instead, these isotopic contrasts may reflect the differences in the formation age of the basement on which the arc system was built. This raises questions about the current view that the Gyeongsang Arc was a simple southwestward extension of the Japanese arc (Chough and Sohn, 2010), but the possibility of intra-arc variation cannot be excluded considering the relatively small isotopic differences.

CONCLUDING REMARKS

This study highlights the potential of *in situ* subgrain Hf isotope data of zircon to resolve source components of granitoids generated in young and juvenile arc systems. Using zircon Hf isotopes, we identified three important sources involved in the Cretaceous-Paleogene granitoids in the Gyeongsang Arc; the Paleozoic basement, the asthenospheric mantle, and the Precambrian basement (or its Mesozoic derivatives). Zircon Hf isotopes indicate that the Gyeongsang granitoids are principally a product of

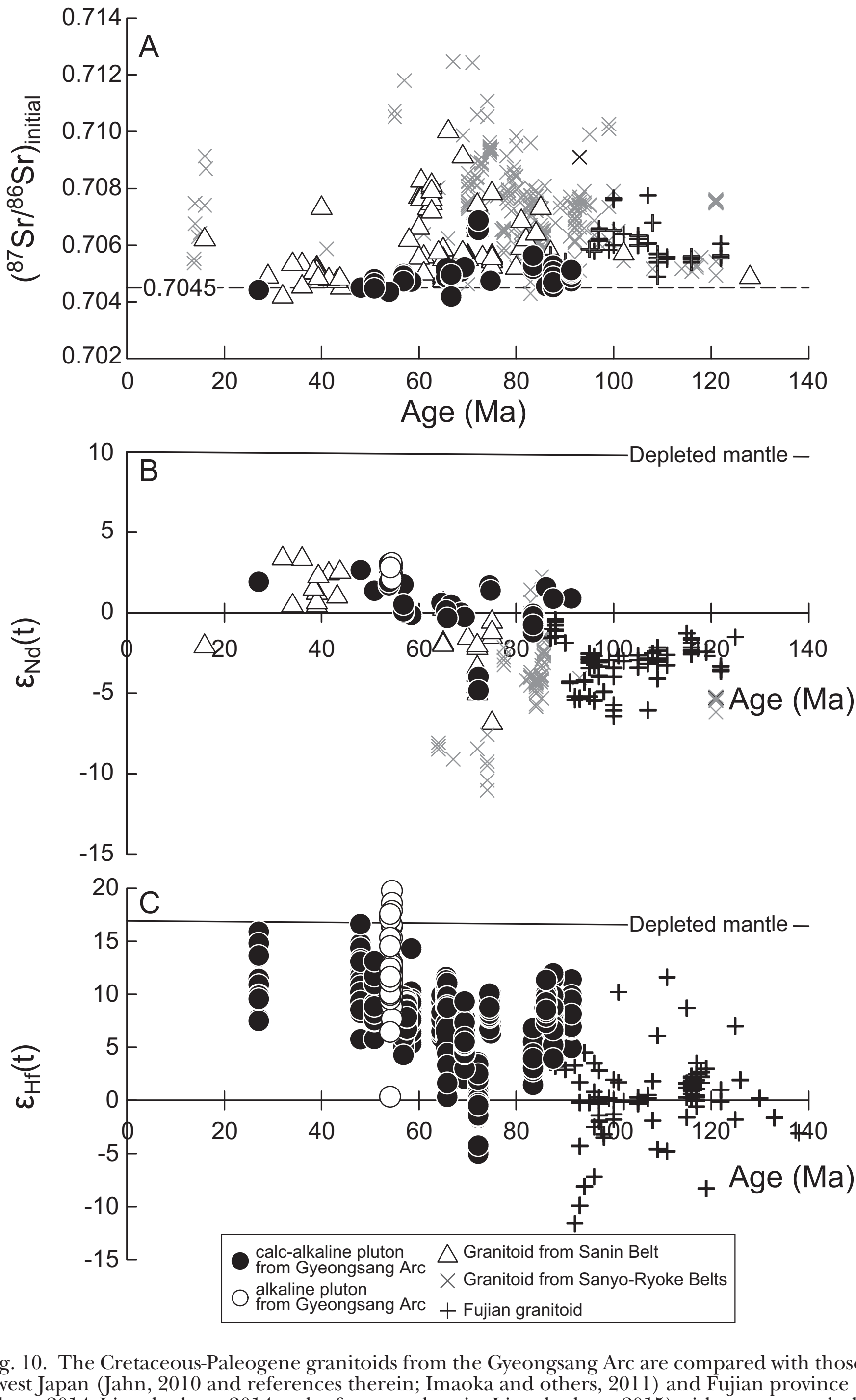

Fig. 10. The Cretaceous-Paleogene granitoids from the Gyeongsang Arc are compared with those from Southwest Japan (Jahn, 2010 and references therein; Imaoka and others, 2011) and Fujian province (Chen and others, 2014; Li and others, 2014 and references therein; Li and others, 2015) with respect to whole-rock initial $^{87}Sr/^{86}Sr$ ratios (A), $\varepsilon_{Nd}(t)$ values (B), and zircon $\varepsilon_{Hf}(t)$ values (C). For clarity, data for the xenocrystic zircon cores are not shown in (C).

crustal reworking. Such information cannot be obtained easily from whole-rock isotope data. The Sr-Nd-Hf isotopic contrasts of the Late Cretaceous granitoids between the Gyeongsang Arc and adjacent accretionary systems in Southwest Japan and southeastern China reflect differences in the formation age of the basement involved in the arc magmatism.

ACKNOWLEDGMENTS

This article is dedicated to the memory of the late Professor Bor-ming Jahn (1940-2016). He devoted his entire career to the basic understanding of the formation and evolution of the continental crust. Namhoon Kim, Keewook Yi, Youn-Joong Jeong, Tae-Ho Lee, and Chan-Soo Park are acknowledged for their help in sample collection and analytical work. We also acknowledge the gracious hospitality we received from Huai-kun Li and Jian-zhen Geng (Tianjin) during zircon Hf analysis in 2014. Constructive comments and corrections from Peter Cawood, Sung-Tack Kwon, and an anonymous reviewer are gratefully appreciated. This work was supported by the Korea Basic Science Institute grant (T36414) and the National Research Foundation of Korea (NRF) grant funded by the Korea government (MSIP) (2016R1A2B4007283) to A.C.S. Cheong.

REFERENCES

Anderson, J. L., editor, 1990, The Nature and Origin of Cordilleran Magmatism: Geological Society of America Memoirs, v. 174, 405 p.

Aoki, K., Isozaki, Y., Yamamoto, S., Maki, K., Yokoyama, T., and Hirata, T., 2012, Tectonic erosion in a Pacific-type orogen: Detrital zircon response to Cretaceous tectonics in Japan: Geology, v. 40, n. 12, p. 1087–1090, https://doi.org/10.1130/G33414.1

Armstrong, R. L., 1988, Mesozoic and early Cenozoic magmatic evolution of the Canadian Cordillera: Geological Society of America Special Papers, v. 218, p. 55–92, https://doi.org/10.1130/SPE218-p55

Arndt, N. T., 2013, Formation and evolution of the continental crust: Geochemical Perspectives, v. 2, n. 3, p. 405–533, https://doi.org/10.7185/geochempersp.2.3

Arndt, N. T., and Goldstein, S. L., 1987, Use and abuse of crust-formation ages: Geology, v. 15, n. 10, p. 893–895, https://doi.org/10.1130/0091-7613(1987)15<893:UAAOCA>2.0.CO;2

Barton, M. D., 1996, Granitic magmatism and metallogeny of southwestern North America: Geological Society of America Special Papers, v. 315, p. 261–280, https://doi.org/10.1130/0-8137-2315-9.261

Bindeman, I., 2008, Oxygen isotopes in mantle and crustal magmas as revealed by single crystal analysis: Reviews in Mineralogy and Geochemistry, v. 69, p. 445–478, https://doi.org/10.2138/rmg.2008.69.12

Blichert-Toft, J., and Albarède, F., 1997, The Lu-Hf isotope geochemistry of chondrites and the evolution of the mantle-crust system: Earth and Planetary Science Letters, v. 148, n. 1–2, p. 243–258, https://doi.org/10.1016/S0012-821X(97)00040-X

Cawood, P. A., and Buchan, C., 2007, Linking accretionary orogenesis with supercontinent assembly: Earth-Science Reviews, v. 82, n. 3–4, p. 217–256, https://doi.org/10.1016/j.earscirev.2007.03.003

Cawood, P. A., Kröner, A., and Pisarevsky, S., 2006, Precambrian plate tectonics: Criteria and evidence: GSA Today, v. 16, n. 7, p. 4–11, https://doi.org/10.1130/GSAT01607.1

Cawood, P. A., Kröner, A., Collins, W. J., Kusky, T. M., Mooney, W. D., and Windley, B. F., 2009, Accretionary orogens through Earth history: Geological Society, London, Special Publications, v. 318, p. 1–36, https://doi.org/10.1144/SP318.1

Cawood, P. A., Hawkesworth, C. J., and Dhuime, B., 2013, The continental record and the generation of continental crust: Geological Society of America Bulletin, v. 125, n. 1–2, p. 14–32, https://doi.org/10.1130/B30722.1

Chappell, B. W., and White, A. J. R., 1992, I- and S-type granites in the Lachlan Fold Belt: Geological Society of America Special Papers, v. 272, p. 1–26, https://doi.org/10.1130/SPE272-p1

Chen, J. Y., Yang, J. H., Zhang, J. H., and Sun, J. F., 2014, Geochemical transition shown by Cretaceous granitoids in southeastern China: Implications for continental crustal reworking and growth: Lithos, v. 196–197, p. 115–130, https://doi.org/10.1016/j.lithos.2014.03.003

Cheong, C. S., and Chang, H. W., 1997, Sr, Nd, and Pb isotope systematics of granitic rocks in the central Ogcheon Belt, Korea: Geochemical Journal, v. 31, n. 1, p. 17–36, https://doi.org/10.2343/geochemj.31.17

Cheong, C. S., and Kim, N., 2012, Review of radiometric ages for Phanerozoic granitoids in southern Korean Peninsula: Journal of the Petrological Society of Korea, v. 21, p. 173–192 (in Korean with English abstract).

Cheong, C. S., Kwon, S. T., Kim, J., and Chang, B. U., 1998, Geochemical and isotopic study of the Onjeongri granite in the northern Gyeongsang Basin, Korea: Comparison with Cretaceous to Tertiary granitic rocks in the other part of the Gyeongsang Basin and the Inner Zone of Southwest Japan: Journal of the Petrological Society of Korea, v. 7, p. 77–97 (in Korean with English abstract).

Cheong, C. S., Kwon, S. T., and Sagong, H., 2002, Geochemical and Sr–Nd–Pb isotopic investigation of Triassic granitoids and basement rocks in the northern Gyeongsang Basin, Korea: Implications for the young basement in the East Asian continental margin: The Island Arc, v. 11, n. 1, p. 25–44, https://doi.org/10.1046/j.1440-1738.2002.00356.x

Cheong, C. S., Yi, K., Kim, N., Lee, T. H., Lee, S. R., Geng, J. Z., and Li, H. K., 2013, Tracking source materials of Phanerozoic granitoids in South Korea by zircon Hf isotopes: Terra Nova, v. 25, n. 3, p. 228–235, https://doi.org/10.1111/ter.12027

Cheong, C.S., Jeong, Y. J., and Kwon, S. T., 2014a, Correction of spike contribution for strontium isotopic measurement by thermal ionization mass spectrometry: A test for spike-standard mixed solutions: Journal of Analytical Science and Technology, 5:26, https://doi.org/10.1186/s40543-014-0026-1

Cheong, C. S., Kim, N., Kim, J., Yi, K., Jeong, Y. J., Park, C. S., Li, H.-K., and Cho, M., 2014b, Petrogenesis of Late Permian sodic metagranitoids in southeastern Korea: SHRIMP zircon geochronology and elemental and Nd-Hf isotope geochemistry: Journal of Asian Earth Sciences, v. 95, p. 228–242, https://doi.org/10.1016/j.jseaes.2014.06.005

Cheong, C. S., Kim, N., Kim, J., and Cho, M., 2015, The Silurian–Devonian magmatism recorded in detrital zircons from the Andong area, northeastern Yeongnam Massif, Korea: Geosciences Journal, v. 19, n. 2, p. 393–405, https://doi.org/10.1007/s12303-014-0060-4

Cheong, D. K., and Kim, Y. I., 1996, Sedimentological study of the Nakdong Formation to analyse the forming and evolving tectonics of the Cretaceous Gyeongsang Basin, I: depositional setting, source, and paleocurrent analyses of the Nakdong Formation in the southwestern Gyeongsang Basin: Economic and Environmental Geology, v. 29, p. 639–660 (in Korean with English abstract).

Cherniak, D. J., Hanchar, J. M., and Watson, E. B., 1997, Diffusion of tetravalent cations in zircon: Contributions to Mineralogy and Petrology, v. 127, n. 4, p. 383–390, https://doi.org/10.1007/s004100050287

Chiaradia, M., Schaltegger, U., Spikings, R., Wotzlaw, J. F., and Ovtcharova, M., 2013, How accurately can we date the duration of magmatic-hydrothermal events in porphyry systems?—An Invited Paper: Economic Geology, v. 108, n. 4, p. 565–584, https://doi.org/10.2113/econgeo.108.4.565

Cho, D. L., and Kwon, S. T., 1994, Hornblende geobarometry of the Mesozoic granitoids in South Korea and the evolution of the crustal thickness: Journal of the Geological Society of Korea, v. 30, p. 41–61 (in Korean with English abstract).

Choi, P. Y., Lee, S. R., Choi, H. I., Hwang, J. H., Kwon, S. K., Ko, I. S., and An, G. O., 2002, Movement history of the Andong Fault System: Geometric and tectonic approaches: Geosciences Journal, v. 6, n. 2, p. 91–102, https://doi.org/10.1007/BF03028280

Choi, T., Lee, Y. I., and Orihashi, Y., 2012, Mesozoic detrital zircon U-Pb ages of modern river sediments in Korea: Implications for migration of arc magmatism in the Mesozoic East Asian continental margin: Terra Nova, v. 24, n. 2, p. 156–165, https://doi.org/10.1111/j.1365-3121.2011.01050.x

Chough, S. K., and Sohn, Y. K., 2010, Tectonic and sedimentary evolution of a Cretaceous continental arc–backarc system in the Korean peninsula: New view: Earth-Science Reviews, v. 101, n. 3–4, p. 225–249, https://doi.org/10.1016/j.earscirev.2010.05.004

Chough, S. K., Kwon, S. T., Ree, J. H., and Choi, D. K., 2000, Tectonic and sedimentary evolution of the Korean peninsula: A review and new view: Earth-Science Reviews, v. 52, n. 1–3, p. 175–235, https://doi.org/10.1016/S0012-8252(00)00029-5

Chu, N. C., Taylor, R. N., Chavagnac, V., Nesbitt, R. W., Boella, R. M., Milton, J. A., German, C. R., Bayon, G., and Burton, K., 2002, Hf isotope ratio analysis using multi-collector inductively coupled plasma mass spectrometry: An evaluation of isobaric interference corrections: Journal of Analytical Atomic Spectrometry, v. 17, p. 1567–1574, https://doi.org/10.1039/b206707b

Collins, W. J., 2002, Hot orogens, tectonic switching, and creation of continental crust: Geology, v. 30, p. 535–538, doi:10.1130/0091-7613(2002)030<0535:HOTSACba>2.0.CO;2.

DeCelles, P. G., Ducea, M. N., Kapp, P., and Zandt, G., 2009, Cyclicity in Cordilleran orogenic systems: Nature Geoscience, v. 2, p. 251–257, https://doi.org/10.1038/ngeo469

Dhuime, B., Hawkesworth, C., and Cawood, P., 2011, When continents formed: Science, v. 331, n. 6014, p. 154–155, https://doi.org/10.1126/science.1201245

Ducea, M. N., 2001, The California arc: Thick granitic batholiths, eclogitic residues, lithospheric-scale thrusting, and magmatic flare-ups: GSA Today, v. 11, n. 11, p. 4–10, https://doi.org/10.1130/1052-5173(2001)011<0004:TCATGB>2.0.CO;2

Ducea, M. N., and Barton, M. D., 2007, Igniting flare-up events in Cordilleran arcs: Geology, v. 35, n. 11, p. 1047–1050, https://doi.org/10.1130/G23898A.1

Ducea, M. N., Paterson, S. R., and DeCelles, P. G., 2015a, High-volume magmatic events in subduction systems: Elements, v. 11, n. 2, p. 99–104, https://doi.org/10.2113/gselements.11.2.99

Ducea, M. N., Saleeby, J. B., and Bergantz, G., 2015b, The architecture, chemistry, and evolution of continental magmatic arcs: Annual Review of Earth and Planetary Sciences, v. 43, p. 299–331, https://doi.org/10.1146/annurev-earth-060614-105049

Eby, G. N., 1990, The A-type granitoids: A review of their occurrence and chemical characteristics and speculations on their petrogenesis: Lithos, v. 26, n. 1–2, p. 115–134, https://doi.org/10.1016/0024-4937(90)90043-Z

Engebretson, D. C., Cox, A., and Gordon, R. G., 1985, Relative motions between oceanic and continental plates in the Pacific Basin: Geological Society of America Special Papers, v. 206, p. 1–60, https://doi.org/10.1130/SPE206-p1

Ernst, W. G., Tsujimori, T., Zhang, R., and Liou, J. G., 2007, Permo-Triassic collision, subduction-zone metamorphism, and tectonic exhumation along the East Asian continental margin: Annual Review of Earth and Planetary Sciences, v. 35, p. 73–110, doi:10.1146/annurev.earth.35.031306.140146.

Frost, B. R., Barnes, C. G., Collins, W. J., Arculus, R. J., Ellis, D. J., and Frost, C. D., 2001, A geochemical classification for granitic rocks: Journal of Petrology, v. 42, n. 11, p. 2033–2048, https://doi.org/10.1093/petrology/42.11.2033

Gerdes, A., and Zeh, A., 2006, Combined U-Pb and Hf isotope LA-(MC-)ICPMS analyses of detrital zircons: Comparison with SHRIMP and new constraints for the provenance and age of an Armorican metasediment in Central Germany: Earth and Planetary Science Letters, v. 249, n. 1–2, p. 47–61, https://doi.org/10.1016/j.epsl.2006.06.039

Gill, J., 1981, Orogenic andesites and plate tectonics: Berlin, Springer-Verlag, 390 p.

Griffin, W. L., Pearson, N. J., Belousova, E. A., Jackson, S. E., O'Reilly, S. Y., van Achterberg, E., and Shee, S. R., 2000, The Hf isotope composition of cratonic mantle: LAM-MC-ICPMS analysis of zircon megacrysts in kimberlites: Geochimica et Cosmochimica Acta, v. 64, n. 1, p. 133–147, https://doi.org/10.1016/S0016-7037(99)00343-9

Grove, T. L., Till, C. B., and Krawczynski, M. J., 2012, The role of H_2O in subduction zone magmatism: Annual Review of Earth and Planetary Sciences, v. 40, p. 413–439, https://doi.org/10.1146/annurev-earth-042711-105310

Hawkesworth, C. J., Dhuime, B., Pietranik, A. B., Cawood, P. A., Kemp, A. I. S., and Storey, C.D., 2010, The generation and evolution of the continental crust: Journal of the Geological Society, London, v. 167, p. 229–248, https://doi.org/10.1144/0016-76492009-072

Hwang, B. H., 2012, Petrogenesis of the Eonyang granitoids, SE Korea: New SHRIMP-RG zircon U-Pb age and whole-rock geochemical data: International Geology Review, v. 54, n. 1, p. 51–66, https://doi.org/10.1080/00206814.2010.497245

Hwang, B. H., McWilliams, M., Son, M., and Yang, K., 2007, Tectonic implication of A-type granites across the Yangsan Fault, Gigye and Gyeongju areas, Southeast Korean Peninsula: International Geology Review, v. 49, n. 12, p. 1094–1102, https://doi.org/10.2747/0020-6814.49.12.1094

Hwang, B. H., Ernst, W. G., McWilliams, M., and Yang, K., 2008, Geometric model of conjugate faulting in the Gyeongsang Basin, southeast Korea: Tectonics, v. 27, n. 6, TC6015, https://doi.org/10.1029/2008TC002343

Hwang, B. H., Ernst, W. G., and Yang, K., 2012, Two different magma series imply a Palaeogene tectonic transition from contraction to extension in the SE Korean Peninsula: International Geology Review, v. 54, n. 11, p. 1284–1295, https://doi.org/10.1080/00206814.2011.636990

Iida, K., Iwamori, H., Orihashi, Y., Park, T., Jwa, Y. J., Kwon, S. T., Danhara, T., and Iwano, H., 2015, Tectonic reconstruction of batholith formation based on the spatiotemporal distribution of Cretaceous–Paleogene granitic rocks in southwestern Japan: Island Arc, v. 24, n. 2, p. 205–220, https://doi.org/10.1111/iar.12103

Iizuka, T., and Hirata, T., 2005, Improvements of precision and accuracy in *in-situ* Hf isotope microanalysis of zircon using the laser ablation-MC-ICPMS technique: Chemical Geology, v. 220, n. 1–2, p. 121–137, https://doi.org/10.1016/j.chemgeo.2005.03.010

Imaoka, T., Kiminami, K., Nishida, K., Takemoto, M., Ikawa, T., Itaya, T., Kagami, H., and Iizumi, S., 2011, K-Ar age and geochemistry of the SW Japan Paleogene cauldron cluster: Implications for Eocene-Oligocene thermo-tectonic reactivation: Journal of Asian Earth Sciences, v. 40, n. 2, p. 509–533, https://doi.org/10.1016/j.jseaes.2010.10.002

Ishihara, S., 1998, Granitoid series and mineralization in the Circum-Pacific Phanerozoic granitoid belts: Resource Geology, v. 48, n. 4, p. 219–224, https://doi.org/10.1111/j.1751-3928.1998.tb00019.x

Isozaki, Y., Aoki, K., Nakajima, T., and Yanai, S., 2010, New insight into a subduction-related orogen: A reappraisal of the geotectonic framework and evolution of the Japanese Islands: Gondwana Research, v. 18, n. 1, p. 82–105, https://doi.org/10.1016/j.gr.2010.02.015

Jahn, B. M., 2010, Accretionary orogen and evolution of the Japanese Islands-Implications from a Sr-Nd isotopic study of the Phanerozoic granitoids from SW Japan: American Journal of Science, v. 310, n. 10, p. 1210–1249, https://doi.org/10.2475/10.2010.02

Jahn, B. M., Usuki, M., Usuki, T., and Chung, S. L., 2014, Generation of Cenozoic granitoids in Hokkaido (Japan): Constraints from zircon geochronology, Sr-Nd-Hf isotopic and geochemical analyses, and implications for crustal growth: American Journal of Science, v. 314, n. 2, p. 704–750, https://doi.org/10.2475/02.2014.09

Jahn, B. M., Valui, G., Kruk, N., Gonevchuk, V., Usuki, M., and Wu, J. T. J., 2015, Emplacement ages, geochemical and Sr–Nd–Hf isotopic characterization of Mesozoic to early Cenozoic granitoids of the Sikhote-Alin Orogenic Belt, Russian Far East: Crustal growth and regional tectonic evolution: Journal of Asian Earth Sciences, v. 111, p. 872–918, https://doi.org/10.1016/j.jseaes.2015.08.012

Jeong, Y. J., Lee, T. H., Kim, S. J., Yi, K., and Cheong, C. S., 2015, Introduction of laser ablation multi-collector ICP MS of Korea Basic Science Institute: Results of zircon U-Th-Pb dating and Hf isotope analysis: Petrological Society of Korea Abstracts with Programs, p. 57–58 (in Korean).

Jo, H. J., Cheong, A. C. S., Ryu, J. S., Kim, N., Yi, K., Jung, H., and Li, X. H., 2016, *In situ* oxygen isotope records of crustal self-cannibalization selectively captured by zircon crystals from high-δ^{26}Mg granitoids: Geology, v. 44, n. 5, p. 339–342, https://doi.org/10.1130/G37725.1

Jwa, Y. J., Lee, Y. I., and Orihashi, Y., 2009, Eruption age of the Kusandong Tuff in the Cretaceous Gyeongsang Basin, Korea: Geosciences Journal, v. 13, p. 265–273, https://doi.org/10.1007/s12303-009-0026-0

Kemp, A. I. S., Wilde, S. A., Hawkesworth, C. J., Coath, C. D., Nemchin, A., Pidgeon, R. T., Vervoort, J. D., and DuFrane, S. A., 2010, Hadean crustal evolution revisited: New constraints from Pb–Hf isotope systematics of the Jack Hills zircons: Earth and Planetary Science Letters, v. 296, n. 1–2, p. 45–56, https://doi.org/10.1016/j.epsl.2010.04.043

Keto, L. S., and Jacobsen, S. B., 1987, Nd and Sr isotopic variations of Early Paleozoic oceans: Earth and Planetary Science Letters, v. 84, n. 1, p. 27–41, https://doi.org/10.1016/0012-821X(87)90173-7

KIGAM (Korea Institute of Geoscience and Mineral Resources), 2001, Tectonic map of Korea: Seoul, South Korea, Sungji Atlas Co. Ltd, scale 1:1,000,000.
Kim, C. S., and Kim, G. S., 1997, Petrogenesis of the early Tertiary A-type Namsan alkali granite in the Kyongsang Basin, Korea: Geosciences Journal, v. 1, p. 99–107, https://doi.org/10.1007/BF02910481
Kim, G. S., Kim, J. Y., Jung, K. K., Hwang, J. Y., and Lee, J. D., 1995, Rb-Sr whole rock geochronology of the granitic rocks in the Kyeongju-Gampo area, Kyeongsangbugdo, Korea: Journal of Korean Earth Science Society, v. 16, p. 272–279 (in Korean with English abstract).
Kim, J., Yi, K., Jeong, Y. J., and Cheong, C. S., 2011, Geochronological and geochemical constraints on the petrogenesis of Mesozoic high-K granitoids in the central Korean peninsula: Gondwana Research, v. 20, n. 2–3, p. 608–620, https://doi.org/10.1016/j.gr.2010.12.005
Kim, N., Cheong, C. S., Yi, K., Song, Y.-S., Park, K. H., Geng, J. Z., and Li, H. K., 2014, Zircon U-Pb geochronological and Hf isotopic constraints on the Precambrian crustal evolution of the north-eastern Yeongnam Massif, Korea: Precambrian Research, v. 242, p. 1–21, https://doi.org/10.1016/j.precamres.2013.12.008
Kim, S. W., Kwon, S., Ryu, I. C., Jeong, Y. J., Choi, S. J., Kee, W. S., Yi, K., Lee, Y. S., Kim, B. C., and Park, D. W., 2012, Characteristics of the Early Cretaceous igneous activity in the Korean Peninsula and tectonic implications: The Journal of Geology, v. 120, n. 6, p. 625–646, https://doi.org/10.1086/667811
Kim, S. W., Kwon, S., Park, S. I., Lee, C., Cho, D. L., Lee, H. J., Ko, K., and Kim, S. J., 2016, SHRIMP U-Pb dating of the Cretaceous plutonic rocks in the Korean Peninsula: A new tectonic model of the Cretaceous Korean Peninsula: Lithos, v. 262, p. 88–106, https://doi.org/10.1016/j.lithos.2016.06.027
Klimetz, M. P., 1983, Speculations on the Mesozoic plate tectonic evolution of Eastern China: Tectonics, v. 2, n. 2, p. 139–166, https://doi.org/10.1029/TC002i002p00139
Koh, J. S., Yoon, S. H., and Lee, S. W., 1996, Petrology and geochemical characteristics of A-type granite with particular reference to the Namsan granite, Kyongju: Journal of the Petrological Society of Korea, v. 5, p. 142–160 (in Korean with English abstract).
Lee, J. I., Kagami, H., and Nagao, K., 1995, Rb-Sr and K-Ar age determinations of the granitic rocks in the southern part of the Kyeongsang basin, Korea: Implication for cooling history and evolution of granitic magmatism during late Cretaceous: Geochemical Journal, v. 29, n. 6, p. 363–376, https://doi.org/10.2343/geochemj.29.363
Lee, S. G., Shin, S. C., Kim, K. H., Lee, T., Koh, H., and Song, Y. S., 2010, Petrogenesis of three Cretaceous granites in the Okcheon Metamorphic Belt, South Korea: Geochemical and Nd–Sr–Pb isotopic constraints: Gondwana Research, v. 17, n. 1, p. 87–101, https://doi.org/10.1016/j.gr.2009.04.012
Lee, T. H., Yi, K., Cheong, C. S., Jeong, Y. J., Kim, N., and Kim, M. J., 2014, SHRIMP U-Pb zircon geochronology and geochemistry of drill cores from the Pohang Basin: Journal of the Petrological Society of Korea, v. 23, p. 167–185 (in Korean with English abstract).
Lee, T. H., Park, K. H., Yi, K., Geng, J. Z., and Li, H. K., 2015, SHRIMP U-Pb ages and Hf isotopic composition of the detrital zircons from the Myogok Formation, SE Korea: Development of terrestrial basin and igneous activity during the early Cretaceous: Geosciences Journal, v. 19, n. 2, p. 189–203, https://doi.org/10.1007/s12303-014-0042-6
Li, S., Santosh, M., and Jahn, B. M., 2012a, Evolution of the Asian continent and its continental margins: Journal of Asian Earth Sciences, v. 47, p. 1–4, https://doi.org/10.1016/j.jseaes.2012.02.001
Li, X. H., 2000, Cretaceous magmatism and lithospheric extension in Southeast China: Journal of Asian Earth Sciences, v. 18, n. 3, p. 293–305, https://doi.org/10.1016/S1367-9120(99)00060-7
Li, X. H., Li, Z. X., Li, W. X., and Wang, Y., 2006, Initiation of the Indosinian orogeny in South China: Evidence for a Permian magmatic arc on Hainan Island: The Journal of Geology, v. 114, n. 3, p. 341–353, https://doi.org/10.1086/501222
Li, Y., Ma, C. Q., Xing, G. F., Zhou, H. W., Zhang, H., and Brouwer, F. M., 2015, Origin of a Cretaceous low-^{18}O granitoid complex in the active continental margin of SE China: Lithos, v. 216–217, p. 136–147, https://doi.org/10.1016/j.lithos.2014.12.018
Li, Z. X., and Li, X. H., 2007, Formation of the 1300-km-wide intracontinental orogen and postorogenic magmatic province in Mesozoic South China: A flat-slab subduction model: Geology, v. 35, n. 2, p. 179–182, https://doi.org/10.1130/G23193A.1
Li, Z. X., and Powell, C. M., 2001, An outline of the palaeogeographic evolution of the Australasian region since the beginning of the Neoproterozoic: Earth-Science Reviews. v. 53, n. 3–4, p. 237–277, https://doi.org/10.1016/S0012-8252(00)00021-0
Li, Z. X., Li, X. H., Chung, S. L., Lo, C. H., Xu, X., and Li, W. X., 2012b, Magmatic switch-on and switch-off along the South China continental margin since the Permian: Transition from an Andean-type to a Western Pacific-type plate boundary: Tectonophysics, v. 532–535, p. 271–290, https://doi.org/10.1016/j.tecto.2012.02.011
Li, Z., Qiu, J. S., and Yang, X. M., 2014, A review of the geochronology and geochemistry of Late Yanshanian (Cretaceous) plutons along the Fujian coastal area of southeastern China: Implications for magma evolution related to slab break-off and rollback in the Cretaceous: Earth-Science Reviews, v. 128, p. 232–248, https://doi.org/10.1016/j.earscirev.2013.09.007
Ludwig, K. R., 2008, User's manual for Isoplot 3.6: a geochronological toolkit for Microsoft Excel: Berkeley Geochronology Center Special, Publication 4, p. 77.
——— 2009, User's manual for Squid 2.50: Berkeley Geochronology Center Special, Publication 5, p. 110.
Martin, H., Smithies, R. H., Rapp, R., Moyen, J. F., and Champion, D., 2005, An overview of adakite, tonalite-trondhjemite-granodiorite (TTG) and sanukitoid: Relationships and some implications for crustal evolution: Lithos, v. 79, n. 1–2, p. 1–24, https://doi.org/10.1016/j.lithos.2004.04.048
Maruyama, S., Liou, J. G., and Terabayashi, M., 1996, Blueschists and eclogites of the world and their exhumation: International Geology Review, v. 38, p. 485–594, https://doi.org/10.101610.1080/00206819709465347

Maruyama, S., Isozaki, Y., Kimura, G., and Terabayashi, M., 1997, Paleogeographic maps of the Japanese Islands: Plate tectonic synthesis from 750 Ma to the present: Island Arc, v. 6, n. 1, p. 121–142, https://doi.org/10.1111/j.1440-1738.1997.tb00043.x

McDonough, W. F., and Sun, S. S., 1995, The composition of the Earth: Chemical Geology, v. 120, n. 3–4, p. 223–253, https://doi.org/10.1016/0009-2541(94)00140-4

Murakami, N., 1974, Some problems concerning late Mesozoic to early Tertiary igneous activity on the inner side of Southwest Japan: Pacific Geology, v. 8, p. 139–151.

Noh, J. H., and Park, H. S., 1990, Mineral diagenesis of sandstones from the Kyongsang Supergroup in Goryeong area: Journal of the Geological Society of Korea, v. 26, p. 371–392 (in Korean with English abstract).

Paces, J. B., and Miller, J. D., Jr., 1993, Precise U–Pb ages of Duluth Complex and related mafic intrusions, Northeastern Minnesota: Geochronological insights to physical, petrogenic, paleomagnetic, and tectonomagmatic processes associated with the 1.1 Ga midcontinent rift system: Journal of Geophysical Research-Solid Earth, v. 98, n. B8, p. 13997–14013, https://doi.org/10.1029/93JB01159

Park, C. S., Shin, H. S., Oh, H., Moon, J. H., Cho, H., and Cheong, C. S., 2013, Determination of trace elements in geological reference materials G-3, GSP-2 and SGD-1a by low-dilution glass bead digestion and ICP-MS: Geostandards and Geoanalytical Research, v. 37, n. 3, p. 361–368, https://doi.org/10.1111/j.1751-908X.2012.00212.x

Paterson, S. R., and Ducea, M. N., 2015, Arc magmatic tempos: Gathering the evidence: Elements, v. 11, n. 2, p. 91–98, https://doi.org/10.2113/gselements.11.2.91

Paterson, S. R., Okaya, D., Memeti, V., Economos, R., and Miller, R. B., 2011, Magma addition and flux calculations of incrementally constructed magma chambers in continental margin arcs: combined field, geochronologic, and thermal modeling studies: Geosphere, v. 7, n. 6, p. 1439–1468, https://doi.org/10.1130/GES00696.1

Peacock, S. M., Rushmer, T., and Thompson, A. B., 1994, Partial melting of subducting oceanic crust: Earth and Planetary Science Letters, v. 121, n. 1–2, p. 227–444, https://doi.org/10.1016/0012-821X(94)90042-6

Qian, Q., and Hermann, J., 2013, Partial melting of lower crust at 10–15 kbar: Constraints on adakite and TTG formation: Contributions to Mineralogy and Petrology, v. 165, n. 6, p. 1195–1224, https://doi.org/10.1007/s00410-013-0854-9

Rickwood, P. C., 1989, Boundary lines within petrologic diagrams which use oxides of major and minor elements: Lithos, v. 22, n. 4, p. 247–263, https://doi.org/10.1016/0024-4937(89)90028-5

Rollinson, H., 1993, Using geochemical data: Evaluation, presentation, interpretation: Singapore, Prentice Hall, 352 p.

Rubatto, D., 2002, Zircon trace element geochemistry: Partitioning with garnet and the link between U-Pb ages and metamorphism: Chemical Geology, v. 184, n. 1–2, p. 123–138, https://doi.org/10.1016/S0009-2541(01)00355-2

Rudnick, R. L., 1995, Making continental crust: Nature, v. 378, p. 571–578, https://doi.org/10.1038/378571a0

Rudnick, R. L., and Gao, S., 2003, Composition of the continental crust, *in* Rudnick, R. L., editor, The Crust: Treatise on Geochemistry, v. 3, p. 1–64, https://doi.org/10.1016/B0-08-043751-6/03016-4

Sagong, H., Kwon, S. T., and Ree, J.-H., 2005, Mesozoic episodic magmatism in South Korea and its tectonic implication: Tectonics, v. 24, n. 5, TC5002, https://doi.org/10.1029/2004TC001720

Scherer, E., Münker, C., and Mezger, K., 2001, Calibration of the lutetium-hafnium clock: Science, v. 293, n. 5530, p. 683–687, https://doi.org/10.1126/science.1061372

Sohn, Y. K., Son, M., Jeong, J. O., and Jeon, Y. M., 2009, Eruption and emplacement of a laterally extensive, crystal-rich, and pumice-free ignimbrite (the Cretaceous Kusandong Tuff, Korea): Sedimentary Geology, v. 220, n. 3–4, p. 190–203, https://doi.org/10.1016/j.sedgeo.2009.04.020

Stacey, J. S., and Kramers, J. D., 1975, Approximation of terrestrial lead isotope evolution by a two-stage model: Earth and Planetary Science Letters, v. 26, n. 2, p. 207–221, https://doi.org/10.1016/0012-821X(75)90088-6

Sun, S. S., and McDonough, W. F., 1989, Chemical and isotopic systematics of oceanic basalts: Implications for mantle composition and processes: Geological Society, London, Special Publications, v. 42, p. 313–345, https://doi.org/10.1144/GSL.SP.1989.042.01.19

Tatsumi, Y., 2005, The subduction factory: How it operates in the evolving Earth: GSA Today, v. 15, n. 7, p. 4–10, https://doi.org/10.1130/1052-5173(2005)015[4:TSFHIO]2.0.CO;2

Tatsumi, Y., and Eggins, S., 1995, Subduction zone magmatism: Cambridge, Massachusetts, Blackwell Science, 211 p.

Valley, J. W., 2003, Oxygen isotopes in zircon: Reviews in Mineralogy and Geochemistry, v. 53, p. 343–385, https://doi.org/10.2113/0530343

Vervoort, J. D., Patchett, P. J., Söderlund, U., and Baker, M., 2004, Isotopic composition of Yb and the determination of Lu concentrations and Lu/Hf ratios by isotope dilution using MC-ICPMS: Geochemistry, Geophysics, Geosystems, v. 5, n. 11, Q11002, https://doi.org/10.1029/2004GC000721

Walker, J. D., Geissman, J. W., Bowring, S. A., and Babcock, L. E., compilers, 2012, Geologic Time Scale v. 4.0: Geological Society of America, https://doi.org/10.1130/2012.CTS004R3C

Wee, S. M., Choi, S. G., Ryu, I. C., and Shin, H. J., 2006, Geochemical characteristics of the Cretaceous Jindong granites in the southwestern part of the Gyeongsang Basin, Korea: Focused on adakitic signatures: Economic and Environmental Geology, v. 39, p. 555–566 (in Korean with English abstract).

Wee, S. M., Kim, Y., Choi, S. G., Park, J. W., and Ryu, I. C., 2007, Adakitic signatures of the Jindong granitoids: Economic and Environmental Geology, v. 40, p. 223–236 (in Korean with English abstract).

Whalen, J. B., Currie, K. L., and Chappell, B. W., 1987, A-type granites: Geochemical characteristics, discrimination and petrogenesis: Contributions to Mineralogy and Petrology, v. 95, n. 4, p. 407–419, https://doi.org/10.1007/BF00402202

White, L. T., and Ireland, T. R., 2012, High-uranium matrix effect in zircon and its implications for SHRIMP U-Pb age determinations: Chemical Geology, v. 306–307, p. 78–91, https://doi.org/10.1016/j.chemgeo.2012.02.025

Williams, I. S., 1998, U-Th-Pb geochronology by ion microprobe, *in* McKibben, M. A., Shanks W. C., III, and Ridley, W. I., editors, Applications of microanalytical techniques to understanding mineralizing processes: Reviews in Economic Geology, 7, p. 1–35, https://doi.org/ 10.5382/Rev.07.01

Woodhead, J., Hergt, J., Shelley, M., Eggins, S., and Kemp, R., 2004, Zircon Hf-isotope analysis with an excimer laser, depth profiling, ablation of complex geometries, and concomitant age estimation: Chemical Geology, v. 209, n. 1–2, p. 121–135, https://doi.org/10.1016/j.chemgeo.2004.04.026

Wu, F. Y., Han, R. H., Yang, J. H., Wilde, S. A., Zhai, M. G., and Park, S. C., 2007, Initial constraints on the timing of granitic magmatism in North Korea using U–Pb zircon geochronology: Chemical Geology, v. 238, n. 3–4, p. 232–248, https://doi.org/10.1016/j.chemgeo.2006.11.012

Yi, K., Cheong, C. S., Kim, J., Kim, N., Jeong, Y. J., and Cho, M., 2012a, Late Paleozoic to Early Mesozoic arc-related magmatism in southeastern Korea: SHRIMP zircon geochronology and geochemistry: Lithos. v. 153, p. 129–141, https://doi.org/10.1016/j.lithos.2012.02.007

Yi, K., Cheong, C. S., Kim, N., Lee, S., and Choi, M. S., 2012b, Mixing effects in zircon U-Pb ion microprobe dating: An example from a quartzofeldspathic dyke in the Yeongdeok pluton, southeastern Korea: Geochemical Journal, v. 46, p. 261–266, https://doi.org/10.2343/geochemj.2.0202.

Yi, K., Lee, S., Kwon, S., and Cheong, C. S., 2014, Polyphase tectono-magmatic episodes as revealed by SHRIMP U-Pb geochronology and microanalysis of zircon and titanite from the central Okcheon belt, Korea: Journal of Asian Earth Sciences, v. 95, p. 243–253, https://doi.org/10.1016/j.jseaes.2014.04.021

Zhang, Y. B., Zhai, M., Hou, Q. L., Li, T. S., Liu, F., and Hu, B., 2012, Late Cretaceous volcanic rocks and associated granites in Gyeongsang Basin, SE Korea: Their chronological ages and tectonic implications for cratonic destruction of the North China Craton: Journal of Asian Earth Sciences, v. 47, p. 252–264, https://doi.org/10.1016/j.jseaes.2011.12.011

Zhang, S. H., Zhao, Y., Davis, G. A., Ye, H., and Wu, F., 2014, Temporal and spatial variations of Mesozoic magmatism and deformation in the North China Craton: Implications for lithospheric thinning and decratonization: Earth-Science Reviews, v. 131, p. 49–87, https://doi.org/10.1016/j.earscirev.2013.12.004

Zhu, K. Y., Li, Z. X., Xu, X. S., and Wilde, S. A., 2014, A Mesozoic Andean-type orogenic cycle in southeastern China as recorded by granitoid evolution: American Journal of Science, v. 314, n. 1, p. 187–234, https://doi.org/10.2475/01.2014.06